Myeloid AMPK in Atherosclerosis: therapeutic potential and associated mechanisms

Nicholas LeBlond

A thesis submitted in partial fulfillment of the requirements for the
Doctorate in Philosophy degree in Biochemistry

Supervisor: Dr. Morgan Fullerton

The department of Biochemistry, Microbiology, and Immunology
Faculty of Medicine
University of Ottawa

ABSTRACT

Atherosclerosis propagates when innate immune cells, myeloid-derived macrophages, undergo unregulated uptake of cholesterol-rich modified low-density lipoproteins (LDL). Excess storage and retention of this cholesterol leads to development of lipid-laden macrophage foam cells, that accumulate within the intima of arteries as developing plaque. Formation of atherosclerotic lesions reduces blood flow and can further lead to more serious complications such as myocardial infarction, stroke, and cardiovascular disease. AMP-activated protein kinase (AMPK), a master regulator of cellular energetics, has been shown to participate in many anti-atherogenic pathways within myeloid cells such as (but not limited to) the inhibition of cholesterol synthesis and stimulation of reverse cholesterol transport. However, a recent report described a pro-atherogenic role for myeloid AMPK, showing it is expression required for myeloid cell recruitment and longevity within the atherosclerotic microenvironment. Despite this, multiple reports all corroborate describing a protective role for systemic pharmacological AMPK activation. We sought to determine the consequence of modified LDL variants in myeloid AMPK signaling and to further clarify the role of myeloid AMPK signaling within atherosclerosis.

In cultured macrophages primed with modified LDL variants underwent AMPK activation, which was also associated with increased markers of autophagy. In an in vivo model of intermediate atherosclerosis, we observed that neither myeloid AMPK expression nor systemic AMPK-activating therapy influenced lesion myeloid content, necrosis, or autophagic markers. Furthermore, despite a suggestive trend, both myeloid AMPK and AMPK-therapy did not significantly influence lesion size in male or female mice. Interestingly, we found that in animals lacking AMPK signaling to only one substrate, HMGCR (the rate limiting enzyme

in cholesterol synthesis), knock-in mice developed accelerated atherosclerosis when compared to their wild-type littermate. Furthermore, we determined that AMPK signaling to HMGCR in the hematopoietic compartment alone is enough to protect against atherogenesis. Taken together, these studies show the benefit of interrogating specific AMPK-regulated pathways in the context of atherosclerosis, and sheds light on the benefit of utilization of single point mutation knock-in models opposed to global or cell type-specific knockout models for investigations into AMPK within atherosclerosis.

AKNOWLEDGEMENTS:

First and foremost, I would like to provide appreciation to my Thesis supervisor, Dr. Morgan Fullerton, for his continued support and guidance for the duration of my doctoral studies. I especially would like to thank Morgan for involving myself in numerous fruitful collaborations as well as his scientific training and advice for all aspects of my research and professional career. In addition, I would also like to thank all members of the Fullerton Lab past and present for their continued support both scientifically and emotionally.

I would also like to thank the members of my thesis advisory committee, Dr. Derrick Gibbings, Dr. Katey Rayner, and Dr. Mireille Ouimet. Throughout the duration of doctoral studies, each member has provided essential advice for my research and has aided me directly by sharing procedures, reagents, and general scientific knowledge. I would also like to thank my collaborator Dr. Suresh Gadde for all his help and direct contribution for my experimentation. Lastly, I would like to thank Michael Culcheith, Zachary Golding, and Bryan Thompson, who all have acted as my number one support system for a time spanning greater than my doctoral research.

CONTRIBUTION OF COLLABORATORS:

There are certain parts of the data presented that were obtained through collaboration, which must be clearly acknowledged.

Chapter 1: Dr. Suresh Gadde (University of Ottawa) ran the high-performance liquid chromatography (HPLC) measurements of AMP and ATP, depicted in Figure 3. Dr. Gadde aided in the quantification and interpretation HPLC measurements. Sabrina Robichaud from Dr. Mireille Ouimet's laboratory (University of Ottawa) performed the experiment in Figure 4, providing the protein lysates for analysis via immunoblot, which I conducted. Additionally, the Ouimet laboratory provided the CD36 antibody for expression validation. The $CD36^{-/+}$ mice were provided to them by Dr. Kathryn Moore's laboratory (New York University). Lastly, the University of Ottawa's Flow Core Facility ran the samples to address all fluorescent-based lysosomal parameters.

Chapter 2: The University of Ottawa Histology Core Facility performed all hematoxylin and eosin of aortic sinuses from atherosclerosis studies used for the interpretation of lesion necrotic areas. Dr. Peyman Ghorbani and Conor O'Dwyer of Dr. Morgan Fullerton's laboratory aided in harvesting tissue from all experimental mice for *in vivo* atherosclerosis experiments. Dr. Peyman Ghorbani was responsible for all intravenous injections of PCSK9-AAV into experimental animals for *in vivo* studies into atherosclerosis. Additionally, Dr. Peyman Ghorbani helped with the identification/quantification of necrotic areas within atherosclerotic lesions. Under the supervision of Natasha Trzaskalski from Dr. Erin Mulvihill laboratory (University of Ottawa Heart Institute) Dr. Peyman Ghorbani ran the MSD MULTI-SPOT Assay to assess circulating chemical messengers isolated from all animals within *in vivo*

studies in atherosclerosis. The assay plate was assessed by Eric Brunette from human health and therapeutics at the National Research Council.

Chapter 3: Both the irradiation of mice along with associated bone marrow transplantation was completed by Dan Devette of the Animal Care and Veterinary Service at the University of Ottawa Heart Institute. Tyler Smith of Dr. Morgan Fullerton's laboratory (University of Ottawa) helped with all experiments depicted in Figures 21-23 including analysis and interpretation of data. Additionally, Tyler aided in the isolation of bone marrow for the bone marrow transplantation. Dr. Peyman Ghorbani (University of Ottawa) aided in the isolation of bone marrow for the bone marrow transplantation. Additionally, Dr. Peyman Ghorbani aided in harvesting tissue from WB and BMT mice for *in vivo* atherosclerosis experiments. Under the supervision of Natasha Trzaskalski from Dr. Erin Mulvihill laboratory (University of Ottawa Heart Institute) Dr. Peyman Ghorbani ran the MSD MULTI-SPOT Assay to assess circulating chemical messengers isolated from all animals within *in vivo* studies in atherosclerosis. The assay plate was assessed by Eric Brunette from human health and therapeutics at the National Research Council.

Table of Contents:

Table 1. List of abbreviations used.

Abbreviation	Definition
1-ELAM	Endothelial leukocyte adhesion molecule 1
ABCA1	ATP-binding cassette transporter A1
ABCG1	ATP-binding cassette transporter G1
ACC	Acetyl -CoA carboxylase
ACSS2	Acyl-CoA Synthetase Short Chain Family Member 2
ADP	Adenosine diphosphate
AICAR	5-Aminoimidazole-4-carboxamide ribonucleotide
AMP	Adenosine monophosphate
AMPK	AMP-activated protein kinase
AMPKK	AMPK kinase
ApoA-I	Apolipoprotein A-I
ATGL	Adipose triglyceride lipase
ATP	Adenosine triphosphate
BHA	Butylated hydroxy anisole
BMDM	bone-marrow derived macrophages
BMT	Bone-marrow transplant
BSA	Bovine serum albumin
CaMKKβ	Calcium/Calmodulin Dependent Protein Kinase Kinase β
CARM1	Coactivator-associated arginine methyltransferase
CC	Cholesterol crystals
CCR2	C-C chemokine receptor type 2
CD36	Cluster of differentiation 36
CE	Cholesterol esters
CLEAR	Coordinated lysosomal expression and regulation motif
CPT1	Carnitine palmitoyl transferase
DKO	Double knockout
DMEM	Dulbecco's Modified Eagle's Medium
DMSO	dimethyl sulfoxide
ER	Endoplasmic reticulum
FAO	Fatty acid oxidation
FASN	Fatty acid synthase
FBS	Fetal bovine serum
FC	Free cholesterol
FITC	Fluorescein
FOXO3	Forkhead Box O3
GGTase-I	Geranylgeranyl transferase type I
GLUT(1/4)	Glucose transporter type (1/4)

GPAT (mtGPAT)	Glycerol-3-Phosphate Acyltransferase 3 (mitochondrial)
GS	Glycogen synthase
HDL	high-density lipoprotein
HK2	hexokinase 2
HMGCR	3-Hydroxy-3-Methylglutaryl-CoA Reductase
HPLC	High-performance liquid chromatography
HSC	Hematopoietic stem cell
HSL	Hormone-sensitive lipase
HUVEC	Human umbilical vein endothelial cells
I.P.	Intraperitoneal
IFN	Interferon
IL	Interleukin
INSIG	Insulin-induced gene 1
IREα	Iron-responsive element
KD	Kinase dead
KI	Knock-in
KO	Knockout
LAL	Lysosomal acid lipase
LD	Lipid droplets
LDLr	Low-density lipoprotein receptor
LKB1	Liver kinase B1
LPS	lipopolysaccharide
MEF	Mouse embryonic fibroblasts
MacKO	Myeloid AMPKα1α2 knockout
mTOR	Mechanistic (mammalian) target of rapamycin
mTORC(1/2)	Mechanistic (mammalian) target of rapamycin complex (1/2)
NALP3	NACHT, LRR and PYD domains-containing protein 3
NPC1	Niemann-Pick disease, type C1
NPC2	NPC Intracellular Cholesterol Transporter 2
PCR	Polymerase chain reaction
PCSK9	Proprotein convertase subtilisin/kexin type 9
PFA	Paraformaldehyde
PFK	6-Phosphofructokinase
PLGA	Poly(lactic-co-glycolic acid)
PPAR	Peroxisome proliferator activated receptor
qPCR	Quantitative polymerase chain reaction
RAPTOR	Regulator-associated protein of mTOR
RCT	Reverse cholesterol transport
ROS	reactive oxygen species

ROS	reactive oxygen species
SCAP	SREBP cleavage-activating protein
SCD1	Stearoyl-CoA Desaturase
SDS-PAGE	Sodium dodecyl sulfate polyacrylamide gel electrophoresis
SKP2	S-phase kinase associated protein 2
Snf1	Sucrose Non-fermenting 1
SREBP	Sterol regulatory-element binding protein
T2D	Type 2 diabetes
TAK1	Transforming growth factor β-activated kinase 1
TFEB	Transcription factor EB
TICE	Transintestinal cholesterol efflux
TNF	Tumor necrosis factor
TSC2	Tuberous Sclerosis Complex 2
TUNEL	Terminal deoxynucleotidyl transferase dUTP nick end labeling
UCP2	Uncoupling protein 2
ULK1	Unc-51 like autophagy activating kinase
UPR	Unfolded protein response
VCAM-1	Vascular cell adhesion protein 1
VLDL	Very low-density lipoprotein
VSMC	vascular smooth muscle cells
WB	Whole-body
WT	Wild type

1.0 INTRODUCTION:

1.1 Atherosclerosis – Discovery and early molecular events.

1.1.1 Atherosclerosis and the economic burden on Canada.

The incidence of metabolic pathologies such as obesity and metabolic syndrome are elevating with little deviation. An obese physiological state prompts an individual to develop other metabolic complications such as fatty liver, hypertension and hyperlipidemia, and is an independent risk factor for cardiovascular disease (CVD). Within the developed world CVD has become a prevalent leading cause of mortality. In Canada alone, 1 in 12 people (or 2.4 million Canadians) over the age of 20 live with diagnosed CVD, with the direct and indirect costs cumulating to ~20 billion dollars of economic burden for the nation[1]. CVD is a class of disease that arises from numerous complications within the heart and/or blood vessels. Despite the range and complexity of cardiac and circulatory complications leading to CVD, atherosclerosis is an underlining causative event that precedes many complications such as (but not limited to) myocardial infarction and stroke, which eventually leads to CVD. Investigations into atherosclerosis are aimed at having a better understanding of the molecular pathways, cell types, and other confounding events to shed light on the best avenues for novel treatment and prevention strategies.

1.1.2 Early investigations into atherosclerosis.

The term ‘atherosclerosis’ has been in use for over a century being first introduced in 1904 by Felix Marchand, however it was in 1913 that the Russian physician Nikolai Anichkov made the serendipitous discovery that dietary cholesterol alone could induce atherosclerosis in rabbits[2]. In addition, Anichkov illustrated by hand his observations in atherosclerotic

vasculature isolated from rabbits, depicting smooth muscle cells, lymphoid cells, and lipid-laden macrophages that he coined cholesterinesterphagozyten (now described as 'foam cells')[2]. Building on Anichkov's influential findings, Dr. John Gofman and associates confirmed a causative role for cholesterol in the pathogenesis of atherosclerosis in the 1950s. Utilizing ultra-centrifugal technologies that were not available at the time of Anichkov's pivotal discovery, Gofman fractionated blood and observed differential cholesterol proportions of high and low-density. Gofman and colleagues further showed in humans that the low-density cholesterol fraction was responsible for rapid progression of atherosclerosis, inspiring an influx of research in related questions within atherosclerosis[3]. By delineating low-density and high-density cholesterol fractions, now defined as low-density lipoproteins (LDL) and high-density lipoproteins (HDL), their antagonizing roles in disease progression became apparent. Elevated proportions of low-density cholesterol predisposed cardiac complications where high levels of high-density lipoproteins had a protective effect, a discovery that inspired the next evolution of research in atherosclerosis to spawn.

1.1.3 Discovery of the LDL receptor and its use as a molecular tool in atherosclerosis.

Understanding the keystone molecular events that trigger a macrophage's ability to develop, propagate, and accumulate within arterial walls came from Goldstein and Brown's investigations into a condition called familial hypercholesterolemia (FH), a hereditable disease-causing high level of circulating LDL-cholesterol. Treating cultured fibroblasts with LDL and measuring cholesterol synthesis through enzymatic kinetics measurements of 3-hydroxy-3-methyl-glutaryl-coenzyme A reductase (HMGCR), they observed that LDL (but not HDL) reduced HMGCR activity[4]. This illuminated a process where LDL provided feedback regulation of sterol *de novo* synthesis. Following, they assessed the enzymatic

kinetics of suppression of HGMCR with LDL, which implicated possible involvement of a high-affinity receptor. Furthermore, Goldstein and Brown further showed that FH ensued from problems in extracting LDL-cholesterol and not cholesterol itself. This led to the discovery of the causative protein to FH, and resulted in the discovery of both the LDL receptor (LDLr) and the idea of receptor-mediated endocytosis by clathrin coated pits[4–7].

Genetically removing the LDL receptor in mice (LDLr-knockout mice; LDLr-KO) delays clearance of very low-density lipoprotein (VLDL) and LDL from plasma, raising total plasma cholesterol levels. When placed on a western diet (WD) rich in cholesterol the inability to properly removed VLDL and LDL from circulation causes hypercholesterolemia that was reversed by adeno-viral gene delivery of LDLr[8]. The ability to trigger diet-induced hypercholesteremia within LDLr-KO mice has made it a prominent mouse model to investigate atherosclerosis, where numerous genetic, pharmacological, and other therapeutic strategies are performed in WD-fed LDLr-KO to assess their ability to modulate atherosclerosis.

Recently, the next advancement has been made in utilization of LDLr-expression as a molecular tool to investigate atherosclerosis. This has been accomplished by exploiting the endogenous regulator of LDL receptor expression, Proprotein convertase subtilisin/kexin type 9 (PCSK9), where PCSK9 targets LDLr for lysosomal degradation promoting atherogenesis[9]. While multiple studies have looked at therapeutics to lower levels of circulating PCSK9 to combat atherogenesis[10,11], recently a gain-of-function PCSK9 adenoviral vector was used with the purpose of induction of hypercholesterolemia within wild-type (WT) mice. Treating WT mice with PCSK9-AAV (Asp377Tyr) reduced LDLr-expression, elevated plasma cholesterol levels, and lead to diet induced atherosclerosis[12,13]. These studies described the PCSK9-AAV

as a molecular tool to mimic the LDLr-KO mouse phenotype, which allows for the generation of an atherosclerotic model from any pre-existing mouse model to negate the need for complex breeding schemes or transplantation of bone-marrow to investigate atherosclerosis.

1.1.4 Cholesterol trafficking and foam cell formation.

Following the major achievements in early stages of atherogenesis, research bloomed looking to map out other associated molecular events within atherogenesis predominantly within developing macrophage foam cells. Summarized below are the key molecular events within macrophage foam cell formation. Areas with compromised endothelial barrier allow for accumulation of LDL particles, which are prone to modifications such as aggregation or oxidation leading to endothelial cell activation[14–21]. Activated endothelial cells increase expression of leukocyte adhesion molecules vascular cell adhesion protein 1 and endothelial-leukocyte adhesion molecule 1 (VCAM-1 and ELAM-1, respectively) as well as chemoattractant protein messengers monocyte chemoattractant protein 1 and interleukin 8 (MCP-1 and IL-8, respectively) that signal circulating pro-inflammatory LY6C^{hi} monocytes to recognize and transmigrate into the subendothelial space where they further differentiate into macrophages[22–24].

Scavenger receptors such as cluster of differentiation 36 (CD36) present on macrophages surface recognize modified LDL and initiate unregulated continued uptake of modified LDL particles accumulated within the subendothelial space[25–30]. The LDL particles are processed at the lysosome, where the cholesterol is released and handled by soluble Niemann-Pick disease intracellular cholesterol transporter 2 (NPC2) within the lysosomal lumen where it releases the cholesterol to the lysosomal membrane protein Niemann-Pick disease type C1 (NPC1) where it is then shuttled to the endoplasmic reticulum where free

cholesterol (FC) is esterified by Acetyl-CoA acetyltransferase 1 (ACAT1)[23,31]. Esterified cholesterol (CE) is retained within cytoplasmic lipid droplets (LD); accumulation of LD is what gives macrophages a 'foamy' appearance giving rise to the nomenclature 'foam cell'. Accumulation of foam cells within the subendothelial space further stimulates the pro-inflammatory nature of the developing plaque through excretion of chemoattractant messengers, leading to further recruitment of additional myeloid and other immune cells into the developing lesion[23,31].

1.1.5 Reverse cholesterol transport.

For removal of stored cholesterol from peripheral tissue out of the body, a necessary first step is to hydrolyse stored CE to FC prior to export. It was originally thought that CE hydrolysis was accomplished by cytoplasmic neutral hydrolases exclusively, however inhibition of neutral hydrolases only accounted for a 50% reduction in CE hydrolysis and cholesterol efflux to extracellular acceptors[32]. It was then uncovered that LD rich in CE can be mobilized to the lysosome for degradation by the 'self-eating' process known as autophagy, where inhibition of autophagy alone reduces CE hydrolysis and cholesterol efflux by 50%. Inhibiting both neutral hydrolases and autophagy negates all CE hydrolysis and cholesterol efflux in culture[32].

In autophagy mediated CE hydrolysis, LD are shuttled to the lysosome through for catalysis, where the CE are hydrolyzed producing free cholesterol (FC). FC is then shuttled from the lysosome to ATP Binding Cassette Subfamily A Member 1 and ATP-binding cassette sub-family G member 1 (ABCA1 or ABCG1, respectively), where cholesterol is exported out of the cell to extracellular acceptors apolipoprotein-A1 (ApoA-1 or nascent-HDL) and HDL, respectively[33–35]. The cholesterol is then carried through circulation to the liver, where it is

removed from circulation. The liver processes the lipoproteins and extracts the cholesterol to either redistribute the cholesterol to tissues in need, or to facilitate removal from the body through the gallbladder into feces[36]. The process of removing cholesterol from peripheral tissue to its excretion in feces is known as reverse cholesterol transport (RCT), an athero-protective process (first described in 1968)[37]. Stimulating RCT is a therapeutically attractive pathway to target for reducing arterial plaque burden and ameliorating atherosclerosis.

Additionally, the lymphatic system contributes to macrophage RCT, where lymphatic vasculature within atherosclerotic lesions account for approximately 50% of cholesterol delivery to blood from lipid-laden macrophage foam cells[38–40]. Alternative the hepatobiliary routes for cholesterol removal from the body, RCT can be facilitated by transintestinal cholesterol efflux (TICE), where cholesterol from the blood is transported by enterocytes into the lumen of the intestine for removal of the body[41,42]. Despite the route that enables RCT, the hydrolysis of stored CE from LD must be accomplished before FC is exported out of the cell. Initially this was thought to be performed by cytoplasmic neutral hydrolases exclusively, however it was uncovered that the lysosome attributed to approximately 50% of cholesterol hydrolysis[32]. Furthermore, evidence emerged showing that this occurs through autophagic processing of LD, such that pharmacological or genetic disruption of this pathway reduces cholesterol efflux *in vitro* and lessens RCT *in vivo*[32]. This study illuminated autophagy as a targetable pathway to stimulate the removal of cholesterol from atherosclerotic lesions and out of the body.

1.1.6 Myeloid-derived monocytes and macrophages in atherosclerosis.

Accumulation of cholesterol-rich apolipoprotein B-containing lipoproteins (modified LDL) within areas of disturbed laminar flow causes the activation of endothelial cells. Once

activated, endothelial cells upregulate expression of chemoattractant proteins (e.g. MCP-1) that can be recognized by C-C chemokine receptor type 2 (CCR2), which is highly expressed on pro-inflammatory LY6C^{hi} monocytes. Activated endothelial cells have increased expression of leukocyte adhesion molecules (e.g. VCAM-1) that facilitates inflammatory monocytes chemotaxis within the subendothelial space[23]. Once localized, monocytes recognize modified LDL variants and differentiate into mononuclear phagocytes (macrophages) and are additionally able to activate any resident macrophages present. Albeit clearance of modified LDL variants from the vasculature by macrophages is initially protective, there is little negative feedback signaling to uptake, resulting in the continuation of myeloid cell recruitment, transmigration, and differentiation promoting lesion development. Macrophage heterogeneity plays an essential role in atherosclerosis, where their pro- or anti-inflammatory state corresponds to either lesion progression or regression, respectively[43,44].

Myeloid-derived monocytes/macrophages are a functionally heterogenous cell population that play multiple critical roles within the body such as immune surveillance, pathogen killings, and tissue repair. Macrophages possess phenotypic plasticity allowing them to develop into multiple distinct phenotypic subtypes that accommodate the desired unique immunological output dependent the signals they sense within their microenvironment. Despite their capability to exhibit many unique phenotypic subtypes, these functional subtypes are often associate with two main branches for simplification of their broad functional roles, they are often classified as classically activated M1 macrophages (pro-inflammatory) or alternatively activated M2 macrophages (anti-inflammatory)[23,24,45].

Classical activation of macrophages into an M1-like phenotype is triggered by Toll-like receptor ligands like lipopolysaccharide (LPS) and interferon gamma (INF-γ). M1

macrophages further aid atherogenesis through secretion of pro-inflammatory cytokines such as interleukin 1β, interleukin 12, tumor necrosis factor-α, (IL-1β, IL-12, TNF-α, respectively) promoting lesion inflammation[23,45,46]. Opposingly, alternative activation of macrophages in a M2-like phenotype occurs from stimulation with interleukin 4 and interleukin 13 (IL-4 and IL-13, respectively). M2 macrophages aid in resolution of inflammation through secretion of anti-inflammatory cytokines interleukin 1 receptor antagonist and interleukin 10 (IL-1RA and IL-10, respectively)[23,47]. Macrophage heterogeneity plays a prominent role in atherosclerosis contributing both to the continuation of atherogenesis (by M1-like macrophages) or the regression of atherosclerosis (by M2-like macrophages). Strategies to resolve macrophage inflammation, either pharmacologically or genetically, have shown to be therapeutically relevant to protect against further recruitment of immune cells to the lesion thus promoting lesion reduction[48].

Alternative to stimulation by chemical messengers within their microenvironment, macrophage metabolism has been shown to dictate their phenotypic output. Macrophages undergo metabolic reprogramming to accommodate immunological output, where M1-like macrophages rely on glycolysis while M2-like macrophages rely on oxidative phosphorylation to meet energy demands[49,50]. This highlights a targetable pathway to attenuate inflammation within developing lesions during atherosclerosis. Cellular metabolism is largely regulated by two antagonizing master regulators, AMP-activated protein kinase (AMPK) and mechanistic target of rapamycin complex 1 (mTORC1), which stimulate catabolic and inhibits anabolic pathways, respectively. AMPK is a potent activator of pathways that stimulate oxidative phosphorylation for adenosine triphosphate (ATP) generation, resulting in its implication as a molecular target to combat metabolic pathologies such as obesity and diabetes[51–54].

1.2 AMP-activated protein kinase.

AMPK is an evolutionarily conserved serine/threonine kinase responsible for sensing and maintaining energy balance. Under low-energy conditions, AMPK is able to stimulate catabolic process to generate energy such as (but not limited to) glucose uptake, fatty acid oxidation, and mitochondrial biogenesis. AMPK is a heterotrimeric enzyme, composed of an α-catalytic subunit, and β- and γ-regulatory subunits. All subunits are transcribed from different genes, with both the α and β subunits possessing two different isoforms while the γ possesses three, all with differential tissue expression[55,56]. AMPK undergoes autoregulation possessing an NH_2-terminal autoinhibitory sequence (residues 313-335) on the catalytic α-subunit[57,58].

Endogenous AMPK activity absolutely requires phosphorylation by upstream kinases (discussed below) at αThr172 (herein referred to as Thr172) present within the activation loop on the α-subunit, while many natural occurring polyphenols and synthetic small molecule compounds are capable of binding and inducing allosteric activation[59–61]. The β-subunit acts as a scaffolding protein allowing for the binding/docking of both the α and γ subunits, its presence being crucial for enzymatic function and protection from proteolytic degradation[62–64]. Additionally, an alternate role for the β-subunit have been shown for membrane association (via an NH_2-terminal myristoyl group), subcellular localization, and glycogen binding[65,66]. The γ-subunit is responsible for sensing adenine energy nucleotides, possessing four tandem repeat sequences called Cystathionine-β-synthase (CBS) motifs (CBS 1-4) allow for binding/sensing adenosine monophosphate (AMP), adenosine diphosphate (ADP), and ATP. In mammals, under physiological conditions CBS 2 remains empty while CBS 4 tightly binds AMP. CBS 1 and CBS 3 has competitive binding of AMP, ADP, and ATP, where its postulated that CBS 3

is the main site for sensing/activation since it is the only site with direct interactions with the α-subunit[67–71].

As mentioned above, AMPK regulates cellular and whole-body energy metabolism, which highlights AMPK as potential molecular target for treatment and prevention of multiple metabolic pathologies such as but not limited to diabetes[72], obesity[73], and non-alcoholic fatty liver disease[74]. It's the goal of this thesis to address the role that AMPK plays in atherosclerosis and expand specifically on the role myeloid AMPK and its subsequent activation plays within the progression of atherosclerosis.

1.2.1 Activation of AMPK.

Phosphorylation of Thr172 on the α-catalytic subunit is required for AMPK activation. Early investigations within AMPK's homologue in *Saccharomyces cerevisiae* Snf1 (identified in 1981) lead researchers to theorize there were three candidate kinases responsible for activating AMPK[75]. Further assessment of related sequence homology then lead to the discovery of two main kinases responsible for phosphorylating mammalian AMPK at Thr172, Ca(2+)/calmodulin-dependent protein kinase kinase β and liver kinase B1 (CaMKKβ1 and LKB1, respectively). The first evidence linking CaMKKβ signaling to AMPK activity came in 1995, however it was largely discarded since AMPK from partially purified rat liver was insensitive to calmodulin[76,77]. CaMKKβ was confirmed as one of the two main AMPK kinases, however it activates AMPK when cytosolic ionic calcium concentrations are elevated independent of nucleotide ratios within the cell[77–79].

The enzyme responsible for activating AMPK in response to energy status was identified to be LKB1, first isolated from partially purified rat liver. Knowing what activates

AMPK in response to low-energy conditions led to investigations to fully understand the molecular events that lead from AMPK sensing shifting adenine nucleotide concentrations to its activation by LKB1[76,78,80]. Under low energy conditions where AMP is readily available, AMPKγ senses and binds AMP inducing a conformational change. This conformation change was shown to aid in AMPK's interaction with AXIN, a scaffolding protein shown to form a complex with AMPK and LKB1. AMPK's interaction with AXIN is strengthened in low glucose conditions while both siRNA-mediated knockdown of AXIN or mutating the AMP binding site on AMPKγ eliminates AMP-mediated AMPK activation by LKB1[81].

These studies were very attractive, partially because it helped better understand LKB1-mediated activation of AMPK but primarily because it illuminated how AMPK is so fine tuned to sense energy fluctuations within the cell. These studies illuminated that the protein V-ATPase/RAGULATOR complex could act as a metabolic switch capable of activating crucial regulators of anabolic (mTORC1) and catabolic metabolism (AMPK)[82]. The lysosome is a crucial organelle for numerous metabolic processes, with a critical role in macromolecule catalysis/recycling to produce precursors for numerous metabolic pathways. Considering that AMPK and mTORC1 share a common molecular switch and are localized to the lysosome (along with select substrates), its easier to understand how signal transduction through one metabolic pathway can immediately inhibit the antagonizing pathway in quick succession to metabolic stress.

There are many compounds that are capable of activating AMPK, both by direct and indirect mechanisms. Many polyphenols such as resveratrol will provide indirect activation AMPK by modulating the AMP: ATP ratio within the cell, while compounds such as 5-Aminoimidazole-4-carboxamide ribonucleotide (AICAR) can be converted to AMP

mimetics[83]. In particular interest to this thesis, A769662 is a small-molecule activator of AMPK that allosterically activates AMPK while simultaneously prevents its dephosphorylation[84]. Refer to **Appendix B** for a list of commonly used activators of AMPK used in macrophage research along with their associate mechanism of action.

1.3 The anti-atherogenic properties of AMPK signaling.

1.3.1 AMPK in inflammation.

Chronic low-grade inflammation is a hallmark of many metabolic pathologies such as (but not limited too) atherosclerosis, obesity, and non-alcoholic fatty liver disease. In high-fat induced chronic inflammation, AMPK activity in metabolic tissues such as liver, white adipose tissue (WAT), skeletal muscles and tissue resident macrophages is reduced[85–87]. Complementary to this, germ-free mice or mice treated with antibiotics have enhanced AMPK signaling highlighting the involvement of AMPK signaling in acute immunological processes in response to inflammation. Importantly, this relationship continues to humans where AMPK activity is reduced in high fat diet induced adipose tissue, where its activity is increased in response to diet induced weight loss. Additionally, multiple studies have shown that genetic ablation of AMPK (α1 and β1) results in more pro-inflammatory primed macrophages *in vitro* and increases systemic pro-inflammatory signaling *in vivo*[85–87]. In addition, it is known that through the regulation of lipid metabolism and cellular energetics, AMPK has often been sought out as a molecular target for pharmacological prevention of metabolic pathologies.

1.3.2 Negative regulation of mTOR protects against atherogenesis.

Anabolic processes such as protein synthesis, cell growth, and proliferation are both essential for development and longevity but are energetically costly. Anabolic metabolism is

largely dictated by mammalian target of rapamycin (mTOR) regulation, where mTOR expression is crucial for development and survival such that its genetic removal causes embryonic lethality[88,89]. mTOR is a serine/threonine kinase that associates with other proteins to form mTOR complex 1 (mTORC1; mTOR, RAPTOR, mLST8, and PRAS40) and mTOR complex 2 (mTORC2; mTOR, RICTOR, mLST8, mSIN1, Protor-1)[90–92]. mTORC1 is responsible for nutrient/energy/redox sensing that leads to its regulation of the synthesis of proteins, lipids, and nucleic acid which are essential for cell growth, proliferation, and survival. Furthermore, mammalian target of rapamycin complex 2 (mTORC2) regulates cell migration and cytoskeleton rearrangement along with glucose metabolism, ion transport, and apoptosis[91,93–95]. In addition to its activation of energy utilizing pathways listed above, mTOR is a potent negative regulator of pathways involved in energy generation such as autophagy, lipid catabolism, and glucose uptake[93,96,97]. In activated immune cells mTOR participates in alterations in cell morphology, migrate tissue sites, and upregulation of synthetic pathways to produce large quantities cytokines, chemokines, and lipid mediators to accommodate inflammation[98–100].

Within atherosclerosis, mTOR contributes in the positive regulation of lipogenesis, proliferation, and synthesis of pro-inflammatory mediators all of which encourage atherogenesis. The therapeutic relevance for mTOR inhibiting in atherosclerosis has been investigated in several studies administrating mTOR inhibitors (rapamycin or everolimus) in mice and rabbits (subcutaneously or orally). In all studies, animals treated with mTOR inhibitors developed significantly lesser lesion burden and had reduced expression of markers of myeloid inflammation; MCP-1, CCR2, and TNF-α in Apolipoprotein E-knockout (ApoE-KO)[101–103] and LDLr-KO[104,48,105] mice. In rabbits, suppression of mTOR with rapamycin or

everolimus significantly lowered lesion size and reduced the myeloid content in comparison to vehicle treated control animals[106–108]. Furthermore, lentiviral-mediated silencing of mTOR in ApoE-KO mice protected against lesion development and promoted plaque stability that was explained by enhanced autophagy in response to mTOR-ablation[109]. These studies all corroborate a protective role for mTOR suppression in atherosclerosis, largely explained by reduction in myeloid cell inflammation and alleviating suppression on lesion autophagy.

Interestingly, AMPK is the metabolic antagonist to mTOR and opposingly regulates numerous pathways such as autophagy to counter act mTOR signaling. Outside of shared regulatory pathways, AMPK counteracts anabolic metabolism by directly inhibiting mTOR activity through two distinct mechanisms. The first mechanism for mTOR-inhibition mediated by AMPK is by phosphorylation of Tuberous Sclerosis Complex 2 (TSC2) at Ser1387 by AMPK, which promotes Ras homolog enriched in brain GTPase (Rheb GAP) activation and associated inhibition of mTOR[110]. The second mechanism is AMPK directly phosphorylates Regulatory-associated protein of mTOR (RAPTOR) at Ser722 and Ser792 which encourages 14-3-3 proteins to bind RAPTOR, preventing its association with mTOR and thus preventing mTORC1 complex formation and activity[111]. Taken together, AMPK's suppression of mTOR and its opposing regulation of shared pathways (e.g. autophagy) potentially contributes to the protection against atherosclerosis.

1.3.3 Autophagy regulation and its role in RCT.

Macroautophagy (herein referred to as autophagy) is an evolutionarily conserved 'self-eating' process responsible for degradation and repurposing of cellular constituents such as (but not limited to) protein aggregates, cellular debris, dysfunctional organelles, and intracellular pathogens[97,112]. In brief, autophagic degradation of cellular cargo initiates from the formulation and sequestration of cargo within a lipid bilayer vesicle denoted as an autophagosome. Autophagosomes are then trafficked to the lysosome where it fuses, exposing its cargo to the highly acidic microenvironment and catalysis by lysosomal hydrolases[112–114]. Importantly, defects in autophagy have been associated with numerous diseases in humans such a myopathy, neurodegeneration, and cancer[115,116].

During regressing atherosclerosis, the CE stored within LD must be hydrolysed prior to exportation to extracellular acceptors ApoA-I and HDL that is facilitated by ABCA1 and ABCG1, respectively. Cholesterol ester hydrolysis was originally thought to be dependent on neutral hydrolases within the cytoplasm, however following inhibition of these hydrolases only suppressed cholesterol efflux to extracellular acceptors by approximately 50%, which suggests alternate hydrolases were participating in CE hydrolysis. The remaining 50% of CE hydrolysis was shown to be dependent on lysosomal processing, where chemical inhibition of lysosomal acid lipase (LAL) or the lysosomal-dependent process autophagy (with lalistat 1 and chloroquine, respectively) suppressed cholesterol efflux by approximately 50%. Lastly, suppression of both neutral hydrolases and autophagy completely blocked CE hydrolysis[32].

Interestingly, it was determined that autophagy was facilitating LD mobilization and CE hydrolysis by LAL such that pharmacological inhibiting LAL (with lalistat 1) or autophagy (with chloroquine) significantly enhanced CE burden within macrophages in addition to

significantly reduced cholesterol efflux to ApoA-I and HDL. Lastly, this study addressed the significance of autophagy within RCT *in vivo* by addressing macrophages genetically devoid of autophagy (isolated from autophagy related 5 knockout mice; ATG5-KO) capacity to expel stored cholesterol from the body[32]. When injected into recipient WT mice, Atg5-KO macrophages had poor capacity to stimulate RCT as evidenced by reduced radio-labeled cholesterol present within the serum, liver, gal bladder, and feces in references to WT mice receiving macrophages isolated from WT mice[32]. Taken together, this study created a paradigm shift showing that autophagy is required for normal levels of RCT and implicated as a targetable pathway to ameliorate atherogenesis. In succession, within an alternate study, it was shown that the progression of atherosclerosis measured in ApoE-KO mice attributed to defective autophagy shown with the accumulation of p62 (a hallmark of defective autophagy) and Beclin-1 protein levels assessed in aortic lysates and within the lesion itself (by immunofluorescent labeling techniques). Additionally, in ATG5-KO mice exhibited enhanced pro-inflammatory signaling and inflammatory activation, which accelerated the progression of atherosclerosis[117].

Despite the oversimplification above, autophagy is a complicated process with over 30 different proteins involved, most of which are subjected to multiple levels of regulation fine tuning the process. Of particular interest, it was shown that, Unc-51 like autophagy activating kinase 1 (ULK1; a crucial kinase within autophagy initiation complex), is directly regulated by phosphorylation by both AMPK and mTORC1[118]. AMPK directly activates ULK1 by phosphorylation of several serine residues (Ser317, Ser555, and Ser777 are the best characterized), inducing ULK1's autophosphorylation and propagation of signaling by the autophagy initiation complex (ULK1, FIP200, ATG101, and ATG13) for autophagosome

biosynthesis[112,118]. Alternatively, AMPK's negative regulation of mTORC1 (discussed above) alleviates mTORC1-mediated suppression of ULK1 (Ser757 phosphorylation of ULK1), which is another mechanism for AMPK-mediated autophagy initiation[119]. AMPK's regulation of ULK1 is the best characterized facet of AMPK-mediated autophagy regulation, however AMPK has been implicated in signaling to other proteins in autophagy and involved in events such as autophagosome biosynthesis and autophagosome-lysosome fusion[120,121].

1.3.4 Lysosomal biogenesis.

As mentioned above, the lysosome is a crucial organelle intimately involved in maintaining regulation of multiple metabolic processes. Defects in lysosomal homeostasis, lysosomal proteins, and autophagy (lysosomal dependent) is a characteristic of many disorders and diseases, highlighting the importance of pathways for improving lysosomal function and biosynthesis[115,122–124]. Interestingly, using pattern discovery analysis of promotor regions of known lysosomal genes led to the discovery of common gene network regulating and linking lysosomal biosynthesis, lysosome function, and autophagy. It was shown that enriched within the promotor region of numerous lysosomal genes there is a 10-base E-box like palindromic sequence motif (GTCACGTGAC) denoted as the coordinated lysosomal expression and regulation motif (CLEAR motif)[125]. It was determined that the basic helix-loop-helix leucine zipper transcription factor, Transcription Factor EB (TFEB), was responsible for recognizing the CLEAR motif for positive regulation transcription of multiple lysosomal genes, including itself. This discovery was later expanded by elucidating that many autophagy related genes posses the CLEAR motif and undergo transcriptional regulation by TFEB[126,127].

With insight of TFEB's role as a potent regulator of lysosomal biogenesis and autophagy allowed researchers to postulate that exploitation of TFEB's regulation could be

used to combat metabolic pathologies. This led to multiple investigations to elucidate the mechanisms and conditions that regulate TFEB's transcriptional activity. Its known that mTORC1 readily localizes to the lysosome where it is able to senses nutrients and amino acids and respond accordingly[128,129]. It was unknown if mTORC1 was implicated in any feedback regulation that could be involved in lysosome homeostasis via TFEB regulation. Multiple studies confirmed mTORC1 as a negative regulator of TFEB providing inhibitory phosphorylation of at least three serine residues (Ser122, Ser142, and Ser211)[130–134], which leads to TFEB's association with YWHA/14-3-3 proteins that sequester TFEB within the cytosol[135].

In recent years there have been multiple reports describing AMPK as a TFEB regulator. Interestingly, multiple reports show AMPK regulates TFEB activity by mechanisms independent of its negative regulation of TFEB-repressor mTORC1[136–138]. The first mechanism elucidated for AMPK regulation of TFEB was evidenced by two studies from independent groups, showing that nuclear AMPK indirectly regulates nuclear CARM1 (Coactivator-associated arginine methyltransferase 1) content, a methyl transferase that associates with TFEB in the nucleus aiding in transcription of target genes[136,139]. It was described that AMPK's induction of Forkhead box protein O3 (FOXO3a) activity led to decreased levels of S-Phase Kinase Associated Protein 2 (SKP2), which is associated with ubiquitin-dependent proteolytic degradation of Coactivator Associated Arginine Methyltransferase 1 (CARM1)[136,139]. Additionally, nuclear AMPK activation by glucose deprivation was shown to regulate TFEB activity by inducing phosphorylation of Acyl-CoA Synthetase Short Chain Family Member 2 (ACSS2) at Ser659[138]. Activated nuclear ACSS2 locally generates acetyl-CoA from acetate, promoting histone H3 acetylation within promotor

regions of TFEB regulated genes in lysosome biogenesis and autophagy[138]. Elimination of AMPK's regulation of ACSS2 by mutagenesis also abolished Arginine 17 dimethylation (catalyzed by CARM1)[136] induced by glucose deprivation, which may shed light on cooperation between pathways[138]. Recently, the first evidence was shown implicating that AMPK expression and subsequent activation reduces the negative phosphorylation of TFEB. Treating WT mouse embryonic fibroblasts (MEFs) with AMPK-activators AICAR and the 991-compound (refer to **Appendix B**) led to decreased levels of phosphorylated TFEB at Ser142, an effect lost in AMPKα1α2-DKO MEFs[140]. Additionally, WT MEFs treated with AMPK pharmacological activators increased levels of nuclear TFEB (but not AMPKα1α2-DKO), evidenced by fractionation and immunoblotting techniques[141]. This suggests that AMPK signaling and activation alleviate the negative phosphorylation on TFEB(Ser142) that increases its function, however future studies to interrogate the exact mechanism are warranted.

1.3.5 Transcriptional Control of Lipogenic programs.

The sterol regulatory binding element protein family (SREBP1a, SREBP1c, and SREBP2) are key lipogenic basic-helix-loop-helix leucine zipper class of transcription factors. The SREBP family are responsible for sensing FA and sterol levels, regulating synthesis of key enzymes within FA and cholesterol regulation to maintain lipid homeostasis. Under normal sterol conditions, immature SREBP is retained in the ER complexed to its proteolytic processor sterol regulatory element-binding protein cleavage-activating protein (SCAP) and regulatory insulin induced gene 1 protein (Insig-1). Insig-1 is a potent inhibitor of SREBP processing, when low Insig-1 dissociates from SCAP allowing for SREBP processing and, ER-release ultimately leading to its active mature form. Mature SREBP localizes to the nucleus

where it binds sterol regulatory elements (SRE motifs) on target genes, inducing transcription. SREBP1c regulates transcription of over 30 genes involved in uptake and synthesis of fatty acids, including Acetyl-CoA carboxylase 1, Stearoyl-CoA desaturase, fatty acid synthase (ACC1, SCD1, and FASN, respectively) all of which playing pivotal roles in fatty acid (FA) synthesis. SREBP2 is cholesterol-centric in nature regulating genes involved in the biosynthesis of cholesterol[142–144].

The complete picture of AMPK's regulation of the SREBP family of transcription factors is far from complete, however it is an exciting branch of research growing steadily. The most potent evidence of AMPK's regulation of SREBP1c and SREBP2 came from a study which observed LDLr-KO mice treated with AMPK activator S17834 had reduced SREBP1c and SREBP2 hepatic nuclear accumulation and transcriptional activity. This study was the first to report AMPK's direct phosphorylation of SREBP1c at Ser372 both *in vitro* and *in vivo*, however no specific mechanism was elucidated for SREBP2 suppression[145]. The Ser372Ala SREBP1c mutant proteolytic processing has been observed to still be regulated by AMPK, illuminating an additional avenue of regulation. Recently, AMPK's regulation of Insig-1 in hepatic tissue has been explored showing that Insig-1 protein stability and expression is regulated by AMPK. Furthermore, it was shown that AMPK directly phosphorylate Insig-1 at Thr222, which was confirmed by mutagenesis experimentation[146]. AMPK's regulation of Insig-1 is an attractive mechanism explaining AMPK's regulation of SREBP2 as reported previously, however this has yet to be completely addressed.

In recent years the carbohydrate response element binding protein (ChREBP) has emerged to be a main transcription factor for metabolic regulation at active sites for *de novo* lipogenesis such as the liver, WAT, and brown adipose tissue[147,148]. When glucose levels are

high, ChREBP undergoes multiple post-translational modifications that regulate its stability, enhances its nuclear localization, and enhances its transcriptional activity[149]. ChREBP contains a low glucose inhibitory domain and a glucose-response activation conserved element (GRACE) domain, the latter is activated by glucose metabolites[148]. When transcriptionally active within the nucleus, ChREBP recognizes carbohydrate response elements (ChoRE) motifs on target genes such as (but not limited to) L-pyruvate kinase (L-PK), FASN, ACC, SCD1, and SREBP1c (in response to insulin)[147]. Following its discovery, it was shown in hepatocytes overexpressed with ChREBP, AMPK activation led to suppressed L-PK transcription (ChREBP regulated). Additionally, AMPK was shown to phosphorylate ChREBP at Ser568 to inactivated the DNA binding activity of ChREBP, which could be reversed through single site mutagenesis (Ser568Ala)[150].

1.3.6 Fatty acid metabolism.

In low-energy conditions, peripheral tissue needs to sense and uptake circulating lipids for utilization as substrates for ATP production. When metabolic demands are high within tissue, AMPK stimulates the translocation of CD36 to the plasma membrane to facilitate the import of lipid substrates for energy metabolism stored within circulating lipoproteins[151–153]. In low energy conditions, AMPK shuts down energetically costly programs such as fatty acid synthesis, AMPK accomplishes this by providing an inhibitory phosphate group to both ACC1 (Ser79) and ACC2 (Ser212). ACC1 and ACC2 catalyze the carboxylation reaction of acetyl-CoA to malonyl-CoA, the rate-limiting reaction in FA synthesis.

The main difference between the two ACC isoforms is that ACC2 possesses a NH_2-terminal extension of 146 amino acids that allows it to be localized/retained within the mitochondria, where it resides in close proximation to the mitochondrial protein carnitine

palmitoyltransferase I (CPT1) [154,155]. CPT1 facilitates transport of fatty acids within the mitochondria to be used as substrates for oxidative phosphorylation (fatty acid oxidation). Malonyl-CoA is an allosteric negative regulator of CPT1, such that when malonyl-CoA pools are high CPT1 is inhibited and cannot facilitate the FA translocation into the mitochondrion. Interestingly, AMPK suppression of ACC2 reduces the available pool of malonyl-CoA and allows for CPT1 to shuttle FAs into mitochondria for ATP production by oxidation of FAs[156–158]. In highly metabolic tissues where lipid synthesis is dispensable (e.g. skeletal muscle), AMPK's regulation of ACC2 stimulates fatty acid oxidation (FAO) is a prominent mechanism by which it enhances energy production (ATP synthesis).

The whole-body physiological impact of AMPK's suppression of ACC1 and ACC2 was determined utilizing a double knock-in mouse that possessed alanine substitutes at Ser79 and Ser212 on ACC1 and ACC2, respectively (ACC-double knock-in; ACC-DKI). In reference to WT control animals, ACC-DKI animals had significantly higher hepatic ACC activity and *de novo* lipogenesis with accompanying reductions in palmitate oxidation. In skeletal muscle, a highly metabolic organ where lipid synthesis is dispensable, there was significantly larger amounts of malonyl-CoA produced and significantly reduced rate of FAO in comparison to WT control animals. Impaired glucose homeostasis and hepatic insulin sensitivity caused by consumption of a high fat diet was shown to be improved by the introduction of the anti-diabetic drug metformin (an indirect activator of AMPK; refer to **Appendix B**) within the diet within WT, but not ACC-DKI mice. Taken together, this illuminated the insulin sensitising effects of metformin were dependent on AMPK's regulation of ACC1 and ACC2 while additionally elaborating on the importance of AMPK-mediated FAO within the whole body[72].

1.3.7 Mitochondrial biogenesis.

The oxidation of lipids by the mitochondria is an essential method of ATP production within mammalian cells. To ensure normal rates of FAO, the cell must ensure adequate mitochondrial content to handle metabolic demands, especially within highly metabolic tissues like skeletal muscle. The majority of genes involved in mitochondrial metabolism are under the transcriptional control of Peroxisome proliferator-activated receptor gamma coactivator **1**-α (PGC-1α), with additional regulation by oestrogen-related receptors and a lesser extent by peroxisome proliferator-activated receptor family (PPAR)[158,159]. There is evidence that AMPK phosphorylates PGC-1α directly at Thr177 and Ser538 *in vitro*, however its unknown if this is physiologically relevant since it has not been shown *in vivo*[160].

Despite the uncertainty of direct regulation of PGC-1α by AMPK, numerous studies have shown that AMPK regulates mitochondrial biogenesis through a PGC-1α-dependent mechanism. AMPK's regulation of mitochondrial biogenesis has been preferentially explored in muscle by numerous studies[161–165], however AMPK has been shown to regulate mitochondrial content in adipocytes[166], macrophages[86], and liver[167]. The strongest mechanistic data illuminating AMPK's control of mitochondrial biogenesis was that AMPK directly phosphorylates PCG-1α, a crucial regulator of many aspects of mitochondrial homeostasis, at Thr177 and Ser538. Furthermore, they observed that the absence of PGC-1α, AMPK activation was not sufficient to induce transcript expression of Glucose transporter type 4 (GLUT4) and other mitochondrial and metabolic proteins[160].

1.3.8 Cholesterol synthesis.

Cholesterol is an important biological molecule that plays diverse roles within whole-body physiology and cellular homeostasis. Cholesterol is an amphiphilic molecule with a hydrophobic hydrocarbon body and a hydrophilic hydroxyl headgroup, allowing for interaction and integration within the plasma membranes within cells to regulate membrane fluidity/rigidity. Cholesterol is also an essential precursor for steroid-derived hormones, essential fat-soluble vitamins, isoprenoids, and bile acids[36,168]. Cholesterol requirements within mammals are met by two interconnected and highly regulated sources; dietary uptake and *de novo* synthesis. There is cross talk within cholesterol biosynthetic pathways and cholesterol absorption, such that influx of cholesterol through one pathway leads to inhibition of the alternative. Thus, when dietary cholesterol levels are insufficient to meet physiological needs *de novo* synthesis of cholesterol occurs to compensate. Cholesterol synthesis is a complicated process that requires 13 enzymes to catalyze numerous reactions where every carbon within the cholesterol molecule is derived from the precursor acetyl-CoA. The commitment step, or rate-limiting reaction, for cholesterol biosynthesis is catalyzed by HMGCR, where it reduces HMG-CoA to mevalonate an important intermediate species for both cholesterol and isoprenoid synthesis[168].

HMGCR and the mevalonate pathway are indispensable, such that genetic removal of HMGCR causes embryonic lethality at the blastocyst stage[169]. While statins are pharmacological inhibitors of HMGCR, AMPK is an endogenous regulator of HMGCR activity that provides inhibitory phosphorylation of HMGCR at Ser871[170]. To address the impact of AMPK-mediated suppression of HMGCR in physiology, we obtained and characterized mice possessing a Ser871Ala point mutation (HMGCR-KI). HMGCR-KI mice

were hypercholesterolemic, with enhanced *in vivo* hepatic cholesterol synthesis and had elevated levels of circulating and hepatic cholesterol (on a high carbohydrate diet). Removal of AMPK's whole-body regulation of HMGCR at Ser871 promoted hepatic steatosis and insulin resistance[171].

1.3.9 Cholesterol homeostasis.

Outside of its inhibition of cholesterol synthesis, AMPK has been shown to be important for macrophage and WB cholesterol homeostasis. Within J774.A1 cells (macrophage cell-line), it was initially shown that AMPK activation with AICAR was able to prevent oxLDL accumulation and LD density. AMPK activation with AICAR, metformin, and A769662 were all shown to increase protein expression of ABCG1, a critical protein in HDL-mediated cholesterol efflux. However, when a dominant-negative variant of AMPK (DN-AMPK) was present AICAR failed to increase ABCG1 protein expression likely indicating that AMPK is mediating ABGC1 protein expression in response to AICAR. Following this it was shown that AICAR is able to enhance cholesterol efflux to HDL in normal J774.A1 cells, but not cells expressing the dominant negative-AMPK variant[172].

Building on this study, we addressed AMPK's regulation of cholesterol efflux using primary bone-marrow derived macrophages (BMDMs) isolated from WT and AMPKβ1-knockout mice (AMPKβ1-KO). We observed in WT BMDMs treated with AMPK activators (A769662 and salicylate) had reduced total cholesterol content caused by acetylated low density lipoprotein (acLDL) incubation, where AMPKβ1-KO BMDMs had no change in total cholesterol content between control and AMPK-activated conditions[173]. Additionally, we have supported previous findings showing that AMPK activation in primary macrophages enhances transcript expression of ABCG1 and ABCA1. This result was confirmed functionally as we

observed basal expression was necessary for normal levels of cholesterol efflux to ApoA-I and HDL, but further stimulation of AMPK with A769662 and salicylate significantly increased efflux to each acceptor, an effect lost in AMPKβ1-KO macrophages[173]. Lastly, we evidenced the significance in WB physiology through an *in vivo* RCT assay where we observed that AMPKβ1-KO BMDMs had significantly less *in vivo* RCT described by less of the radioactive-cholesterol tracer present within the serum, liver, and feces[173]. Taken together these studies show that AMPK is implicated in multiple aspects of cholesterol homeostasis outside of HMGCR suppression, which plays an important role in macrophage and WB cholesterol homeostasis.

1.4 AMPK's role in Atherosclerosis.

1.4.1 Global AMPK expression in atherosclerosis:

It was shown that siRNA-mediated knockdown of AMPKα2 in cultured endothelial cells promoted the unfolded protein response, denoted by increased protein abundance of phosphorylation of protein kinase R (PKR)-like endoplasmic reticulum kinase, Eukaryotic translation initiation factor 2A, c-Jun N-terminal kinase, and increased abundance of X-box binding protein 1 (pPERK, pelF2α, and pJNK, and XBP-1, respectively), which is indicative of endoplasmic reticulum (ER) stress. Furthermore, within aortic endothelial cells isolated from AMPKα2-knockout mice (AMPKα2-KO), there was significantly higher levels of expression of ER stress markers pPERK, XBP-1, and Activating Transcription Factor 6 (ATF6). ER stress markers were restored to normal levels when AMPKα2-KO animals were transduced with a constituently active AMPK adenoviral construct (CA-AMPK)[174]. Following, these findings were investigated in the context of atherosclerosis by breeding AMPKα2-KO animals to an LDLr-KO background (AMPKα2/LDLr-DKO) and atherogenesis was assessed after 10-weeks of WD feeding. Animals lacking WB expression of AMPKα2 on an LDLr-KO background (AMPKα2/LDLr-DKO) were shown to develop significantly more atherosclerotic lesions within their aortic root. Additionally, lesions from AMPKα2/LDLr-DKO animals had enhanced levels of expression of the ER stress markers ATF6 and XBP-1[174].

Shortly after, the role of global expression of AMPKα2 and its therapeutic activation was assessed within the ApoE-KO model of atherosclerosis. Similar to the phenotype observed in AMPKα2/LDLr-DKO animals, AMPKα2/ApoE-DKO animals developed significantly more atherosclerosis within their aortic root than ApoE-KO control animals. Furthermore, the

AMPK activator, berberine, was shown to significantly reduce lesion development in ApoE-KO animals, but only had a trending protective effect in AMPKα2/ApoE-DKO animals[175]. Mechanistically, it was shown that berberine significantly reduced the expression of leukocyte adhesion proteins VCAM-1 and intercellular adhesion molecule 1 (1-CAM1) within developing lesions independent of AMPKα2 expression. Furthermore, they observed that berberine significantly increased mitochondrial uncoupling protein 2 (UCP2) protein abundance in an AMPKα2-dependent manner, leading to their *in vitro* characterization of improved mitochondrial biogenesis by berberine-mediated activation of AMPK within Human umbilical vein endothelial cell (HUVEC) cells[175].

1.4.2 Vascular AMPK and plaque stability:

Following their previous studies in AMPKα2 within atherosclerosis (see above), the Zou group looked to further elaborate the potential effects within vascular smooth muscle cells. They show that WD-fed AMPKα2/ApoE-DKO mice developed significantly more atherosclerosis within their aortic root compared to ApoE control animals. Additionally, lesions from AMPKα2/ApoE-DKO mice had a significantly larger necrotic and myeloid component and significantly reduced collagen levels and a smaller fibrous cap, all of which signifies reduced plaque stability present in animals lacking AMPKα2 expression[176]. To address if AMPKα2 in vascular smooth muscle cells (VSMC) were responsible for protection, they generated AMPK$^{SM\alpha2}$-KO animals by Cre recombinase (Cre) mediated deletion of the AMPKα2 floxed allele driven by the SM22 promoter, they bred this animal to ApoE-KO mouse to produce AMPK$^{SM\alpha2}$/ApoE-DKO animals for subsequent studies[176].

In reference to ApoE-KO control animals, AMPK$^{SM\alpha2}$/ApoE-DKO animals fed a WD developed significantly more atherosclerosis within their aortic root, accompanied by elevated

levels of lesion necrosis, less collagen content, and a smaller fibrous cap. Additionally, AMPK activation with Pravastatin did not effect lesion size, but it did lead to significantly reduced lesion necrosis, and enhanced collagen content and the presence of the fibrous cap in ApoE-KO animals, but not AMPK$^{SM\alpha2}$/ApoE-DKO animals[176]. Mechanistically this was explained by showing in cultured VSMCs, that siRNA-mediated knockdown of AMPKα2 induces a phenotypic switch in VSMCs, reducing the expression of (transcript and protein) of contractile proteins SM-α-actin and calponin while enhancing synthetic markers vimentin and osteopontin[176].

It was shown that in ApoE-KO mice lacking AMPKα1, but not AMPKα2, had significantly increased lesion calcification than ApoE-control mice, denoted by increased Alizarin red staining. In late atherosclerosis (24-week WD feeding), it was shown that ApoE-KO mice treated with the (indirect) AMPK activator, metformin, had significantly lower lesion calcification than untreated ApoE-KO mice. Furthermore, the protective effects against lesion calcification by metformin were only observed in ApoE-KO animals expressing AMPKα1[177]. In ApoE-KO animals, cell type specific double knockouts for AMPKα1 within smooth muscle cells (SMC) and myeloid cells (driven by Cre recombinase expression by the promoters SM22 and lysozyme, respectively) were generated to further investigate what cells are crucial for AMPKα1-mediated protection from lesion calcification. It was found that SMC AMPKα1, but not myeloid, was responsible for reducing lesion calcification by regulating runt-related transcription factor 2 (Runx2) expression, a key protein in osteoblast differentiation[177].

1.4.3 Myeloid AMPK in atherosclerosis:

Global expression of AMPKα2 in ApoE-KO mice (AMPKα2/ApoE-DKO) was shown to be atheroprotective[174,175], however whether this was a myeloid-specific effect was

undetermined. Generating AMPKα2 myeloid specific knockout on an ApoE-KO background (AMPK$^{M\Phi\alpha2}$/ApoE-DKO), it was observed that the level of DNA methylation on cytosine within cytosine-guanine dinucleotide islands was enhanced for vascular endothelial growth factor (VEGF) and matrix metalloproteinase 9 (MMP9) were enhanced in AMPK$^{M\Phi\alpha2}$/ApoE-DKO mice in reference to ApoE-KO control mice. These changes were accompanied by a slight skew to macrophage polarization to a pro-inflammatory M1 phenotype and significantly accelerated the progression of atherosclerosis[178]. An important consideration was that myeloid cells predominantly express the AMPKα1 isoform opposed to AMPKα2. The next steps to understand myeloid AMPK's role in atherogenesis came from addressing the role of myeloid expression of AMPKα1 and its possible contribution to atherogenesis. The first study with a primary focus on myeloid AMPKα1 within the progression of atherosclerosis used the Cre-mediated deletion driven by the lysozyme (LysM) promoter to generate AMPK$^{M\Phi\alpha1}$-KO mice, which were then crossed to LDL-KO mice producing AMPK$^{M\Phi\alpha1}$/LDLr-DKO animals. Following a 16-period of WD-feeding, it was observed that AMPK$^{M\Phi\alpha1}$/LDLr-DKO animals developed significantly more atherosclerosis within the aortic root compared to LDLr-KO control animals[179].

Inflammation promotes lesion development and enhances recruitment of myeloid and other immune cells, since its known that AMPK exhibits anti-inflammatory properties, the role of AMPK$^{M\Phi\alpha1}$ in regulation of inflammation during atherogenesis was a potential leading anti-atherogenic mechanism. Isolated macrophages from AMPK$^{M\Phi\alpha1}$/LDLr-DKO animals showed significant increased expression of pro-inflammatory genes TNF-α, interleukin 6 (IL-6), IL-1β, MCP-1, and inducible nitric oxide synthase (iNOS) when elicited with LPS or IFN-γ, in reference to LDLr-KO control mice. Furthermore, in macrophages isolated from the aorta,

AMPK$^{M\Phi\alpha1}$-deletion significantly increased the expression of pro-inflammatory proteins TNF-α, IL-1β, MCP-1, and NACHT, LRR and PYD domains-containing protein 3 (NLRP3; an inflammasome marker)[179]. In addition, it was shown both *in vivo* that AMPKMΦα1/LDLr-KO mice had increased levels of LY6C^{hi} monocyte within circulation, this led to enhanced migration to atherosclerotic regions. To drive this point home, they stained for the macrophage-like cell marker cluster of differentiation 68 (CD68) within the lesion, showing that AMPK$^{M\Phi\alpha1}$/LDLr-DKO animals had significantly larger macrophage-like cells within their lesions compared to LDLr-KO control animals[179].

Taken together, this study was the first to describe myeloid AMPKα1 having a protective effect against lesion development. Mechanistically, this was explained by dampening inflammation within the lesion microenvironment to reduce myeloid cell recruitment and transmigration into developing lesions. Additionally, the authors did observe a significantly higher proportion of total cholesterol (TC) and triglycerides (TG) within circulation within AMPK$^{M\Phi\alpha1}$/LDLr-DKO signifying that the regulation of circulating lipids may also be contributing to the phenotype observed[179].

Interestingly, the next study addressing at myeloid AMPKα1 within atherosclerosis yielded controversial and confounding data to what was been shown previously. The Zou group, who previously elaborated on AMPKα2 within the WB and VSMCs during atherosclerosis, generated AMPK$^{M\Phi\alpha1}$/ApoE-DKO mice to further elaborate on myeloid AMPKα1's role in atherogenesis[174,176]. Surprisingly, they found that AMPK$^{M\Phi\alpha1}$/ApoE-DKO animals developed significantly less atherosclerosis in comparison to ApoE-KO control animals. This was surprising since this was the first evidence describing a negative role for AMPKα1 in atherogenesis.

They investigated AMPK activity from THP-1 monocytes and shown that over time, incubation with pro-inflammatory macrophage colony-stimulating factor (M-CSF) significantly increased AMPK activity. Furthermore, inflammatory and atherogenic components (such as oxidized low density lipoprotein; oxLDL) increased AMPK activation by enhanced Thr172 phosphorylation[180]. In isolated peritoneal cells it was shown that there were significantly higher proportions of inflammatory LY6C^{hi} monocytes and reciprocally lower anti-inflammatory LY6C^{lo} monocytes isolated from AMPK$^{M\Phi\alpha1}$/ApoE-DKO animals in comparison to ApoE-KO control animals[180]. Furthermore, they shown that in isolated peritoneal cells from AMPK$^{M\Phi\alpha1}$-KO and AMPK$^{M\Phi\alpha1}$/ApoE-DKO mice had increased rates of apoptosis (assessed by positive Terminal deoxynucleotidyl transferase dUTP nick end labeling) and increased expression of apoptotic marker cleaved caspase-3. They lastly highlighted that within AMPK$^{M\Phi\alpha1}$/ApoE-DKO animals there was significantly reduced lesion myeloid component (less lesion F4/80 expression), and more apoptotic macrophages (CD68+TUNEL+ cells within lesions) in comparison to ApoE-KO control animals[180].

1.4.4 Systemic AMPK activation in atherosclerosis.

The potential for systemic AMPK activation to reduce atherosclerosis was first assessed using AICAR (which is metabolized to 5-aminoimidazole-4-carboxamide ribonucleotide an AMP analogue) in ApoE-KO mice. It was shown that in the J774.A1 macrophage cell line, treatment with AICAR enhanced cholesterol efflux to HDL, mechanistically explained by increasing ABCG1 transcript and protein expression[172]. Following these findings, they fed two cohorts of ApoE-KO mice a WD for 12 weeks, one group received daily systemic injections of AICAR and the other were subjected to a saline control. It was found that AICAR significantly reduced lesion generation[172], however there

was no genetic control to account for AMPK-specificity. Genetic controls are is important when using compounds such as AICAR since it is metabolized to ZMP, an AMP mimetic, that can regulate alternative AMP-binding enzymes. Shortly after, and mentioned previously above, investigations using berberine and the in ApoE-KO and AMPKα2/ApoE-DKO showing a protective effect against lesion development through modulating immune cell recruitment and mitochondrial dynamics within the lesion microenvironment[175].

Two back to back reports from the Zou group have illuminated many aspects of the therapeutic potential for systemic AMPK activation in atherosclerosis. Within their first study, multiple AMPK activators (A769662, AICAR, Metformin, and H007) were used to assess RCT, where it was found that when ApoE-KO mice were treated with an AMPK activator (A769662 and H007 performing the best) had significantly improved RCT to plasma, liver, or feces[181]. They attribute these effects to increased expression of ABCA1 and ABCG1, which aid in increasing cholesterol efflux to ApoA-I and HDL in PMACs under AMPK activated conditions[181]. Furthermore, in ApoE-KO animals fed a WD for 10 weeks, daily systemic injections of A769662, AICAR, Metformin, and H007, all protected against lesion development in the aortic sinus in reference to vehicle treated ApoE-KO control animals[181].

The Zou group followed immediately after with a study investigating the potential for metformin, AICAR, and A769662 to ameliorate atherosclerosis through modulation of myeloid cell inflammation and infiltration. In ApoE-KO animals, it was shown that systemic injections of metformin, AICAR, and A769662 all reduces total numbers of monocytes in circulation, as well as reducing the proportions of $LY6C^{hi}$ monocytes, with $LYC6^{lo}$ monocyte subsets being unaffected[182]. Reductions in inflammatory monocytes were also observed in the bone-marrow and spleen of ApoE-KO animals treated with AMPK activators, furthermore

AMPK activation lead to decreased CCR2 expression on monocytes. Lastly, they assessed atherogenesis in ApoE-KO mice following 12-weeks on a WD, receiving daily systemic injections of metformin, AICAR, or A769662. All AMPK activators significantly protected against lesion development within the aortic root. Following digestion of lesions and labeling of monocyte subsets, AICAR and A769662-treated animals were shown to have significantly reduced $LYC6^{hi}$ monocyte population within lesions[182].

1.5 Thesis Hypotheses and Objectives.

As outline above, we are beginning to understand the role that AMPK (in various cell types) is playing during the progression of atherosclerosis. However, due to conflicting data regarding myeloid AMPK has made its role within atherogenesis elusive at best. Despite this, its been shown in separate reports that therapeutic intervention of WD-fed ApoE-KO with various AMPK activators (including A769662) significantly protects against lesion generation. While most reports show a protective role for WB AMPKα2 and myeloid AMPKα1, there is evidence suggesting that both myeloid AMPKα1 and AMPKα2 participates in an athero-causative role within ApoE-KO mice. Based on previously published work and preliminary pilot studies, our overarching **hypothesis** is that myeloid AMPK-signaling and pharmacological activation play protective roles against the progression of atherosclerosis. We sought out to test this hypothesis with three **objectives:**

(1) Elucidate the role of modified LDL variants in modulating macrophage AMPK activity and its down stream consequences on lysosomal homeostasis.

(2) Determine if myeloid AMPK and its pharmacological activation protects against the progression of atherosclerosis.

(3) Illuminate whether AMPK's suppression of endogenous cholesterol synthesis protects against the development of atherosclerosis.

2.0 CHAPTER 1 – The regulation of BMDM AMPK by modified LDL variants and its implications on lysosomal homeostasis.

2.1 Study Rationale:

Within macrophages, the lysosome plays a crucial role in regulating and maintaining cholesterol homeostasis during atherosclerosis. Impaired or defective lysosomal programs (caused by pharmacological agents or genetic manipulation) have shed light on the importance of normal lysosomal homeostasis for excess cholesterol removal in culture and *in vivo* RCT[32]. Despite being crucial for maintenance of cholesterol homeostasis, it has been shown in cultured macrophages that atherogenic lipids (oxLDL and cholesterol crystals) perturb lysosome function[183]. Additionally, atherogenic lipids also induce the expression and nuclear enrichment of TFEB, a transcriptional factor responsible for regulating genes important within lysosomal biosynthesis and autophagy. This disconnect allowed for postulation that atherogenic lipids may be detrimental to lysosomal function and longevity but may induce a compensatory mechanism through TFEB regulation.

AMPK's regulation of lysosomal programs has been of particular interest, with evidence showing that it is capable to regulate TFEB-mediated lysosomal and autophagy responses[137,140,136]. Despite the growing role for AMPK in regulating autophagy, there has been little work done to address AMPK's possible role in regulating expression of proteins within the pathway. It has been observed that culturing macrophages with oxLDL leads to increased Thr172 phosphorylation on AMPK, indictive of increased activity[180]. Additionally, its known that the scavenger receptor responsible for oxLDL uptake, CD36, participates in a signaling axis with AMPK, where AMPK bridges the link between lipid uptake to downstream use of lipids via FAO[184]. We speculated that modified LDL uptake may be altering AMPK signaling

that could lead to downstream alterations on lysosomal homeostasis. Therefore, we **hypothesized** that modified LDL variants, agLDL and oxLDL, mediate induction of lysosomal biogenesis through regulation of AMPK. Additionally, we speculate that modified LDL variants, agLDL and oxLDL, induce ER stress and are affecting ionic calcium homeostasis that then mediate AMPK activation through CaMKKβ-mediated signaling.

2.2 RESULTS:

2.2.1 Modified LDL variants, agLDL and oxLDL, enhances AMPK-specific signaling.

It was observed that incubation of THP-1 monocytes within oxLDL increased AMPK phosphorylation at Thr172[180]. We sought out to address if modified LDL variants, agLDL and oxLDL, participated in regulation of AMPK within our BMDM model. Culturing BMDM with either agLDL or oxLDL for 18 h led to an increase in phosphorylation of ACC at Ser79, an AMPK specific regulatory site (Figure 1). We observed that 18 h incubation with agLDL (Figure 1A) and oxLDL (Figure 1B) enhanced AMPK signaling by approximately 2- and 5-fold, respectively. We observed that neither agLDL or oxLDL enhanced AMPK signaling on par with pharmacological activation of AMPK with A769662.

2.2.2 Modified LDL variants, agLDL and oxLDL, activate BMDM AMPK partially through the CaMKKβ1/Ca^{2+} pathway.

The ER is responsible for the maintenance of ionic calcium homeostasis within the cell. ER stress initiators cause the release of ionic calcium from the ER into the cytoplasm[185]. Modified LDL variants have been shown to induce ER stress in endothelial cells that are relevant within atherogenesis[186,187], furthermore ER stress promotes pro-atherogenic programs in multiple cell types involved in lesion formation[188,189]. We speculated that excess FC from modified LDL variants trigger ER stress, altering calcium homeostasis resulting in CaMKKβ-mediated activation of AMPK. We sought to test whether CaMKKβ signaling was implicated in agLDL and oxLDL-mediated activation of AMPK.

To delve deeper into potential mechanisms and important steps within this suggested pathway, we sought to address if inhibiting cholesterol trafficking from the lysosome

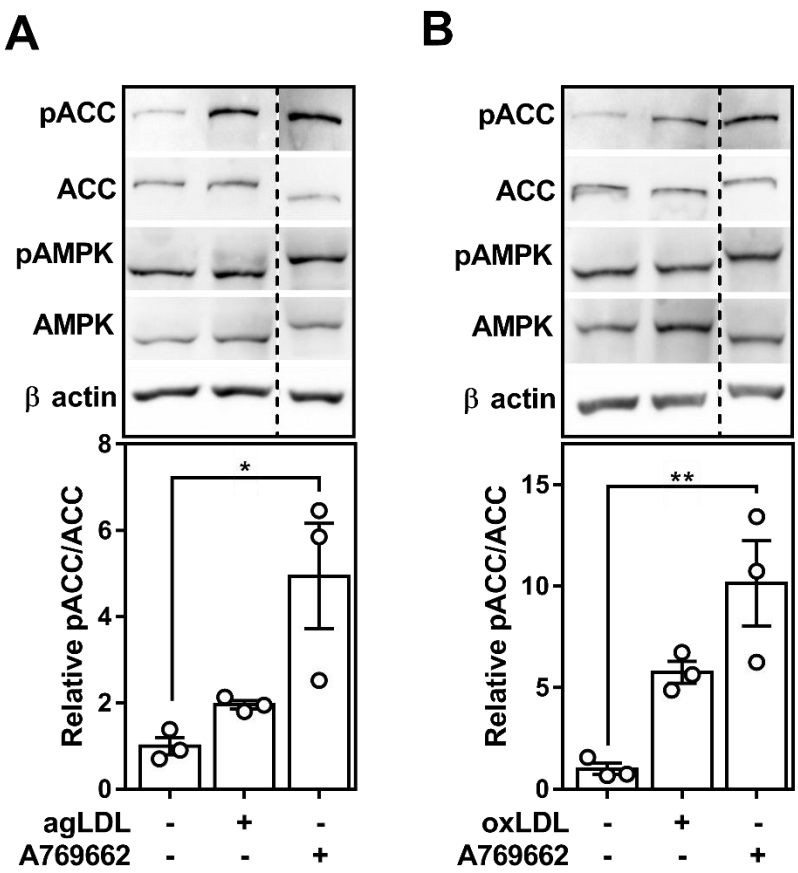

Figure 1. Modified LDL variants, agLDL and oxLDL, augment AMPK-specific signaling in BMDM. (A and B) BMDM were isolated from WT mice, then incubated for 18 h with either agLDL (A; 50 µg/mL), oxLDL (B; 50 µg/mL), or A769662 (100 µM) as a positive control for AMPK activation. Black doted line represents where the immunoblot was cropped to produce the representative image. Datum is representative of 3 independent experiments from BMDMs isolated from WT mice. Datum is reported as the mean value ± SEM, where *P<0.05 and **P<0.005 was calculated by a one-way ANOVA using Prism8 software.

(U18666A; NPC1 inhibitor), ER calcium release (Ryanodine), oxidative stress (BHA), or CaMKKβ directly (STO-609) could negate the effects of agLDL and oxLDL on AMPK activation. Incubating WT BMDMs with agLDL increased AMPK-mediated signaling to ACC at Ser79, which was accompanied with increased expression of the ER stress marker IREα (Figure 2A and 2C). We observed that co-incubating BMDM with agLDL with STO-609, U18666A, and Ryanodine reduced AMPK-specific signaling to ACC, however it remained elevated in reference to basal conditions (Figure 2B). A similar but less pronounce trend was observed within oxLDL-treated BMDM, where in CaMKKβ, NPC1, or Ryanodine-inhibited conditions reduced oxLDL potential to enhance AMPK signaling to ACC (Figure 2C and 2D). Additionally, inhibiting the generation of ROS (oxidative stress) was observed to reduce oxLDL, but not agLDL, ability to increase AMPK signaling (Figure 2C and 2D). Taken together, this datum suggests that the CaMKKβ/Ca^{2+} pathway participates in agLDL and oxLDL-mediated activation of AMPK, however it is not exclusively responsible.

Following our observations that both agLDL and oxLDL enhance AMPK-mediated signaling to ACC, which was partially attributed to CaMKKβ-signalling, we then wanted to assess LKB1's potential contribution. LKB1 activates AMPK in response to a shift in adenine nucleotide concentrations, such that when AMP: ATP ratio is elevated AMPK undergoes a conformational change and becomes a substrate for LKB1. We measured AMP and ATP in cultured WT BMDMs incubated with agLDL and oxLDL to interrogate if there are any shifts in the AMP: ATP ratio. Both agLDL and oxLDL provided a slight trending increase in AMP: ATP ratios measured by high performance liquid chromatography (HPLC), supporting a possible mechanistic role for LKB1-mediated activation (Figure 3).

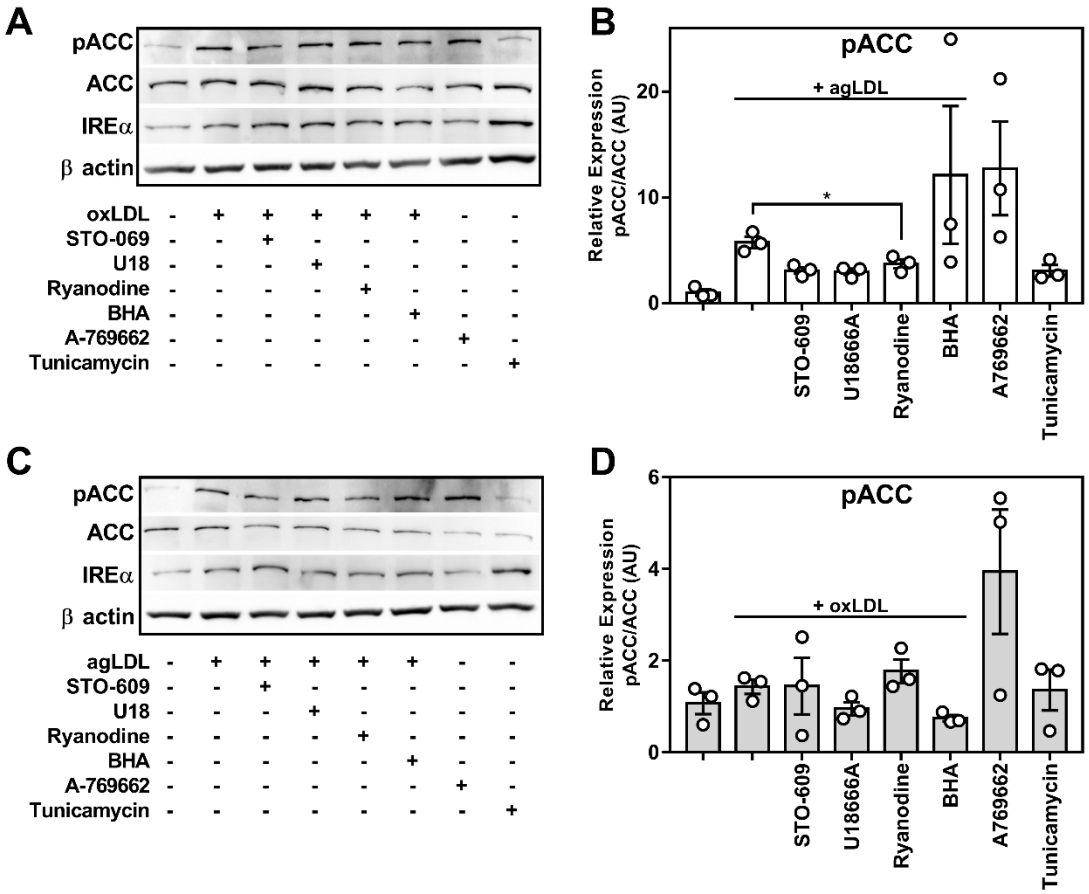

Figure 2. The CaMKKβ/Ca^{2+} pathway is partially involved in regulating AMPK activity in response to agLDL and oxLDL in BMDM. (A-D) BMDM were isolated from WT mice, then incubated with either (A and B; 50 µg/mL) or oxLDL (C and D; 50 µg/mL), ± chemical inhibitors for CaMKKβ (STO-609; 20µM), NPC1 (U18666A; 1 µM), ER calcium release (Ryanodine; 10 µM), or oxidative stress (BHA; 100 µM). BMDM were incubated with A769662 (100 µM) and Tunicamycin (2.5 µg/mL) were used as a positive control for AMPK activation and ER stress induction, respectively. Quantifications for agLDL (C) and oxLDL (D) signaling were completed from immunoblots from each independent experiment. Datum is representative of 3 independent experiments from BMDMs isolated from WT mice. Datum is reported as the mean value ± SEM, where *P<0.05 calculated by a one-way ANOVA using Prism8 software. Datum is representative of 3 independent experiments from BMDMs isolated from WT mice. (B and D) Datum is reported as the mean value ± SEM, where *P<0.05 was calculated by a one-way ANOVA using Prism8 software.

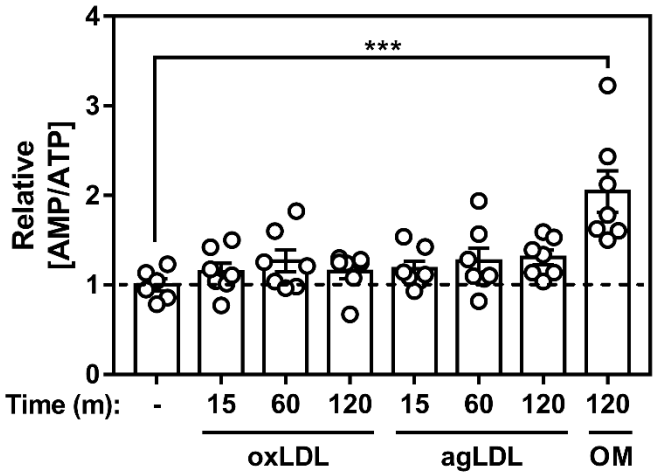

Figure 3. Acute incubation with agLDL or oxLDL shifts cellular energy levels in BMDM. BMDM were cultured in the presence of agLDL (50 µg/mL), oxLDL (50 µg/mL), or oligomycin (5 µM) as a positive control for increase AMP: ATP ratios. BMDM were incubated within each respective treatment as indicated above. AMP and ATP from cellular extracts were measured by high performance liquid chromatography. Datum is representative of 7 independent experiments from BMDMs isolated from WT mice. Datum is reported as the mean value ± SEM, where ***P<0.001 was calculated by a one-way ANOVA using Prism8 software.

2.2.3 CD36 links oxLDL uptake to AMPK-mediated autophagy initiation.

In the context of atherosclerosis, the scavenger receptor CD36 plays a pivotal role through recognition and unregulated uptake of modified LDL such as oxLDL[27]. In addition it has been shown that AMPK and CD36 participate in shared signaling axis[153,190], we speculated that CD36-mediated uptake is an early event for oxLDL regulation of lysosomal programs and AMPK activity. We incubated BMDMs from WT ($CD36^{+/+}$) or mice lacking one allele for CD36 ($CD36^{-/+}$) with oxLDL and assessed phospho-signaling to ULK1 at the AMPK specific residue Ser555 (Figure 4A). We observed an increase of signaling to ULK1 at Ser555 in WT BMDMs, however this was blunted in CD36-/+ BMDM (Figure 4B). This datum suggests that both CD36 and AMPK are involved in oxLDL-mediated induction of autophagy within BMDM.

2.2.4 BMDM isolated from AMPKβ1-KO mice show signs of perturbed lysosomal function.

With more insight into AMPK's regulation of autophagic and lysosomal pathways, we wanted to address if basal AMPK expression in macrophages is implicated in specific lysosomal parameters. To assess total cellular acidity, we stained WT and AMPKβ1-KO macrophages with a dye that fluoresces at an acidic pH. We observed a significant decrease in fluorescence in AMPKβ1-KO macrophages, which is indicative of a more neutral pH corresponding to less acidic compartments within the cell (Figure 5A). Assessing total cellular pH is suggestive of the lysosomal content; however, there are acidic compartments such as late endosomes that may be contributing to the result. Following, we assessed the lysosomal processing of DQ-ovalbumin, a quenched fluorescent probe that when catabolized at the lysosome emits fluorescence. Albeit not reaching statistical significance, there was a trending

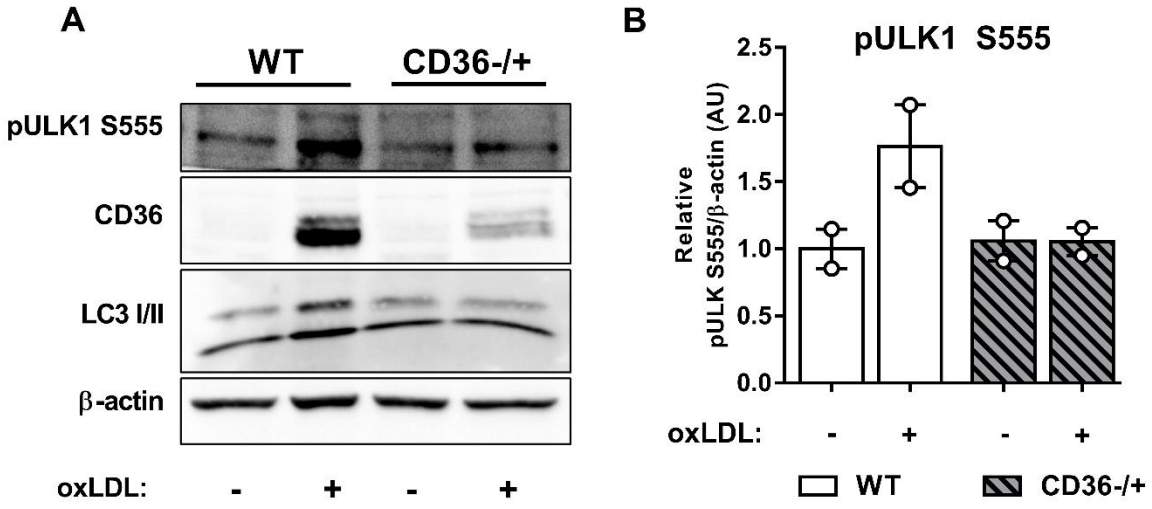

Figure 4. AMPK links CD36-mediated uptake of oxLDL to early signaling events in autophagy initiation. (A and B) BMDM isolated from WT or $CD36^{-/+}$ mice were incubated with oxLDL (50 µg/mL) for 24 h. Regulation of autophagy assessed by AMPK-specific signaling to ULK1 at Ser555 (B) and lipidation of LC3 was used as a general measure of autophagic flux. (A and B) Datum is representative of 2 independent experiments from BMDMs isolated from WT and $CD36^{-/+}$ heterozygote knockout mice. Datum is representative of 2 independent experiments from BMDMs isolated from WT mice. Datum is reported as the mean value ± SEM, results were analyzed by a one-way ANOVA using Prism8 software and found unsignificant.

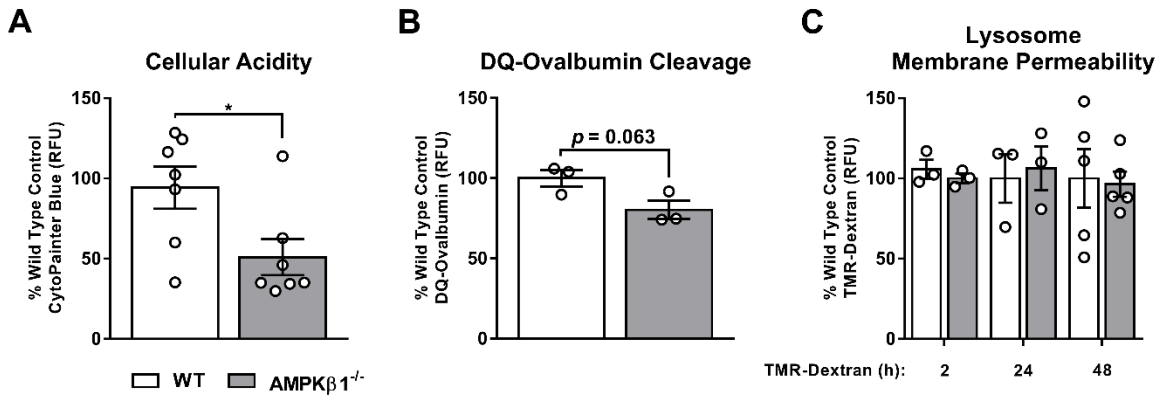

Figure 5. AMPKβ1-KO BMDM show signs of perturbed parameters associated with lysosomal dysfunction. BMDM isolated from WT and AMPKβ1-KO mice were stained and assessed for (A) Cellular pH, (B) Lysosomal DQ-ovalbumin cleavage, and (C) membrane permeability. (A) Cellular acidity was measured by incubating WT and AMPKβ1-KO macrophages with CytoPainter blue working reagent at a 10% dilution (v/v) for 30 minutes prior to analysis by flow cytometry. (B) Lysosomal DQ-ovalbumin cleavage was assessed by incubating WT and AMPKβ1-KO macrophages with 10 µg/mL DQ-ovalbumin for 2 h prior to analysis by flow cytometry. (C) Lysosomal membrane permeability was assessed by incubating WT and AMPKβ1-KO macrophages with 10000 MW tetramethylrhodamine-conjugated dextran (25 µg/mL) prior to analysis by flow cytometry. Datum is representative of 3-7 independent experiments from BMDMs isolated from separate WT and AMPKβ1-KO mice. Datum is reported as the mean value ± SEM, where *P<0.05 was calculated by a student's t test using Prism8 software.

effect for a decrease in lysosomal processing of DQ-ovalbumin (p = 0.063) in AMPKβ1-KO BMDM (Figure 5B). We also probed into lysosomal membrane permeability assessing the release of TMR-Dextran from the lysosome, however AMPK expression did not alter lysosomal membrane permeability at the time points assessed (Figure 5C).

2.2.5 BMDM AMPK regulates signaling events within autophagy and TFEB's nuclear enrichment.

Autophagy is a tightly controlled process with numerous levels of regulation for signaling within the pathway along with the biogenesis of enzymes and substrates involved. It has been established that AMPK and its metabolic antagonist mTORC1 signal through autophagy at various stages. A key protein in autophagy initiation, ULK1, has been shown to be regulated by phosphorylation by AMPK and its metabolic antagonist mTORC1 at several serine residues[97,118]. At this point in time regulation of ULK1 by phosphorylation is not completely understood, however there have been several serine residues phosphorylated by AMPK (Ser317, Ser555, and Ser757) and mTORC1 (Ser757) characterized for their positive and negative effects on autophagy initiation, respectively[97,118].

We confirm that in BMDM, A769662 the small molecule direct activator of AMPK increases signaling to ULK1 at Ser555 in basal conditions and when autophagy is chemically disrupted by chloroquine (Figure 6). Interesting, we observe that there seemed to be a trending decrease in protein expression in proteins involved in autophagy in AMPKβ1-KO BMDM (Figure 6). Regulation of proteins within autophagy is tightly controlled by TFEB, thus we investigated whether acute AMPK activation can influence TFEB activity. In WT BMDM, we observed that acute pharmacological activation of AMPK with A769662 significantly increased the co-localization of fluorescently labeled TFEB with the nuclear stain DAPI

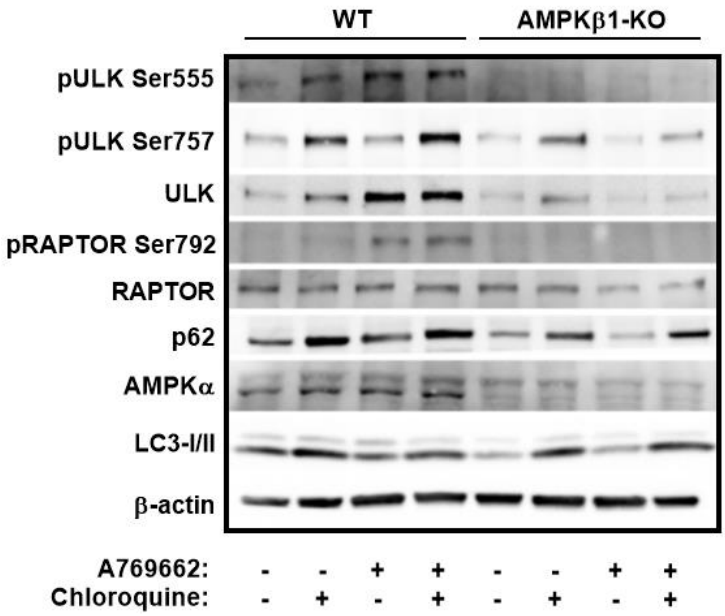

Figure 6. Activation of BMDM AMPK regulates signaling events within the autophagy pathway. Immunoblot is representative of 4 independent experiments from BMDMs isolated from WT and AMPKβ1-KO mice, where a 5 h incubation with A769662 (100 μM) and Chloroquine (50 μM) were used to pharmacologically activate AMPK and inhibit autophagy, respectively.

(Figure 7B). We observed that TFEB's nuclear localization was unresponsive to A769662 in AMPKβ1-KO BMDM compared to untreated conditions (Figure 7A).

2.2.6 BMDM AMPK expression and pharmacological activation regulates expression of key enzymes within autophagy.

To further explore AMPK's role in the synthesis of autophagic machinery, we investigated AMPK's regulation of transcript expression of *Tfeb* (Figure 8A) and TFEB-regulated downstream effector genes (Figure 8B-D). We observe a trending decrease in transcript expression of *Tfeb* and TFEB-regulated genes under basal conditions between WT and AMPKβ1-KO BMDMs. Under AMPK-activated conditions, a significant increase in transcript expression for *Tfeb* and TFEB-regulated genes was observed in WT BMDMs while AMPKβ1-KO macrophages were unresponsive (Figure 8A-D). To confirm these results on a translational level, we treated WT and AMPKβ1-KO BMDM with A769662 for 24 hour and assessed protein expression of TFEB-regulated proteins, ULK1 and Beclin-1. In BMDM isolated from WT mice, we observed that A769662 significantly increased the expression of ULK1 and Beclin-1, an effect lost in AMPKβ1-KO BMDM (Figure 8E-G). Additionally, there was a significant reduction in basal expression in AMPKβ1-KO BMDM in reference to WT control cells (Figure 8F-G). This suggests that basal AMPK expression and its subsequent activation both play an important role in regulating the synthesis of TFEB-regulated proteins important for autophagy.

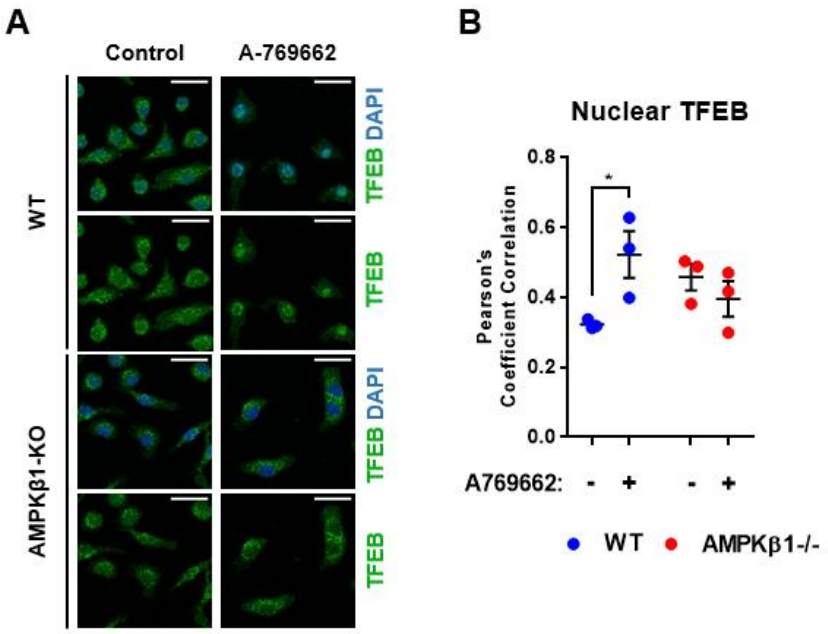

Figure 7. Acute pharmacological activation of BMDM AMPK induces the nuclear localization of TFEB. WT and AMPKβ1-KO BMDM and incubated with A769662 (100 μM) for 2 h. (A) Representative Z-projection for maximum intensity immunofluorescent image showing AMPK-activation leads to TFEB (Green) localization to the nucleus (Blue). (B) Pearson's coefficient correlation for the co-localization of TFEB and DAPI across the entire Z-stack images, where 1 represents 100% co-localization and 0 represents 100% no co-localization. (A and B) Datum is representative of 3 independent experiments from BMDMs isolated from separate WT and AMPKβ1-KO mice. Datum is reported as the mean value ± SEM, where *P<0.05 was calculated by a two-way ANOVA using Prism8 software.

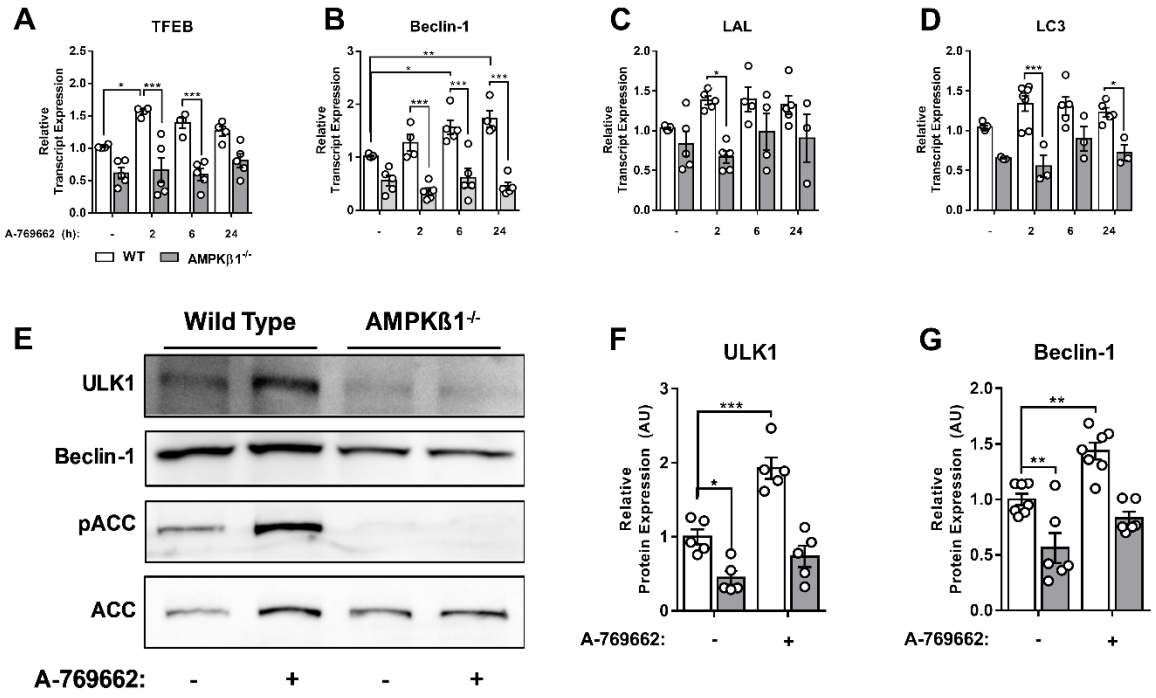

Figure 8. AMPK regulates the transcript and protein expression of TFEB and TFEB-regulated genes important for lysosomal homeostasis and autophagy. (A-D) The effect of basal AMPK expression and its pharmacological activation on relative transcript expression for (a) *Tfeb* and TFEB-regulated (B) *Becn1*, (C) *Lipa*, and (D) *Map1lc3b*, relative to WT control. (E) Representative immunoblot depicting ULK1 and Beclin-1 protein content is regulated by AMPK expression and its pharmacological activation. (F and G) Quantification of all corresponding immunoblots for (F) ULK1 and (G) Beclin-1. A769662 (100 μM) was used as an AMPK activator for all experiments, where incubation time is listed above (A-D) or 24 h (E-G). Datum is representative of 3-7 independent experiments from BMDMs isolated from separate WT and AMPKβ1-KO mice. Datum is reported as the mean value ± SEM, where *P<0.05, **P<0.005, and ***P<0.001 was calculated by a two-way ANOVA using Prism8 software.

2.2.7 Modified LDL variants, agLDL and oxLDL, uncouple AMPK from TFEB-regulated transcriptional responses in BMDM.

It was observed in peritoneal macrophages isolated from thioglycolate-elicited mice, that culturing with oxLDL for 3 and 12 h increased the transcription of TFEB-regulated genes within autophagy and lysosomal biogenesis[183]. We sought out to address if a similar effect occurred within our BMDM model, and if this transcriptional response was dependent on AMPK. Using BMDMs as our source of isolated primary macrophages, we incubated WT and AMPKβ1-KO cells with agLDL or oxLDL for 3-12 hours, then assed transcript expression of TFEB and two downstream effector genes (Figure 9). To date, there has been no study addressing agLDL's role in regulating lysosomal homeostasis, however we speculated that it may exhibit regulatory effects as previous observed for oxLDL in peritoneal macrophages[183].

Contrary to our original predictions, we observed no induction of transcript expression for *Tfeb, Becn1*, or *Lipa* by agLDL (Figure 9A-C). In addition, we observed no increase in transcript expression for *Tfeb, Becn1*, and *Lipa* induced by oxLDL (Figure 9E-F) as reported earlier in peritoneal macrophages. This suggests that modified LDL variants, agLDL and oxLDL, are modulating macrophages gene expression within quiescent and lipid-loaded macrophages differentially.

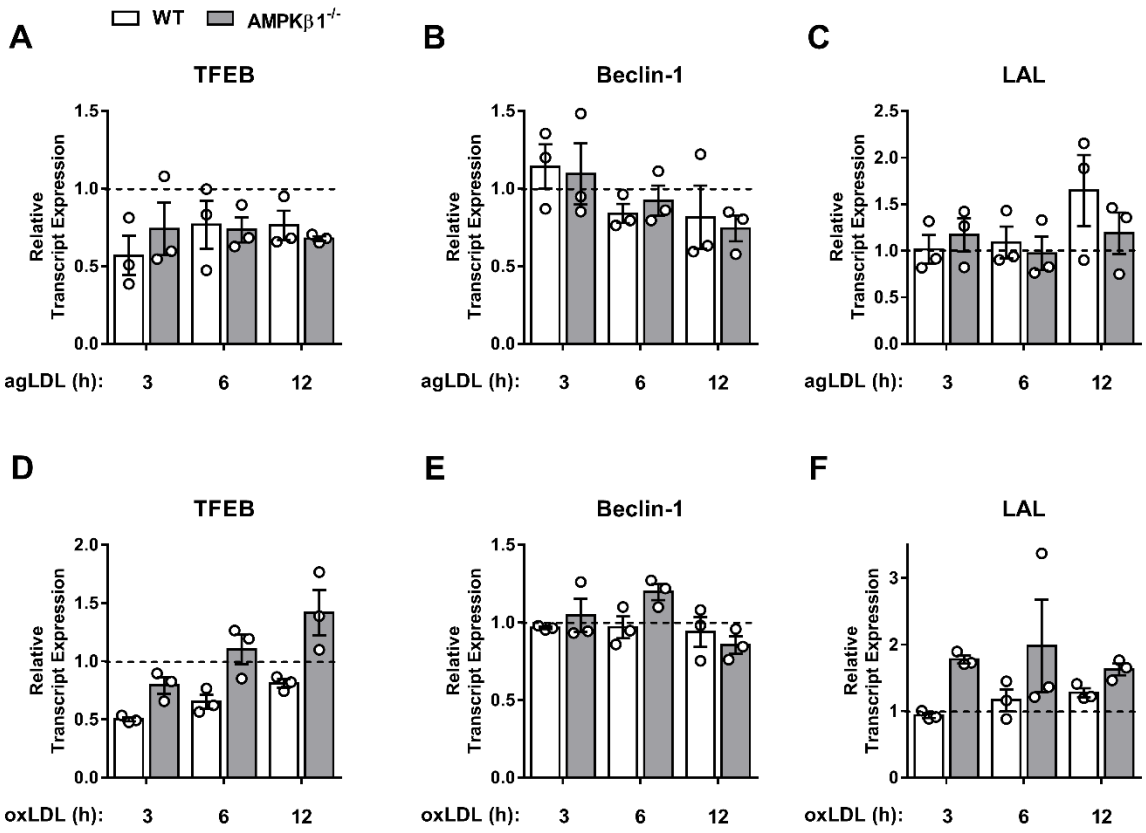

Figure 9. Modified LDL variants, agLDL and oxLDL, do not modulate TFEB or downstream effector genes through AMPK in BMDMs. (A-C) Relative transcript analysis for agLDL's effect on BMDM transcription of (A) *Tfeb*, (B) *Becn1*, and (c) *Lipa*, relative to untreated WT BMDM control. (D-F) Relative transcript analysis of oxLDL's effect on BMDM transcription of (D) *Tfeb*, (E) *Becn1*, and (f) *Lipa*, relative to untreated WT BMDM control. BMDM isolated from mice were cultured with either agLDL (A-C; 50 µg/mL) or oxLDL (D-F; 50 µg/mL) for time points indicated above. Datum is representative of 3 independent experiments from BMDMs isolated from separate WT and AMPKβ1-KO mice. Datum is reported as the mean value ± SEM, where statistical significance was not found through a two-way ANOVA using Prism8 software.

2.3 DISCUSSION:

The unregulated uptake and retention of cholesterol-rich modified lipoproteins is a hallmark of atherogenesis[31,191,192]. Despite this, many of the molecular events caused by modified LDL have yet to be elucidated. Within this study it was our objective to elucidate if modified lipoproteins, agLDL and oxLDL, had a regulatory role within AMPK signaling and if so, the potential mechanism(s) and consequences. Within our BMDM model, we illuminated that various physiological modified LDL variants enhanced AMPK-specific signaling to ACC, which was partially attributed to CaMKKβ signaling and potentially in a CD36 dependent manner. However, the maintenance of lysosomal and autophagic transcriptional pathways (TFEB-regulated processes) accomplished by AMPK was diminished in response to agLDL and oxLDL incubation.

Within the human THP-1 monocyte cell line, AMPK signaling is required for normal monocyte-to-macrophage differentiation[180]. In response to various atherogenic stimuli, including oxLDL treatment, an increase in AMPK activation was observed in THP-1 cells[180]. To our knowledge, this was the first evidence showing a role for oxLDL in the regulation of AMPK activity, which can occur from glucose deprivation (lysosomal activation), adenine nucleotide fluctuations (AMP/ADP binding to the γ-subunit of AMPK), and/or intracellular ionic calcium release (mediated by CaMKKβ)[71,75–77]. It has been observed that oxLDL potentiates ER stress, a process linker to alterations in cytosolic calcium flux[185–187], we predicted that CaMKKβ may be responsible for activation of AMPK in response to agLDL and oxLDL. We observed that in CaMKKβ-inhibited conditions, agLDL and oxLDL exhibited a blunted response in enhancing AMPK signaling. Despite this, AMPK signaling remained

elevated in reference to untreated cells, which is suggestive that CaMKKβ is not the only factor involved these pathways.

Glucose deprivation leads to alterations in energy fluctuations reflected by AMP: ADP: ATP ratios. Incubations with atherogenic lipoproteins trended towards an increased AMP: ATP ratio (Figure 3). The activity of the upstream kinase LKB1 has been described as constituently active, making its activation of AMPK a function of nucleotide binding and AMPK conformation. The recent discovery of the LKB1-AMPK-AXIN lysosomal pathway brings to light whether localization/interaction of these components is important, which will be important to address in future studies. Finally, it is well known that binding of the allosteric drug and metabolite (ADaM) site of the β-subunit by engineered pharmaceuticals allosterically activates AMPK[193]. Interestingly, it has recently been shown that long-chain fatty acyl-CoA esters bind AMPK's ADaM site and induce conformation activation independent of Thr172 phosphorylation on AMPK[194]. This will be important to consider for future studies since it is plausible that modified LDL variants are carrying long-chain fatty acyl-CoA esters that may be partially responsible for enhancing AMPK signaling (independent of CaMKKβ and LKB1).

Our understanding of AMPK's role in AMPK-specific signaling in autophagy is continually expanding. While most studies address AMPK's signaling through autophagy by phosphorylation of multiple substrates, implication of AMPK in regulation of transcriptional responses in autophagy is beginning to emerge[136,139]. TFEB, a master regulator of lysosomal and autophagic programs, has been shown to be subjected to regulation by AMPK through different mechanisms[136,138,139]. Our data suggests that AMPK signaling is required in murine BMDMs for maintenance of normal transcriptional and cellular control of lysosomal programs (Figure 5). To date, the discovery of AMPK signaling to ULK1 has largely overshadowed the

potential of AMPK regulation of transcriptional control of ULK1, with little focus on the potential for ULK1 transcriptional regulation in response to AMPK signaling. Our study corroborates recent work depicting within THP-1 monocytes[180], where protein levels of ULK1 are significantly reduced in BMDM deficient of AMPK. However, to our knowledge, we show the first evidence (in BMDMs) that pharmacological activation of AMPK (via A769662) results in upregulation of ULK1 (and Beclin-1) protein levels (Figure 8). Additionally, acute activation of AMPK by A769662 significant increased TFEB's co-localization with the nucleus (Figure 7), and up-regulation of TFEB-regulated transcriptional responses (Figure 8). With the potential for modified LDL variants to mediate AMPK signaling, which in turn can influence TFEB-regulated pathways, it could be possible that AMPK is mediating a compensatory induction of lysosomal biogenesis by modified LDL variants as reported by others[183].

We predicted that modified LDL variants, agLDL and oxLDL, would regulate transcriptional expression of lysosomal-associated genes through AMPK activation. However, our results were complicated by the fact that neither agLDL nor oxLDL had any effect on TFEB-associated transcript expression in WT BMDMs (Figure 9), which had been shown previously (by oxLDL)[183]. Additionally, and in contrast to basal treatment without modified LDL variants, the expression level observed for TFEB within AMPKβ1-KO cells treated with oxLDL were at times the opposite (Figure 9). Several factors such as differences in batch-to-batch preparations, technical/experimental variations in preparing of oxLDL (also in-house preparation vs. commercial suppliers), and the level of oxidation for oxLDL (minimally oxidized verses highly oxidized) all could be contributing in the experimental differences we observe compared to what has been published[183]. However, the type of macrophages presents

the biggest discrepancy between our and published results. Thioglycolate-elicited peritoneal macrophages are a heterogenous population of infiltrating monocyte-derived macrophages, which are considered much more activated in comparison to the homogenous quiescent population of BMDM. The regulatory differences between these two macrophage populations may result in discrepancies between metabolic and inflammatory characteristics and could provide an explanation for altered responses when incubated with modified LDL variants. Future work using both macrophage models isolated from WT and AMPKβ1-KO mice would be insightful.

We highlight that physiological modified lipoproteins enhance macrophage AMPK signaling partially through CaMMKβ signaling. The expression and activation of macrophage AMPK is implicated in upregulation of lysosomal and autophagic pathways, responses were blunted in macrophages devoid of AMPK expression (Figure 6). Although endogenous AMPK signaling was implicated in multiple aspects of lysosomal homeostasis, in the presence of modified LDL variants, agLDL and oxLDL, AMPK signaling was not sufficient to augment TFEB-regulated transcriptional programs. In the context of initiating and established atherosclerosis, there could exist a futile regulatory cycle, whereby plaque-resident macrophages are relentlessly exposed to atherogenic stimuli that have the capacity to activate AMPK-TFEB regulatory programs. However, the beneficial effects from acute AMPK activation, including induction of autophagy and lysosomal programs are not involved.

2.4 MATERIAL AND METHODS:

Animal Studies: All experiments conducted were in accordance with the Canadian Council of Animal Care and approved by the Animal Care Committee at the University of Ottawa. All mice were housed in ventilated cages at ~23 °C and maintained on a 12/12 h light-dark cycle with *ad libitum* access to a standard rodent chow (44.2% carbohydrates, 6.2% fat, and 18.6% crude protein; diet T.2018, Harlan Teklad).

Isolation and culturing BMDMs: Mice were anesthetized with ketamine (150 mg/kg) and xylazine (10 mg/kg), then euthanized by cervical dislocation. Both hind legs were carefully degloved then each leg was surgically removed from the mouse with precision to ensure the femur and tibia remained completely intact. The surrounding musculature was carefully excised, ligaments connecting the tibia to the femur were then gently cut allowing for ease for bone separation. Once the tibia and femur were completely isolated and devoid of muscle the distal ends of each bone were carefully cut, the tibia and femur were placed a sterile 0.5 mL tube (Thermo Fisher Scientific) containing a hole punctured at the bottom with 18-gauge needle at the bottom of the microfuge tube. The 0.5 mL tube (containing one tibia and one femur) was placed in a sterile 1.5 mL microfuge tube (Thermo Fisher Scientific) containing 100 µL of culture media; Dulbecco's modified Eagle's medium (Wisent) supplemented with 10% FBS (Wisent) and 1% antibiotics (HyClone Penicillin-Streptomycin Solution – Thermo Fisher Scientific). Bone-containing tubes were then centrifuged on a benchtop microcentrifuge at 4000 RPM for 5 min. The 0.5 mL tube containing the femur and tibia (now devoid of bone-marrow) were discarded, then 900 µL of culture media was added to each tube containing the bone marrow pellet. Bone-marrow pellets were gently re-suspended within the 1 mL culture media with gentle pipetting. A sterile 40 µm cell strainer (Thermo Fisher Scientific) was placed

onto a sterile 50 mL conical tube containing 24 mL culture media, suspended bone-marrow samples were gently passed through the cell strainer. An additional 25 mL culture media was passed through the cell strainer into the diluted bone-marrow sample. The diluted bone-marrow samples were then added to a T175 flask (Thermo Fisher Scientific) containing 77.5 mL culture media, flasks were then incubated in a humidified 5% CO_2 incubator at 37ºC for 4 hours. Following, T175 flasks were removed and 22.5 mL of L929-conditioned culture media was added (final volume: 150 mL with 15% L929-conditioned media) as a source of M-CSF to induce macrophage differentiation from hematopoietic stem cells. The sample was mixed thoroughly. Bone-marrow cells were plated within five 150 mm tissue culture plates (25 mL/plate) then incubated in a humidified 5% CO_2 incubator at 37ºC for 7-8 days. Subsequent to the 7-8 incubation, media was removed from each 150 mm plate, cells were washed once with PBS, and then gently scrapped in 8 mL culture media. Cells were counted and seeded as necessary to meet experimental and plating requirements.

LDL aggregation: 1 mL of 5 mg/mL LDL (Alpha Assar) was vortexed at max speed for precisely 60 seconds.

Protein signaling experiments: BMDMs were harvested and plated within a 6-well tissue culture plate (Thermo Fisher Scientific) at a density of 1.2 million cells per well (duplicate wells plated for each experimental condition) in 1 mL of culture media. All experiments began by removing the culture media, cells were washed once with ice-cold PBS (Wisent). Following the PBS was removed and 1 mL of fresh culture media was added to each well along with each respective treatment. Experiments were conducted such that the longest time-points (if applicable) were treated first to ensure all conditions were completed simultaneously. At experimental endpoint, all medium was removed and cells were washed with PBS. PBS was

removed and cells were scraped in 80 µL lysis buffer; 50 mM Tris-HCl pH 7.5 (Tris; Bio basic, HCl; Thermo Fisher Scientific), 150 mM NaCl (Bioshop), 1 mM EDTA (Wisent), 0.5% Triton X-100 (Bioshop), 0.5% NP-40 (Bioshop), 100 µM Na3VO4 (Bioshop), supplemented with a protease inhibitor tablet (Sigma-Alrich). Duplicate lysates were combined and placed in a new 1.5 mL microfuge tube and snap frozen with liquid nitrogen. Lysates were thawed on ice, following samples were centrifugation at 14000 RPM at 4ºC for 5 minutes. The lysate was collected and placed within a new 1.5 mL microtube and the pellet was discarded.

Protein quantification, normalization, and preparation: Protein quantification was performed by Pierce™ BCA Protein Assay Kit as per manufacturers instructions under the microplate procedure. In brief, 25 µL of various BSA protein standards ranging from 25-2000 µg/mL was added to a 96-well tissue culture plate (Thermo Fisher Scientific) in duplicate to produce a standard curve. Additionally, 20 µL water and 5 µL of lysis buffer was loaded onto the plate to account for any absorbance at 562 nm produced from the lysis buffer alone (serving as a blank). In duplicate wells, 20 µL of water and 5 µL protein sample were loaded onto plate the 96-well plate in duplicate. Following, 200 µL of the colorimetric proprietary working reagent was added to each well, the plate was then incubated at 37ºC for 30 minutes. Following, absorbance at 562 nm was measured for the entire 96-well plate using a plate reader (Biotek). Protein concentration was determined based on the plates standard curve using Biotek's Gen5 software. All protein samples were normalized to the 1.34 µg/µL in lysis buffer, then an aliquot was further diluted in 4X loading dye; 200 mM Tris-HCl pH 6.8, 400 mM Dithiothreitol (DTT; Bioshop), 8% Sodium dodecyl sulfate (SDS; Bioshop), 0.4% bromophenol blue (Thermo Fisher Scientific), 40% glycerol (Thermo Fisher Scientific).

Protein samples in loading dye were then boiled at 95ºC for 5 minutes. Samples were stored at -20ºC until ready for analysis by immunoblotting techniques.

CD36 links oxLDL uptake to activation of ULK1 by AMPK: BMDMs were prepared and seeded as detailed above. WT and $CD36^{+/-}$ BMDMs were incubated with 50 µg/mL of oxLDL (Alfa Aesar). Each plate was returned to a humidified 5% CO_2 incubator at 37ºC for 24 hours. At experimental endpoint macrophages were lysed and protein lysates were prepared as detailed above.

Assessing macrophage AMPK's effect on cellular pH: BMDMs were prepared and seeded as detailed above. WT and AMPKβ1-KO macrophages were incubated in CytoPainter blue (Abcam) working reagent at a 10% dilution (v/v) in culture media for 30 minutes. Following, medium was removed and cells were washed three times with ice-cold PBS. PBS was removed, then cells were gently scraped in 250 µL of Hanks buffer saline solution (HBSS), and placed in a 96-well tissue culture plate. The University of Ottawa's Flow Cytometry Core then assessed the relative fluorescent intensity (360/445 ex/em) for each sample using a BD LSRFortessa.

Assessing macrophage AMPK's effect on lysosomal DQ-ovalbumin processing: BMDMs were prepared and seeded as detailed above. WT and AMPKβ1-KO macrophages were incubated with 10 µg/mL DQ-ovalbumin (Thermo Fisher Scientific) in complete media for 2 hours. Following, media was removed and cells were washed three times with ice-cold PBS. PBS was removed, then cells were gently scraped in 250 µL of HBSS, and placed in a 96-well tissue culture plate. The University of Ottawa's Flow Cytometry Core then assessed the relative fluorescent intensity (505/515 ex/em) for each sample using a BD LSRFortessa.

Assessing macrophage AMPK's effect on lysosomal membrane permeability: BMDMs were prepared and seeded as detailed above. WT and AMPKβ1-KO macrophages were incubated with 10 µg/mL of 10000 MW TMR-Dextran (Thermo Fisher Scientific) in culture media for 2, 24, and 48 hours. Following, the medium was removed and cells were washed three times with ice-cold PBS. PBS was removed, then cells were gently scraped in 250 µL of HBSS, and placed in a 96-well tissue culture plate. The University of Ottawa's Flow Cytometry Core then assessed the relative fluorescent intensity (555/580 ex/em) for each sample using a BD LSRFortessa.

Macrophage AMPK's signaling within autophagy: BMDMs were prepared and seeded as detailed above. Both A769662 (100 µM; AdooQ Bioscience) and Chloroquine (50 µM; Sigma-Alrich) were added to corresponding wells, and 0.2% (v/v) of DMSO (Thermo Fisher Scientific) was added to both control and chloroquine conditions to account for the A769662 solvent concentration. Each plate was returned to a humidified 5% CO_2 incubator at 37ºC for 5 hours. At experimental endpoint all media was removed, cells were washed with ice-col PBS and then were lysed and protein lysates were prepared as detailed above.

Macrophage AMPK's regulation of autophagic protein content: Preparation, seeding, and protein harvest was identical to the procedure explained above. A769662 (100 µM) was added to corresponding wells, 0.2% (v/v) of DMSO was added to control wells. Each plate was returned to a humidified 5% CO_2 incubator at 37ºC for 24 hours. At experimental endpoint all medium was removed, cells were washed with ice-col PBS and then were lysed and protein lysates were prepared as detailed above.

Determining if modified LDL variants, agLDL and oxLDL, modulate AMPK activity through CaMKKβ: Preparation, seeding, and protein harvest was identical to the procedure explained above. Prior to the experiment initiation, preparation of agLDL and oxLDL supplemented media was completed. Both agLDL and oxLDL were removed from sealed vials with a 0.5 mL insulin syringe (Thermo Fisher Scientific) to avoid contact with air to avoid further possible oxidation of each modified LDL variant, then the lipids were added to corresponding culture media to a final concentration of 50 µg/mL and mixed thoroughly. Culture media supplemented with modified LDL was aliquoted accordingly for all treatment conditions, various treatments were used at a final concentration as follows; STO-609 (20 µM; Sigma-Alrich), U18666A (1 µM; Sigma-Alrich), Ryanodyne (10 µM; Torcis), BHA (100 µM; Sigma-Alrich), A769662 (100 µM), and Tunicamycin (2.5 µg/mL; Sigma-Alrich). All treatment-containing media (and control culture medium) was supplemented with DMSO and EtOH (Commercial alcohols) until a final concentration of 0.2% v/v for each vehicle was achieved for all conditions. Each plate was returned to a humidified 5% CO_2 incubator at 37ºC for 18 hours. At experimental endpoint macrophages were lysed and protein lysates were prepared as detailed above.

Immunoblotting: Equalized protein samples containing loading dye were loaded (15 µg protein/well) and electrophoresed onto either a 4-20% (BioRad) or 8% SDS-PAGE gel (110 volts for ~1.75 hours). For analysis of relative phosphorylation of target proteins, duplicate gels were electrophoresed in tandem to probe for phosphorylated and total levels of target proteins of interest. Following electrophoresis, each gel was carefully removed and transferred onto PVDF membranes (BioRad) using BioRad's Trans-Blot Turbo system (25 V, 2.5 amps, for 18 min). Membranes were then blocked in TBST supplemented with 5% (w/v) BSA

(Albumin; Bioshop) with gentle rocking (Rocker 25 – Mendel) at room temperature for 1 hour. Membranes were then cut at appropriate molecular weights to isolate multiple proteins of interest per membrane. Each membrane fraction was incubated in the desired primary antibody solution (TBST supplemented with 5% BSA and 1:1000 dilution of primary antibody of interest (refer to **Appendix A**) overnight at 4ºC. The following day the primary antibody solution was collected and membranes were washed four sequential times in TBST for 5 min with gentle rocking at room temperature. After washing, membranes were incubated with anti-rabbit HRP conjugated secondary antibody (TBST supplemented with 5% BSA and 1:10000 dilution of anti-rabbit secondary) for 1h at room temperature with gentle rocking. Following, secondary-antibody solution was discarded and membranes were washed four times as previously done. Image acquisition was completed by gently drying membranes then incubating briefly in Clarity ECL substrate mix (BioRad). Luminescence was measured using the ImageQuant LAS4000 system (GE), obtained image files were processed and densitometry of protein bands was quantified using Image J analysis software.

Relative transcript expression experiment: BMDMs were harvested and plated within a 12-well tissue culture plate (Thermo Fisher Scientific) at a density of 0.6 million cells per well (triplicate wells plated for each experimental condition) in culture media. All experiments began with removal of culture media, cells were washed once with ice-cold PBS. Following the PBS was removed and 0.5 mL of fresh culture medium was added to each well with respective treatments. Experiments were conducted such that the longest time-points (if applicable) were treated first to ensure all conditions were finished simultaneously. At experimental endpoint, all media was removed and 0.5 mL of TriPure reagent (Roche) was added directly to the cells. TriPure containing plates were flash frozen by incubating the plate

in a Styrofoam container with a shallow level of liquid nitrogen. Plates were thawed on ice, then samples in TriPure were collected following visual confirmation that adherent cells are not present (ensuring proper lysis) and placed within a sterile 1.5 mL microfuge tube (replicates were collected separately). Samples were then either stored at -80ºC or were subjected to an RNA isolation (explained below).

Atherogenic lipids effect on lysosomal transcript expression: Preparation, seeding, and protein harvest was identical to the procedure explained above. A769662 (100 µM) was added to corresponding wells at desired time points, 0.2% (v/v) of DMSO was added to control wells. Each plate was returned to a humidified 5% CO_2 incubator at 37ºC following each treatment for a total of 24 hours. At experimental endpoint macrophages were lysed with TriPure as described above.

Modified LDL variants, agLDL and oxLDL, effect on lysosomal transcript expression: Preparation, seeding, and protein harvest was identical to the procedure explained above. Complete media supplemented with either agLDL (50 µg/mL) or oxLDL (50 µg/mL) was prepared prior and added to respective wells as described above.

AMPK activation triggers TFEB's nuclear enrichment: BMDMSs were harvested and plated within an 8-well chamber slide (Ibidi) at a density of 50 thousand cells per chamber, a single replicate was plated for all experimental conditions from each isolation. At the start of the experiment, all culture media was removed and cells were washed once with PBS. A stock culture media sample containing either 100 µM A769662 or 0.2% (v/v) DMSO was prepared prior to experiment. Following, 300 µL of each respective medium was added to corresponding chambers, chamber slide was then returned to a humidified 5% CO_2 incubator at 37ºC for 2

hours. Following, chamber slides were subjected to immunofluorescent labeling (described below).

RNA Isolation: RNA isolations were performed using Roche's TriPure reagent kit as per manufacturers instructions. In brief, thawed samples suspended in TriPure were let equilibrate to room temperature for 5 minutes. Following, 100 µL of chloroform (Bioshop) were added to each sample then each tube was capped tightly and was thoroughly mixed by repetitively and vigorously inverting samples for 15 seconds. Samples were then incubated at room temperature for 5 minutes. Phase separation was accomplished by centrifuging samples at 14000 RPM at 4ºC for 15 minutes. The top colorless phase was carefully collected and placed within a new sterile 1.5 mL microfuge tube. RNA was precipitated by addition of 250 µL of isopropanol (Thermo Fisher Scientific), samples were vigorously mixed for 15 seconds and let incubate at room temperature for 10 minutes. The RNA was pelleted by centrifuging samples at 14000 RPM at 4ºC for 10 minutes, following isopropanol was gently decanted and samples were placed on their side and let air dry at room temperature. Once dry, each RNA pellet was resuspended in 500 µL EtOH and vortexed vigorously. The RNA was pelleted by centrifuging samples at 14000 RPM at 4ºC for 5 minutes, following EtOH was gently poured out and samples were placed on their side and let air dry at room temperature. The RNA pellet was then resuspended in 30 µL of nuclease free water (Wisent) and incubated at 58ºC for 15 minutes. Samples were stored at -80ºC until quantification and synthesis of cDNA were ready to be performed.

RNA quantification: RNA concentration and purity were assessed using a take-3 plate reader (Biotek). In brief, 2 µL of sample was placed on corresponding location within the take-3 plate in duplicate using nuclease free water as a blank. Samples were then measured using Gen5

software, samples with a 260/280 absorbance ratio less than 1.8 or greater than 2.0 were removed from assessment. All samples were then normalized to 20 ng/mL in nuclease free water, now ready for cDNA synthesis.

cDNA synthesis: The synthesis of cDNA from RNA was performed using Applied Biological Material's 5X All-In-One RT Mastermix product as per manufacturers instructions. In brief, genomic DNA was removed using AccuRT Genomic DNA removal kit (Applied Biological Materials) as per manufacturers instructions. In brief, 3 µL of RNA (60 ng of template) were placed within a 0.2 mL PCR-tube (Thermo Fisher Scientific), 1 µL of AccuRT Reaction Mix (4X) was added to the sample and mixed thoroughly by gentle pipetting. Samples were incubated at room temperature for 5 min, then 1 µL of AccuRT Reaction Stopper (5X) buffer was added to the reaction. Following removal of genomic DNA, 2 µL of All-in-One RT Mastermix were added to each sample, samples mixed and placed within a thermocycler. Samples were incubated for 10 min at 25ºC, 15 min at 42ºC, then 5 min at 85ºC to stop the reaction. Following, cDNA was further diluted 1:20 with nuclease-free water prior to transcript expression analysis.

Quantitative PCR: Quantitative PCR reactions were performed within 0.1 mL 4-Strip tubes (Ultident) using 4.75 µL of diluted cDNA template, 0.25 µL of primer of interest (refer to **Appendix A**), and 5 µL of PCR master mix (Taqman master mix; Quiagen). PCR reactions underwent using a thermocycler (Quiagen) under manufacturers protocols for specific probe primer sets.

Immunofluorescent labeling: Upon experimental completion, all media were removed and each chamber was washed once with PBS. PBS was removed, and cells were fixed for 20 min with 300 µL of 2% PFA (Thermo Fisher Scientific) at room temperature. The fixative was

removed and chambers were washed twice with PBS. PBS was removed and fixed cells were blocked/permeabilized for 1 hour at room temperature with 300 µL PBS supplemented with with 5% fatty-acid free BSA, 0.2% Triton X-100 and 0.1% Tween-20 (Thermo Fisher Scientific). Blocking/permeabilizing buffer was removed, chambers were washed once with PBS, then 300 µL of anti-TFEB (refer to **Appendix A**) antibody solution (PBS supplemented with 1:100 anti-TFEB primary antibody, 2% fatty acid-free BSA, 0.2% Triton X-100, 0.1% Tween-20). All chamber slides were incubated in primary antibody solution over night at 4ºC. The following day, the antibody solution was removed, chambers were washed twice with PBS. PBS was removed and chamber slides were incubated in 300 µL secondary antibody solution (PBS supplemented with 1:100 anti-Goat FITC-conjugated secondary antibody (refer to **Appendix A**), 2% fatty acid-free BSA (Thermo Fisher Scientific), 0.2% Triton X-100, 0.1% Tween-20) for 1 hour at room temperature shield from light. Following, secondary antibodies solution was removed and chambers were washed once with PBS. PBS was removed and 300 µL of 300 nM DAPI (Thermo Fisher Scientific) made in PBS were added to each chamber then incubated at room temperature for 5 minutes (shielded from light). Following, DAPI solution was removed and all chambers were washed three times with PBS. Chambers were stored in 300 µL PBS at 4ºC shielded from light until image acquisition was ready to be performed.

Immunofluorescent imaging: Following immunolabeling, multiple Z-stack images spanning the entirety of the cell at 50 µm increments were taken at 40X using a Zeiss Confocal microscope. Image files were processed using Image J Software and representative Z-projection for maximum intensities were used for analysis and generation of representative images.

Measuring the effect of modified LDL variants, agLDL and oxLDL, on relative AMP and ATP ratios: BMDMs were harvested and plated within a 100 mm tissue culture plate (Thermo Fisher Scientific) at a density of 5 million cells per plate in culture media (duplicate plates were seeded for each experimental condition). At experimental start, culture media were removed and cells were washed once with ice-cold PBS. Following, 5 mL of media supplemented with either oligomycin (5 mM), agLDL (50 µg/mL), or oxLDL (50 µg/mL) for respective time points. At the experimental endpoint, media were removed from each plate and cells were washed once with ice-cold PBS. Following, 250 µL ice-cold perchloric acid (10% v/v $HClO_4$, 25 mM EDTA; Sigma-Alrich) were added and cells were scraped/lysed with a rubber policeman. Cellular extracts were transferred to a sterile 1.5 mL microfuge tube and vortexed briefly. Samples were left to incubate on ice for 30 min then precipitated proteins were spun down at 8000 x *g* for 2 min at 4ºC. A 200 µL aliquot was taken and placed in a new microfuge tube, samples pH was adjusted to 6.5-7 using ~130 µL KOH/MOPS (2 N KOH/0.3 M 3-N-morpholino propane sulfonic acid; Sigma-Alrich) with careful mixing and pH confirmation was completed using pH strips (Sigma-Alrich). Lysate was clarified by centrifugation at 8000 x *g* for 2 min at 4ºC. A 200 µL aliquot of neutralized supernatant fraction was pipetted into a new 1.5 mL microfuge tube and was stored at -80ºC until ready for HPLC measurement. HPLC measurements were performed as dictated in Spring's AMPK Methods and Protocols[195].

Statistics: Statistical analysis using a one-way ANOVA was completed for Figure 1 (A-B), Figure 2 (B and D), and Figure 3. Analysis was performed comparing the mean of each group to the mean of WT control. Statistical analysis using a two-way ANOVA was completed for Figure 4 (B), Figure 7 (B), Figure 8 (A-D, F, and G), and Figure 9 (A-F). Analysis was

performed with multiple comparisons comparing the mean value for each group to the mean value to the mean value of alternate groups. Statistical analysis using a student's t test was completed for Figure 5 (A-C) for genotype comparisons. Statistical significance was only reported between genotypes of the same treatment, or treatments within genotype in reference to the untreated control. Statistical significance is represented as follows for each Figure (if applicable); *P<0.05, **P<0.005, ***P<0.001. All statistics were done using Prism 8 software.

3.0 CHAPTER 2. The role of myeloid AMPK signaling in atherogenesis.

3.1 Study Rationale:

Research has illuminated numerous roles for AMPK in protection against atherogenesis, such as improved cholesterol homeostasis, anti-inflammatory properties, lipid lowering effects, and regulation of lysosomal dependent processes necessary for normal RCT to occur[86,141,173,196]. Multiple studies have recently addressed the role of whole-body AMPKα2 expression, vascular AMPKα2 expression, myeloid AMPK expression, and systemic AMPK activation with various activators[177,179,180]. Despite this, the role of myeloid AMPK and its subsequent activation plays in atherosclerosis is not fully understood. Reports focussed on systemic AMPK activation as a therapy to protect against from atherosclerosis all support a role for systemic AMPK activation as an atheroprotective therapy by reducing myeloid chemotaxis into the developing lesion. Despite this, studies aimed to identify myeloid AMPKα1's role in atherosclerosis yielded opposing results such as a causative role on an ApoE-KO background[180] and a protective role on an LDLr-KO background[179]. Importantly, it is unknown if the atheroprotective effects from systemic AMPK activation (by pharmacological activators) is dependent on myeloid AMPK expression.

We sought out to address the contribution of myeloid AMPK and its subsequent activation on atherosclerosis with two separate studies. To date, assessing the contribution of AMPK activation to combat atherosclerosis has been accomplished with prolonged therapies (10-12 weeks) where various AMPK activators (including A769662) were systemically introduced daily to atherogenic mice[181,182]. Alternative to this treatment strategy, we sought out to encapsulate our AMPK activator (A769662) within poly(lactic-co-glycolic acid) (PLGA) nanoparticles (NP) that have been shown to preferentially target atherosclerotic

regions when decorated with Collagen IV binding peptide[197]. With our AMPK activator encapsulated within NP, we sought out to test if we could preferentially activate lesion AMPK acutely to combat atherogenesis. In an alternative approach, we assessed atherogenesis within PCSK9-AAV treated mice devoid of myeloid AMPKα1α2 in combination with systemic A769662 therapy. This second study was designed to assess atherogenesis in mice with complete ablation of myeloid AMPK activity, in addition to determining if the atheroprotective effects of A769662 therapy are dependent on myeloid AMPK expression. We **hypothesized** that myeloid AMPK signaling is critical for normal cellular function in atherosclerosis and that systemic AMPK activation with A769662 is atheroprotective in a myeloid-AMPK-dependent manner.

3.2 RESULTS:

3.2.1 Assessing the efficacy of A769662-NP to activate AMPK.

The therapeutic efficacy of A769662 as an anti-atherogenic agent was first shown in two back-to-back reports from the same laboratory, each study administered systemic A769662 therapy for a 10-12 weeks in ApoE-KO mice fed a WD describing a protective effect for prolonged AMPK activation within atherogenesis[182,198]. We sought to design a treatment regime to increase efficacy and cell type specificity while reducing the length of therapy. To accomplish these goals, we collaborated with Dr. Suresh Gadde whose expertise in nanomedicine allowed for the packaging of A769662 within PLGA nanoparticles. Furthermore, Dr. Gadde was able to decorate the surface of A769662-embedded nanoparticles (A769662-NP) with a Col IV-binding peptide, which has been shown to enhance nanoparticle delivery to areas of damaged vasculature where atherogenesis propagates[197].

We show that in BMDM cultured with A769662-NP had enhanced AMPK signaling to ACC (at Ser79) that was comparable with A769662 alone (Figure 10A). Additionally, we observed that A769662-NP treated macrophages had sustained enhancement of AMPK-signaling to ACC for 48 hours while activity induced by A769662 alone dropped drastically after 4 hours (Figure 10A). To ensure increases in AMPK signaling exhibited by A769662-NP treatment was not caused by any off-target effects from the nanoparticles alone, we treated macrophages with empty-nanoparticles (Empty-NP) over time and showed no alterations in AMPK signaling in comparison vehicle treated cells (Figure 10A).

We next sought to confirm that A769662-NP were capable of activating AMPK *in vivo* and elucidate optimal timing for multiple NP injections. Ideally, we would have liked to

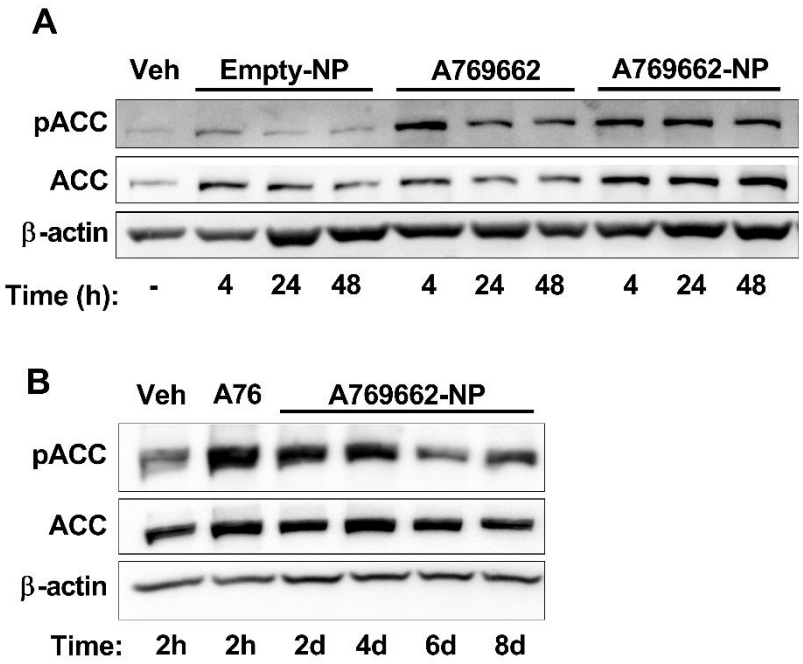

Figure 10. A769662 embedded within poly-lactic acid nanoparticles induces a robust and sustained increase of AMPK signaling to ACC in BMDM and hepatic tissue. (A) BMDM were isolated from WT mice and treated with A769662 (100 μM), A769662-NP (100 μM), or Empty-NP (equivalent dose to A769662-NP) for indicated time. (B) WT mice were treated with one 10 mg/kg dose of either A769662-NP or Empty-NP and sacrificed every second day. A single acute I.P. injection of 30 mg/kg A769662 was completed followed by animal sacrifice 2 h post-injection to serve as a positive control for enhanced hepatic AMPK signaling in response to A769662. (A) Datum is representative of 2 independent experiments performed in BMDM isolated from WT mice. (B) Datum is representative of 4 mice per given time point.

validate A769662-NP potential to activate AMPK within atherosclerotic regions, however to generate atherosclerotic mice would have been time and labour intensive. Alternatively, we decided to treat WT mice with A769662-NP and measure AMPK signaling to ACC within hepatic tissue. We were aware that the regulation of AMPK signaling within hepatic tissue may vary from the lesion microenvironment, however we reasoned that this may be the an acceptable read out for *in vivo* AMPK activation by A769662-NP treatment, in consideration of the time and labour constraints within our study. We treated WT mice with a single dose of A769662-NP (devoid of any targeting peptide) every two days for a period of 8 days. We observed at 2- and 4-days post A769662-NP administration there was enhanced AM PK signaling to ACC (Ser79) compared to vehicle control animals within hepatic tissue (Figure 10B). AMPK signaling to ACC was approximately returned to basal levels by 6 post-nanoparticle injection, illuminating that AMPK activation induced by A769662-NP was highest at 1-4 days post injection (Figure 10B).

3.2.2 A769662-NP therapy is insufficient in reducing diet induced atherosclerosis in male LDLr-KO mice.

Knowing the potential for A769662-NP providing enhanced and sustained AMPK activity (Figure 10), we sought out to investigate the relevance within atherosclerosis in a preliminary study. Using the LDLr-KO model of atherosclerosis for our investigation, we fed mice a WD for 12 weeks prior to administration of our A769662-NP therapeutic regime (Figure 11A). Following previous results (Figure 10B), we treated LDLr-KO mice with intravenous injections of PBS, Empty-NP, or A769662-NP every 4 days for a total of 6 injections (Figure 11A-C). At experimental endpoint (15 weeks) we isolated the hearts from each animal to assess atherosclerosis development within the aortic sinus. We stained each

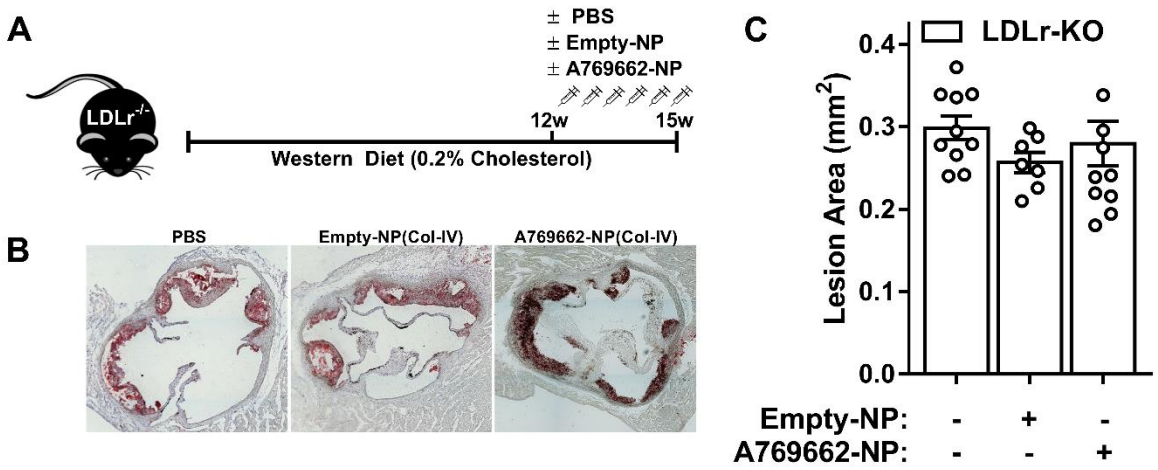

Figure 11. A769662-NP therapy is insufficient for reducing WD-induced lesion development in male LDLr-KO mice. (A) Experimental schematic. (B) Representative brightfield image of Oil Red O stained aortic sinus from LDLr-KO mice for all experimental conditions. (C) Quantification of lesion size; lesions were stained and quantified from Oil Red O stained slides using Image J software, each data point is representative of the average lesion size from 7 serial sections (10 µm thick) spanning the same 700 µm within the aortic sinus of each animal. After 12-weeks of western diet feeding mice received an I.V. (retroorbital) administration of either A769662-NP(Col IV), Empty-NP(Col IV), or vehicle control (PBS) every 4 days for a total of 6 injections (within ~3.4 weeks). Datum is representative of the lesion area from 7-10 LDLr-KO mice. Datum is reported as the mean value ± SEM, where no significance was found by a one-way ANOVA using Prism8 software.

aortic sinus with the neutral lipid dye Oil Red O to aid in lesion quantification (Figure 11B). We observed no alterations in lesion size between A769662-NP treated animals compared to PBS- or Empty-NP control groups (Figure 11C).

3.2.3 A769662-NP therapy does not modulate lesion markers of lesion macrophage-like cells, inflammation, or apoptosis in male LDLr-KO mice.

With no reductions in lesion size between LDLr-KO animals treated with A769662-NP compared to control mice, we sought out to elucidate whether any anti-atherogenic processes may be initiated in response to A769662-NP treatment (Figure 12A). We observed that targeting lesion AMPK with A769662-NP did not change in the expression of CD68 expression within the lesion, which is suggestive that A769662-NP is not implicated in modulating macrophage-like cell content within the developing lesion (Figure 12B). Additionally, in CD68+ cells, we show a trending decrease in both arginase 1 (Arg1) and cleaved caspase-3 (CC3), which are markers for anti-inflammatory macrophages and apoptotic cell death, respectively (Figure 12B-D). However, these trending decreases could not be attributed to A769662 specifically since we observed that Empty-NP-treated mice also exhibited a similar trending effect (Figure 12B and 12C), which may indicate that NP themselves could potentially exhibit regulatory effects within the lesion microenvironment. Since there were no observable effects from A769662-NP treatment on lesion generation or properties, we sought out to validate that A769662-NP was in fact activating AMPK within the atherosclerotic lesion. However, despite our best efforts we did not find any reliable markers to assess lesion AMPK activity by the techniques and resources available to us at the time of the study (Figure 13).

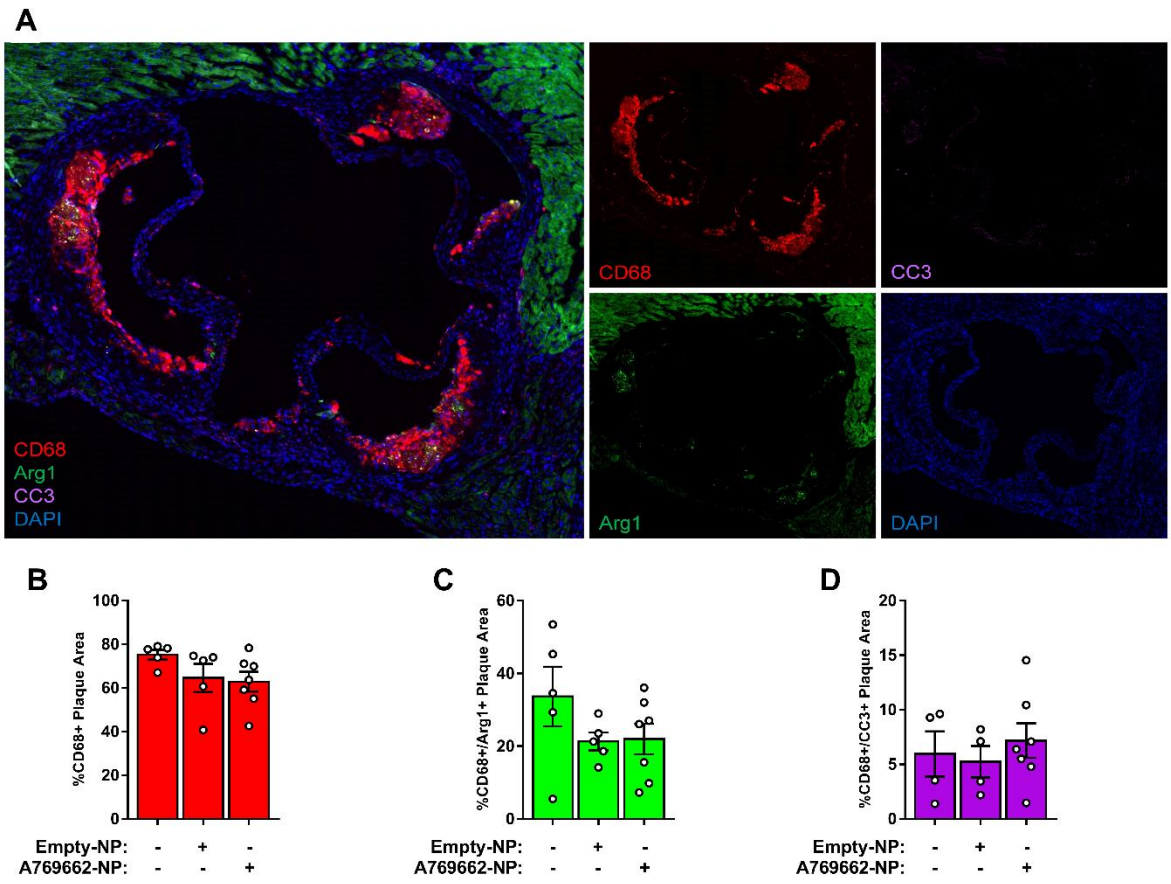

Figure 12. A769662-NPs do not alter lesion macrophage-like cell frequency, anti-inflammatory marker expression, or apoptotic cell death in male mice. (A) Representative immunofluorescent image of immunofluorescent labeled aortic sinus (CD68; RED, Arg1; GREEN, Cleaved Caspase-3; MAGENTA, and Nuclei; BLUE). (B) Quantification of lesion CD68 composition. (C) Quantification of CD68+Arg1+ area within lesion. (D) Quantification of CD68+CC3+ area within lesion. Each quantification was completed from one 10 µm thick section of the aortic sinus within the same section for each animal. Datum is representative of the results from 4-7 LDLr-KO mice. Datum is reported as the mean value ± SEM, where no significance was found by a one-way ANOVA using Prism8 software.

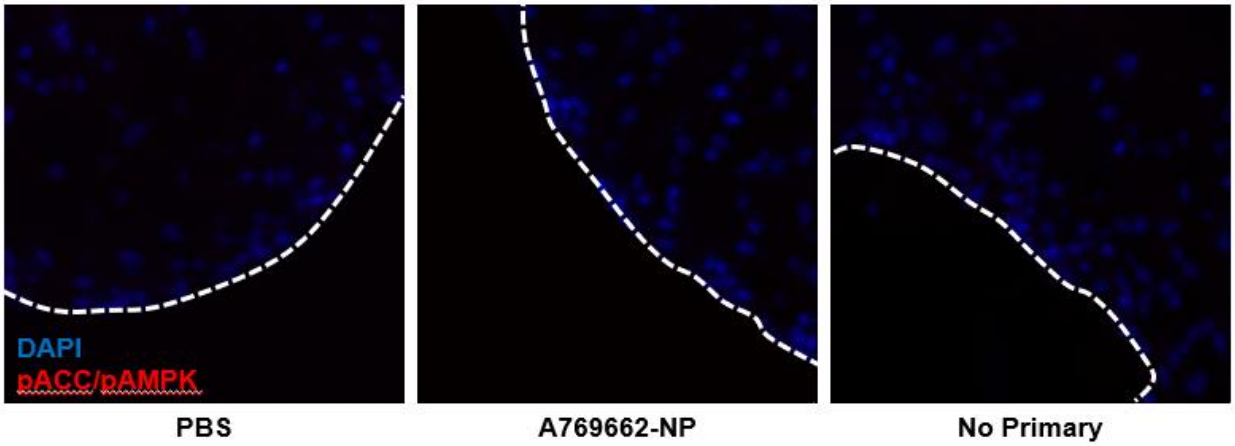

Figure 13. Inability to assess AMPK activity in atherosclerotic lesions via immunofluorescent techniques. Representative immunofluorescent image for staining plaque pACC Ser79 and pAMPK Thr172 (Red) and DAPI to label nuclei (BLUE). No fluorescence was detected within AMPK activation or signaling. Datum is representative of a single interrogation into AMPK signaling within the plaque by immunofluorescent techniques.

While there are many technical considerations regarding this study, which will be discusses below, with the observation that A769662-NP therapy did not alter the progression of atherosclerosis or attenuate any other athero-related parameters we formulated two important questions; (1) is myeloid AMPK within developing lesions responsible for the anti-atherogenic properties observed from A769662 treatment as shown in previous reports, and (2) does our therapeutic window allow for AMPK to exhibit its anti-atherogenic properties to potentiate alterations in lesion generation.

3.2.4 Generation of myeloid AMPKα1α2-DKO atherogenic mice.

While AMPKα1 is the predominant isoform expressed in haematopoietic cells, myeloid deficiency of either AMPKα1 or AMPKα2 has been shown to alter atherosclerosis[178,180]. Moreover, these studies crossed their respective AMPK-deficient mouse models onto the atherogenic LDLr- or ApoE-KO background. To completely disrupt AMPK signaling, we generated mice lacking complete AMPK catalytic activity in myeloid cells (AMPKα1 and AMPKα2 deletion driven by LysM expression of Cre recombinase; MacKO), which was confirmed by assessing AMPK-specific signaling to its downstream target ACC in elicited peritoneal macrophages from floxed (WT-equivalent) and MacKO mice (Figure 14A). We isolated peritoneal cells from thioglycolate elicited MacKO mice and floxed controls 4-days post thioglycolate injection and cultured cells ± A769662 (Figure 14A). We observed that in peritoneal cells isolated from MacKO mice had reduced AMPK-signaling to ACC, any residual signalling to ACC was attributed to non-myeloid cell that was harvested from the peritoneum in tandem (Figure 14A). Additionally, we isolated protein from hepatic tissue from MacKO mice and their floxed controls to confirm normal AMPK signaling persists in non-myeloid cells (Figure 14B).

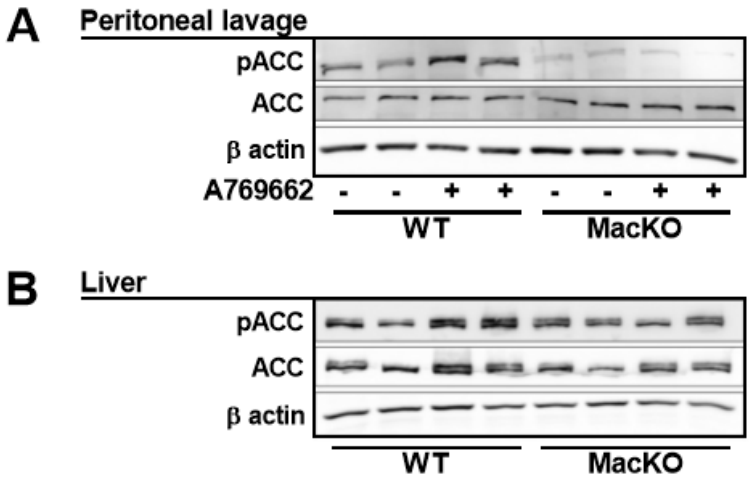

Figure 14. AMPK signaling is retained in liver, but not in primary peritoneal macrophages isolated from thioglycolate-elicited MacKO mice. Representative immunoblot depicting AMPK signaling in (A) peritoneal cells (± A769662) and (B) hepatic tissue isolated from MacKO mice and their floxed (WT equivalent) control mice. (A) Peritoneal cells were isolated from mice after 4-days post thioglycolate elicited immune response, following peritoneal cells were treated with A769962 (100 μM) for 5 h. Images are representative of results obtained from 7 WT and MacKO mice.

3.2.5 AMPK activation therapy helps prevent weight gain induced by western diet feeding in male mice.

To circumvent the time and cost associated with genetic mouse models of atherosclerosis, we used a single intravenous injection of a well characterized gain-of-function PCSK9-AAV (Asp377Tyr) followed by WD-feeding to induce rapid hypercholesterolemia in MacKO and floxed control animals (herein referred to as WT) to drive the progression of atherosclerosis (Figure 15A). AMPK plays numerous roles within cells, tissue, and WB physiology to ensure proper regulation of energy metabolism through regulation of networks to maintain adequate glucose and lipid homeostasis. Following the promotion of diet-induced hypercholesterolemia within WT and MacKO mice, we observed a gradual increase in weight over time regardless of genotype (Figure 15B). At 6-weeks of WD feeding, mice were subjected to daily I.P. injections of either 30 mg/kg A769662 or vehicle control for 6-weeks. We observed that male WT mice treated with A769662 had a significant protection from weight gain (Figure 15C), which is in corroboration with what has been shown previously[199]. In addition, male MacKO had a trending (although not significant) reduction in weight gain in response to A769662-intervention therapy.

3.2.6 Myeloid AMPK and A769662-intervention therapy do not protect against the progression of atherosclerosis male and female mice.

Multiple groups have reported on the numerous effects of AMPK signaling within atherosclerosis, however the role of myeloid AMPK within atherogenesis remains unclear. Moreover, all studies implementing a preventative therapeutic AMPK activation therapy within their study have illuminated a protective effect against atherogenesis largely mediated

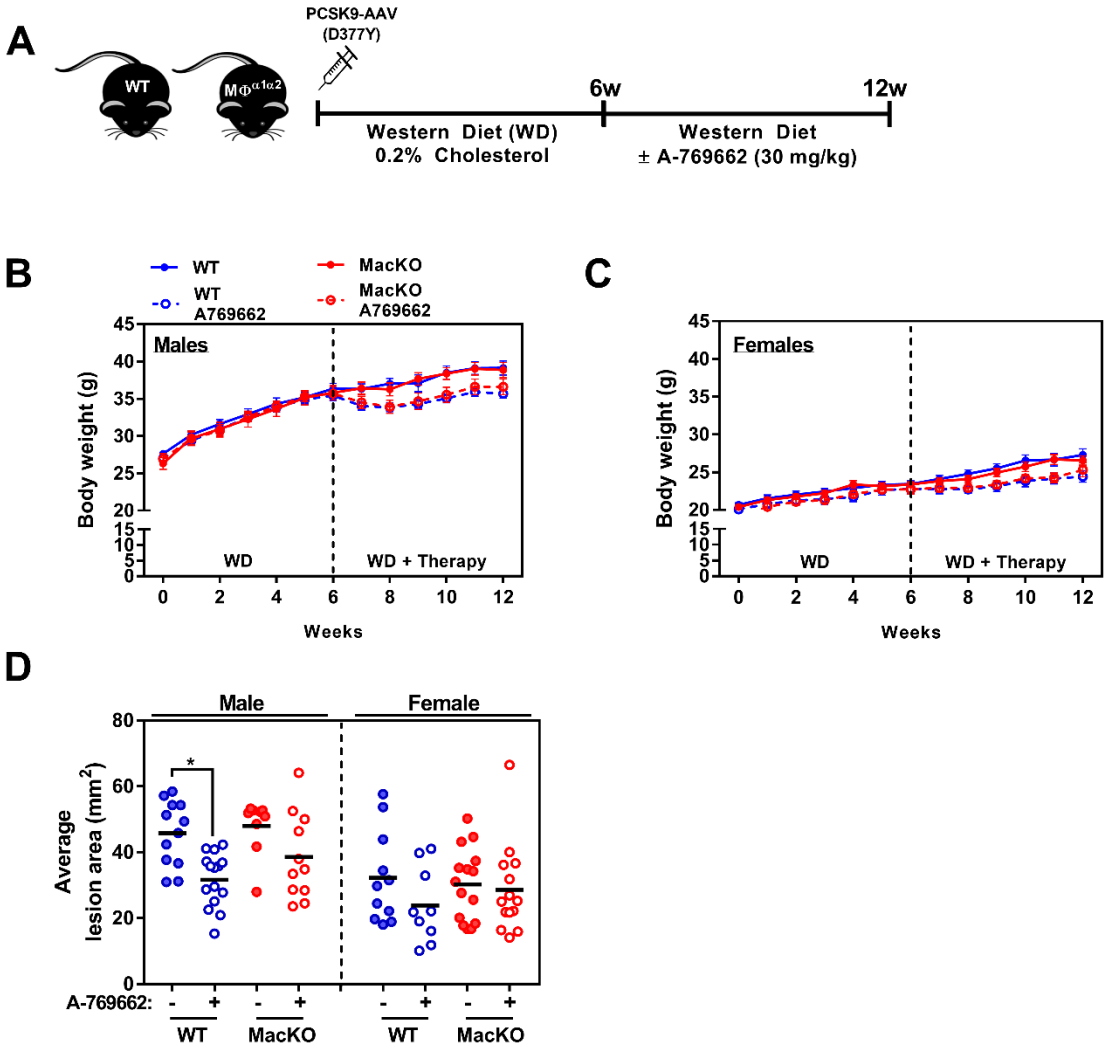

Figure 15. A769662-therapy protects against WD-induced weight gain in male mice. (A) Experimental schematic depicting generation of hypercholesterolaemic male mice (± myeloid AMPKα1α2; MacKO) and therapy regime on a western diet. (B) Weekly body weights for all male experimental groups. (C) Weight gain percentage calculated from baseline to endpoint weights. A769662 was dissolved in DMSO and made up in PBS, mice received daily I.P. injections of either 30 mg/kg of A769662 or vehicle control (5% DMSO v/v in PBS) as depicted in (A). Datum is representative of 7-16 WT and MacKO mice. Datum is reported as the mean value, where *P<0.05 was calculated by a two-way ANOVA using Prism8 software.

by reducing myeloid chemotaxis within the developing lesions[182,198]. We sought out to test whether animals lacking complete myeloid AMPK activity (MacKO) developed accelerated atherosclerosis, and if so, is A769662-therapy protecting against atherogenesis in a myeloid AMPK-dependent manner. We observed that lesion generation within MacKO animals was similar to WT control animals, and 6-week A769662-intervention therapy did not reduce lesion size in all animals regardless of genotype (Figure 16A). However, measuring total neutral lipid content within the aortic sinus (by Oil Red O staining), we saw a trending protective genotype and treatment effect in male mice (Figure 16B). This is suggestive that myeloid AMPK and A769662-intervention therapy play a role in regulating lesion lipid content, highlighting a potential protective effect, albeit not significant within the duration and timing of our study.

3.2.7 Myeloid AMPK signaling does not influence CD68 expression within atherosclerotic lesions in male mice.

Deletion of myeloid AMPK on an ApoE-KO[200] and LDLr-KO background[201] resulted in less and more markers of macrophage-like cell accumulation, respectively. To interrogate this potential effect within our model of PCSK9-induced atherosclerosis, we used CD68 as a general marker of macrophage-like cells within atherosclerotic lesions (Figure 17A). We speculated that within our model of atherosclerosis, which mechanistically resembles the LDLr-KO mice, myeloid AMPK would have a protective effect against myeloid recruitment/transmigration into developing lesions. Furthermore, we predicted that A769662-therapy would further reduce the number of myeloid content as observed in 10 and 12-week systemic therapy evidenced in ApoE-KO mice[181,182]. Despite our original predictions, we detected no difference in the amount of lesion CD68 expression between any groups,

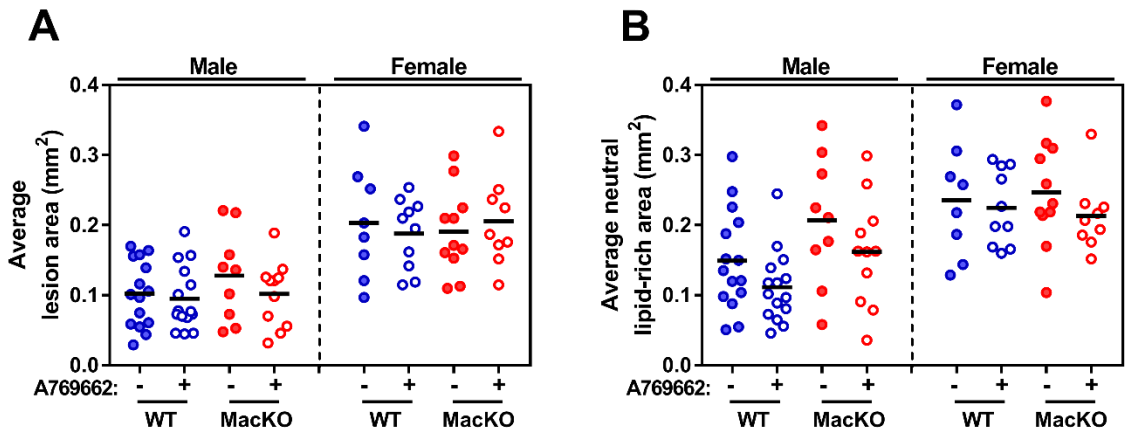

Figure 16. Myeloid AMPK and A769662-intervention therapy are insufficient in protecting against the progression of atherosclerosis in male mice. (A) Quantification of lesion size; lesions were stained and quantified from H&E stained slides using Image J software, each data point is representative of the average lesion size from 5 serial sections (10 µm thick) spanning the same 500 µm within the aortic sinus of each animal. (B) Quantification of Oil Red O area; neutral lipids were stained and quantified from Oil Red O stained slides using Image J software, each data point is representative of the average lesion size from 5 serial sections (10 µm thick) spanning the same 500 µm within the aortic sinus of each animal. (C) Representative brightfield image of Oil Red O (ORO) stained aortic sinus from WT and MacKO ± A769662 therapy. A769662 was dissolved in DMSO and made up in PBS, mice received daily I.P. injections of either 30 mg/kg of A769662 or vehicle control (5% DMSO v/v in PBS). Datum is reported as the mean value for 7-16 WT or MacKO mice, where the results were found to be insignificant calculated by a two-way ANOVA using Prism8 software.

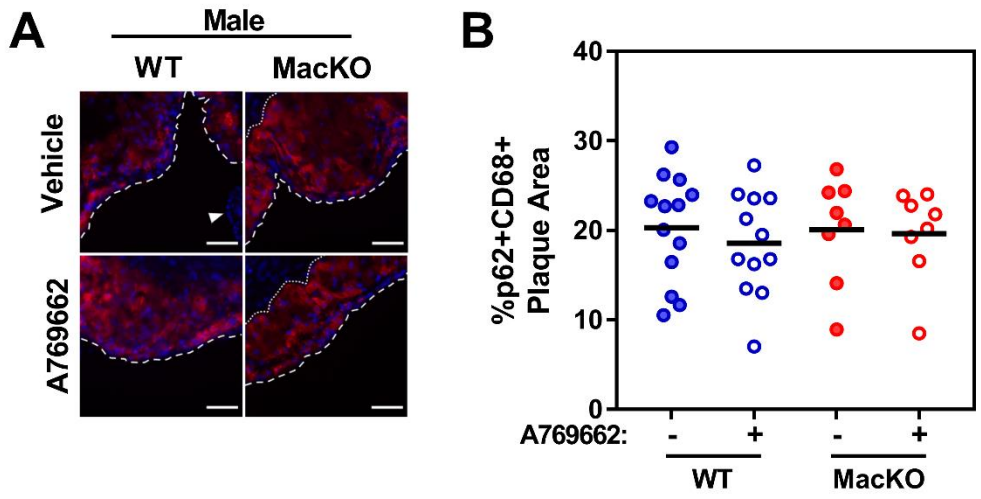

Figure 17. Myeloid AMPK and A769662-therapy don't influence macrophage-like cell frequency within developing lesions in male mice. (A) Representative image of immunofluorescent labeled aortic sinus (CD68; RED and Nuclei; BLUE). (B) Quantification of lesion CD68 composition, each data point is representative of the average CD68+ lesion area fraction from 3 serial sections (10 µm thick) spanning the same 300 µm within the aortic sinus from each animal. Datum is reported as the mean value for 7-12 male WT or MacKO mice, where the results were found to be insignificant calculated by a two-way ANOVA using Prism8 software.

regardless of genotype or treatment (Figure 17B). However, since it is now well established that vascular smooth muscle cells can adopt CD68 expression as atherogenesis progresses, we cannot rule out that shifts between myeloid or VSMCs content could be affecting our interpretation of results[202,203].

3.2.8 Neither myeloid AMPK signaling or A769662 therapy enhance lesion autophagy in male mice.

We next aimed to determine if the AMPK signaling in myeloid cells or A769662-therapy had an effect autophagy within the plaque environment. We stained for lesion p62 (Figure 18A), a key chaperone protein that is processed in an autophagic-dependent manner and serves as a marker of defective autophagy[204]. The average level of lesion p62 was unaffected by the presence or absence of myeloid AMPK, in addition we observed that A769662-therapy had no effect on the levels of p62 staining within lesions (Figure 18B). Furthermore, in CD68+ cells, we observed no difference in p62 expression regardless of genotype or treatment (Figure 18C). Lastly, we observed that the localization of p62 staining within the plaque, which has been linked to its potential sequestration along with its cargo to autophagosomes, was also not regulated by genotype or treatment (Figure 18A).

3.2.9 Myeloid AMPK signaling and A769662-therapy are not protective against lesion necrosis in male or female mice.

Macrophages are professional phagocytes that readily participate in the clearance of apoptotic and necrotic bodies following cell death, this is important to maintain inflammatory mediators within their microenvironment[205–207]. It has been shown that pharmacologically activating AMPK improves macrophage phagocytic capabilities, additionally AMPK plays a

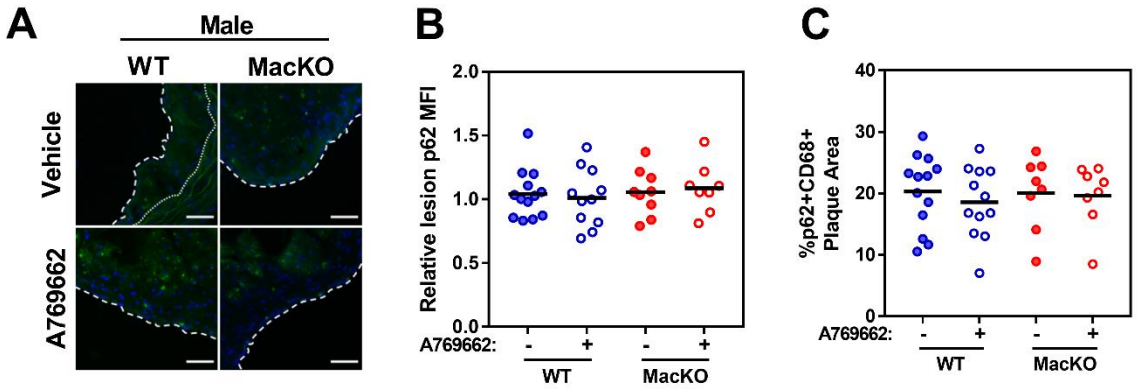

Figure 18. Myeloid AMPK and A769662-therapy do not promote lesion autophagy in male mice. (A) Representative close up image of immunofluorescent labeled aortic sinus (p62; GREEN and Nuclei; BLUE). (B) Relative lesion p62 expression and (C) relative p62 expression in CD68+ cells. The mean fluorescent intensity of p62 within lesions was measured then made relative to WT control mice, each data point is representative of the average from 3 serial sections (10 µm thick) spanning 300 µm within the aortic sinus from each animal. Datum is reported as the mean value for 7-12 male WT or MacKO mice, where the results were found to be insignificant calculated by a two-way ANOVA using Prism8 software.

protective role against cellular stresses leading to apoptotic and necrotic death[208–211]. This led us to predict that myeloid AMPK and A769662-therapy may aid in reducing areas of necrosis within developing lesions. To determine if AMPK was participating in resolution of lesion necrosis, we stained the aortic sinus with hematoxylin and eosin and defined white space within lesions, which are devoid of cellularity, necrotic regions (Figure 19). We observed no difference in the necrotic area within lesions regardless of myeloid AMPK expression in male or female mice (Figure 19). Furthermore, A769662-therapy did not alter lesion necrosis, taken together these results suggest that myeloid AMPK and A769662-therapy do not contribute to resolution of lesion necrosis in male or female mice.

3.2.10 Myeloid AMPK and A769662-intervention therapy are insufficient to induce alterations in total circulating lipids in in male and female mice.

The liver is a major regulator of whole-body lipid and lipoprotein metabolism, where it regulates levels of lipoprotein-associated cholesterol and triglyceride within circulation. While disruption of AMPK was restricted to myeloid cells, there is the potential that LysM-mediated deletion within liver resident macrophages (kupffer cells) could lead to regulatory differences that could contribute to altered circulating lipid levels. Moreover, our experimental design made use of systemic delivery of the A769662 activator, which has well known hepatic effects[199]. We observed within plasma collected from endpoint blood, levels of circulating total cholesterol and triglycerides were equivalent between WT and MacKO mice and were not altered by A769662-therapy (Figure 20). This suggests that the trending difference in neutral lipid area were not caused by modulation of circulating lipid levels.

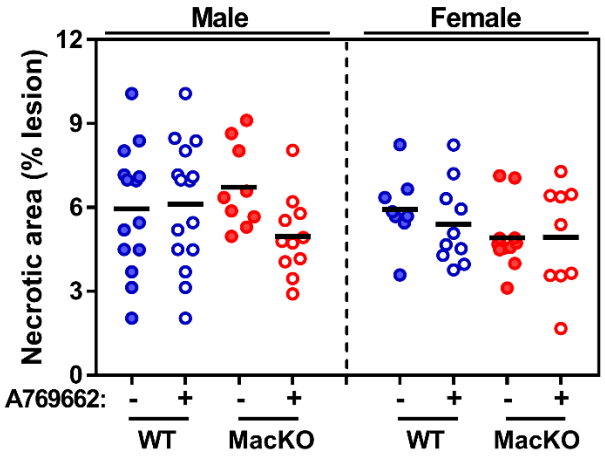

Figure 19. Myeloid AMPK and A769662-therapy do not protect against the resolution of lesion necrosis in male mice. (A) Quantification of necrotic area within lesions (define as areas absent of cellularity – whitespace), each datum point is representative of the average necrotic area measured from 4 serial sections (10 µm thick) spanning the same 400 µm within the aortic sinus of each animal. (B) Representative image showing how necrotic regions were selected and quantified within lesions using Image J software. A769662 was dissolved in DMSO and made up in PBS, mice received daily I.P. injections of either 30 mg/kg of A769662 or vehicle control (5% DMSO v/v in PBS) as depicted in (A). Datum is reported as the mean value for 7-16 WT or MacKO mice, where the results were found to be insignificant calculated by a two-way ANOVA using Prism8 software.

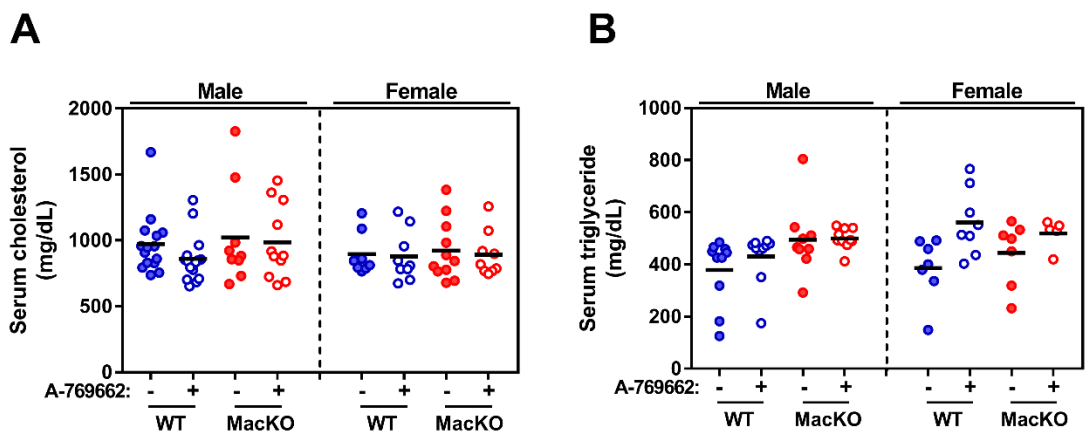

Figure 20. Myeloid AMPK and A769662 therapy do not mitigate anti-atherogenic effects through modulation of total circulating lipids in male or female mice. (A) Total cholesterol and total cholesterol levels from plasma isolated from terminal blood were measured using Infinity Cholesterol Kit as per manufacturers instructions. (B) Terminal plasma triglycerides. Total triglyceride levels were measured using Triglyceride Colorimetric Assay Kit (Cayman Chemical) as per manufacturers instructions. Datum is reported as the mean value for 7-16 WT or MacKO mice, where the results were found to be insignificant calculated by a two-way ANOVA using Prism8 software.

3.2.11 Circulating inflammatory messengers are unaltered by myeloid AMPK signaling or A769662-therapy in male and female mice.

Metabolism and inflammation are recognized as important drivers of atherogenesis. Given the known role for AMPK in modulating both macrophage metabolism and immune programs, we next assessed the systemic (circulating) levels of inflammatory cytokines (IL-10, IL-12p70, IL-6, IL-5, KC, TNF-α, IFNγ, IL-2, and IL-1β). In male mice, at the time of tissue harvest and blood collection, circulating levels of KC/GRO were significantly higher in A769662-treated conditions in comparison to control mice (Figure 21). When comparing vehicle and A769662 treatment, IL-12p70 and IL-5 levels significantly increased in male and female MacKO, respectively (Figure 21). Despite this, we see very little significant shifts in other markers of inflammation (Figure 21).

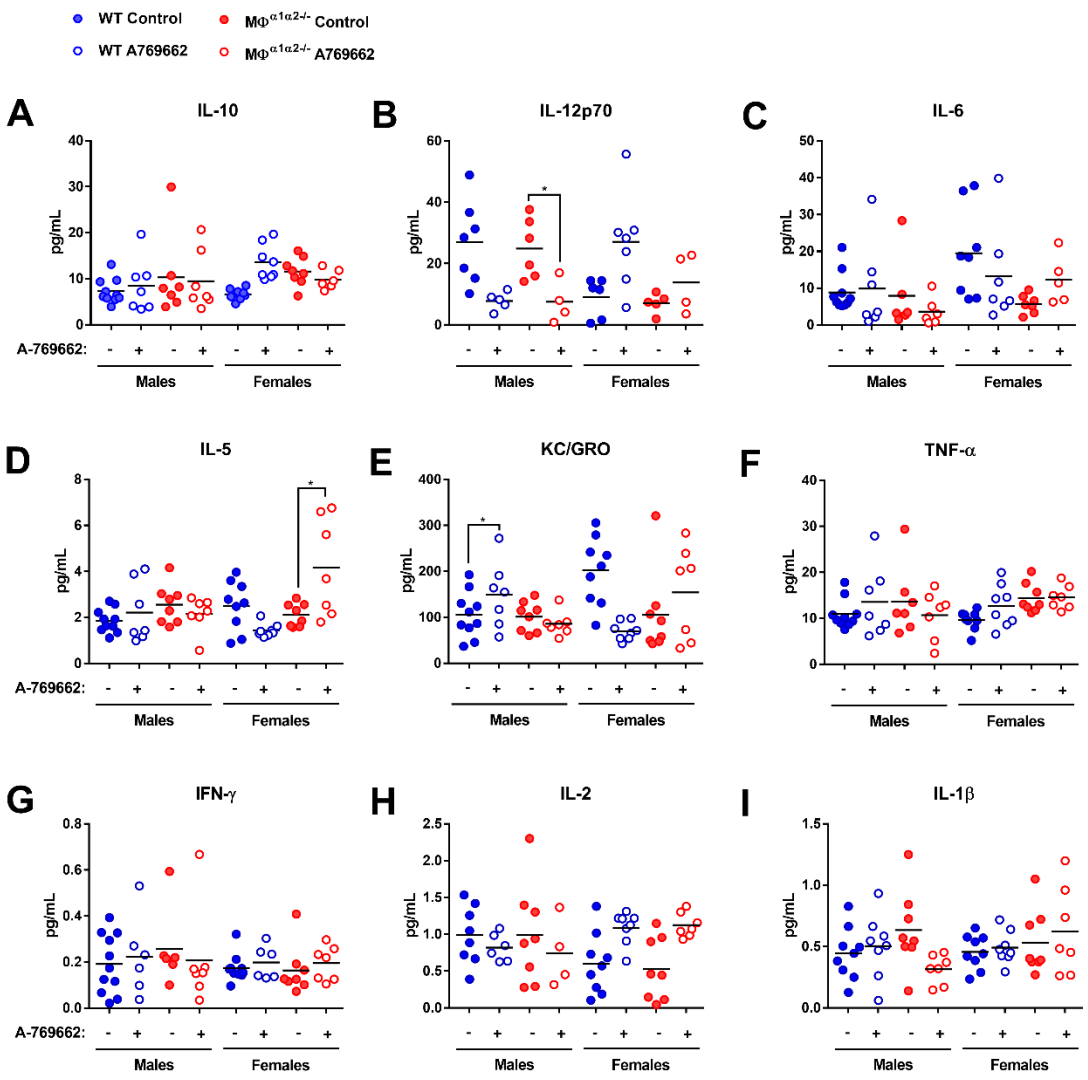

Figure 21. The role of myeloid AMPK and A769662-therapy on circulating inflammatory messengers. Endpoint plasma cytokines (A-I) were analyzed and quantified using the MSD MULTI-SPOT Assay system Meso Scale technologies for Scales Pro-inflammatory Panel 1 (mouse) kit as per manufacturer's instructions. Datum is representative of 4-10 WT and MacKO mice. Datum is reported as the mean value, where *P<0.05 was calculated by a two-way ANOVA using Prism8 software

3.3 DISCUSSION:

The progression of atherosclerosis is causative in the development of CVD. While our mechanistic understanding has translated to effective frontline therapies against cardiovascular disease, incidence and societal burden remain high. There are numerous pathways engaged and cell types initiated at the onset of atherosclerosis; however, metabolic and cell differentiation pathways of myeloid cells have been shown to be critical. Since AMPK is known to regulate multiple immunometabolic programs, we sought to address the importance of AMPK signaling in myeloid cells during the progression of atherosclerosis. Moreover, building on evidence that chronic preventative treatment of WD-fed ApoE-KO mice with AMPK activators (including A769662) protected against lesion development[198,212], we asked whether therapeutic intervention with pharmacological AMPK activation protects against atherogenesis in a myeloid AMPK-dependent manner.

We first sought out to address the contribution of myeloid AMPK activation in atherosclerosis in a preliminary study where we incorporated our pharmacological activator of AMPK, A769662, within highly targetable PLGA nanoparticles to improve drug delivery and efficacy. In attempt to develop therapeutically relevant treatment regimes, opposed to chronic AMPK activation for extended periods of time (10-12 weeks shown previously)[181,212], we intervened WD-fed LDLr-KO mice at 12-weeks with 6 intravenous injections of 7.5 mg/kg A769662-NP at 4-day intervals (Figure 11A). Following, we assessed atherosclerotic burden by staining lesion neutral lipids with Oil Red O (Figure 11B). We did not observe any alterations in lesion size influenced by targeted A769662-NP therapy within our preliminary findings (Figure 11C). With a short intervention time along with a total of 6-injections we predicted that our therapy was not sufficient in time and/or dosage to allow for lesion AMPK

to exhibit its anti-atherogenic effects. One important factor to consider is we could not confirm AMPK activity within the lesion microenvironment. Despite the inclusion of a fluorescent marker within all *in vivo* NP formulations, we failed to observe and enhanced or altered fluorescent output within the plaque contained within the aortic sinus of NP-treated mice. Additionally, using various AMPK-specific substrates (singly or in combination), we were unable to observe AMPK activation within the lesion by immunofluorescent techniques (Figure 13). In future studies, it would be important to find a method to observe AMPK activation within the lesion, with the probable adoption of immunohistochemical assays that have been validated within literature[213]. Building on these findings, we sought out an alternative approach to assess myeloid AMPK and its subsequent activation contribution within the progression of atherosclerosis.

Rather than deal with isoform-specific contributions, we chose to delete both catalytic subunits to best characterize the significance of myeloid AMPK signaling in atherosclerosis. To avoid lengthy breeding schemes and the constitutive nature of LDLr-KO and ApoE-KO mouse models, we administered a validated gain-of-function PCSK9-AAV (Asp377Tyr), which was driven by a liver-specific promoter. One potential limitation to all studies that have used $LysM^{Cre}$ as a driver of myeloid-specific disruption is the chronic and constitutive nature of the targeted deletion. However, even when this is considered, the largest discrepancy between studies that show a protective role and those that show a detrimental role for myeloid AMPK is dependent on genetic background (LDLr-KO vs. ApoE-KO, respectively). Atherosclerosis is lessened in response to myeloid AMPKα1 and AMPKα2 deletion only when on an ApoE-KO background[178,200]. Moreover, AMPKα1/ApoE-DKO mice had no difference in serum cholesterol and AMPKα2/ApoE-DKO mice had higher total cholesterol levels compared to floxed/ApoE-KO control mice, suggesting that these effects were independent of

circulating cholesterol. Contrary to this, circulating cholesterol levels in AMPKα1/LDLr-KO mice were positively correlated with lesion size and were increased when myeloid AMPKα1 was absent. Despite this, within our model we observed in male and female mice that there were no alterations in circulating total cholesterol or triglycerides regardless of phenotype or treatment (Figure 20).

Regardless of the animal's sex, we observed no difference in the progression of atherosclerosis between WT and MacKO animals (Figure 16A). Despite no significant alterations in the development of atherosclerosis, we observed a significant protection against WD-induced weight gain in male WT mice, along with a trending decrease in male MacKO animals (Figure 15C). This is indicates that our daily treatment regime with A769662 is improving WB metabolic features similar to what has been previously reported[199]. We observe a trending increase in neutral lipid-rich areas within male MacKO animals, however when intervened with A769662 these animals had a trending decrease in lesion lipid content comparable to WT controls (Figure 16B). This suggests that myeloid AMPK is playing a role within restraining lipid content within developing lesions, furthermore A769662-intervention therapy further protects against lipid accumulation in a myeloid AMPK-independent fashion (Figure 16B). However, since these effects are only modest, future studies designed to focus on these lipid-centric effects for myeloid AMPK (and A769662-therapy) during atherogenesis should be completed to confidently address any potentially important differences observed.

It has been documented that in response to cellular stressors, AMPK is able to promote that phagocytic capacity for macrophages and protects against cell death[214]. We predicted that AMPK may be involved in the resolution of necrosis within the lesion however we observed no difference in necrotic content regardless of sex, phenotype, or treatment (Figure 19). Despite our interrogations within lesion specific responses, it is our interpretation that

A769662-therapy provided beneficial metabolic effects, such that male WT mice were significantly protected from WD-induced weight gain (Figure 15C). We speculate that these improved metabolic and lipid-centric effects exhibited in male WT A769662-treated mice, is suggestive that A769662-therapy may be an effective therapeutic to protect against atherogenesis (or other metabolic pathologies such as obesity). However, additional studies are required to better optimize the time of intervention and duration of therapy to maximize its potential benefit.

AMPK signaling has been shown to directly[215,216] induce autophagy via activating phosphorylation of ULK1, Beclin-1 and VPS34, and indirectly via inhibition of mTORC1, which is regulated by AMPK-mediated phosphorylation of tuberous sclerosis complex 2 (TSC2) and/or regulatory-associated protein of mTOR (RAPTOR)[215,216]. It is now well established that autophagy is athero-protective[217] due to its clearance of cellular debris, sequestration of defective organelles and liberation of free cholesterol for the purpose of cholesterol efflux. To assess one marker of lesion autophagy, we stained lesions for p62, the accumulation of which is associated with defective autophagy[204]. Despite initial predictions, there were no genotype or treatment effects on the expression or localization p62 within the developed lesions, or macrophage-like cells (Figure 18). It remains entirely plausible and possible that the beneficial effects of AMPK signaling are linked to its regulation of autophagy; however, this is not captured by the staining of p62.

As previously mentioned, when myeloid AMPKα1 deletion was driven by LysM expression on a LDLr-KO background, these mice had more atherosclerotic lesion and plaque area, higher circulating lipids, more $LY6C^{hi}$ monocytes and increased levels of CD68 expression within the lesion[201]. Opposing this, when myeloid AMPKα1 was deleted via LysM expression on an ApoE-KO background, atherosclerotic lesions were smaller and had less

F4/80 expression within lesions[179,180]. This was attributed to an AMPKα1-dependent effect on regulating monocyte-to-macrophage differentiation and autophagy (for F4/80 expression) or an AMPKα2-dependent effect on DNA methylation and expression of extracellular matrix (for CD68 expression), respectively[200,201].

Our study highlights a possible role for myeloid AMPK and A769662-intervention therapy to reduce lipid content within atherosclerosis, however the experimental duration and therapeutic window may not capture the maximum potential for AMPK to restrict the progression of atherosclerosis. However, technical and experimental differences may help to explain discrepancies between ours and previously published work[200,201]. We were surprised to observe no difference in CD68 expression within lesions between conditions since both previous report on myeloid AMPKα1 described myeloid content as a leading contribution explaining their phenotype observed (Figure 17). Speculating about possible differences in molecular events to better interpret and explain the opposite phenotypes produced by $AMPK^{M\Phi\alpha1}$/ApoE-DKO to that of the $AMPK^{M\Phi\alpha1}$/LDLr-DKO we first thought about differential signaling events occurring intracellularly that may differ. Focusing our attentions firstly to the cell surface receptor LDLr, which is lacking in LDLr-KO mice and within our model of atherosclerosis, but not in ApoE-KO mouse models we tried to speculate if this could be contributing to the observable difference in phenotype by different groups. Recently, a novel role for the LDL receptor was describing where its C-terminal has the ability to shield protein-protein interactions, one of which being AMPK[218].

If LDLr exhibits regulatory effects on AMPK's substrate recognition, we speculate that these pathways would diverge between myeloid cells from LDLr-KO and ApoE-KO mice. A recent report made the unexpected observation that aldehyde dehydrogenase 2 (ALDH2) disruption was atheroprotective on an ApoE-KO background but atherogenic on a LDLr-KO

background[218]. In this pathway, the presence of the LDLr shielded AMPK from interacting and phosphorylating ALDH2, which leads to HDAC3-mediated down-regulation of various transcriptional responses. While this may be important to consider for future studies, currently it is unknown within the PCSK9-induced model, whether circulating PCSK9 has LDLr-lowering effects in non-hepatic tissues (specifically circulating monocytes and plaque macrophages), making any interpretation of myeloid AMPK signaling working via LDLr premature.

Implicating the LDL receptor in regulating AMPK substrate specificity, or other aspects of AMPK function and/or localization, allows ease of speculation for how signaling events may differ between macrophages from LDLr-KO and ApoE-KO mice. We observed in **Chapter 1** that the cell surface receptor, CD36, is implicated in regulating AMPK activity in response to lipid uptake (**Chapter 1**; Figure 4). It is possible something similar may be occurring between LDLr and AMPK. LDLr may have a regulatory role in AMPK substrate recognition, however if AMPK associates with LDLr there could be a chanced that it becomes complexed and consequently affect AMPK localization and cytosolic availability. These changes, if true, would impact AMPK signaling in macrophages within LDLr-KO animals but retained (theoretically) in ApoE-KO macrophages. To test the possibility of altered AMPK-signaling between macrophages isolated from either LDLr-KO or ApoE-KO mice, experiments designed to address potential differences in AMPK-regulated processes (and possibly localization) are a high priority in order to understand differences in phenotypes reported. Initial investigations could be performed using both the LDLr-KO and ApoE-KO mouse lines, isolating primary BMDM from both. Following, AMPK signaling and localization could be assessed both basally and in AMPK activated conditions (A769662 treatment) in culture.

To investigate potential differences in AMPK signaling, protein lysates from LDLr-KO and ApoE-KO macrophages (± A769662) could be separated by size by gel electrophoresis, then with immunoblotting techniques we could probe with AMPK's phosphorylation substrate motif antibody (LXRXX(pS/pT)). Probing for global changes in AMPK's phosphorylation of substrates may lead to observable differences in protein banding patterns between conditions and/or treatments. If differential banding patterns between genotypes persist, we could further isolate areas of interest for all conditions and attempt to identify candidate peptides and proteins by tandem mass spectrometry. This would help identify protein candidates subject to differential AMPK regulation within macrophages from different animal models of atherosclerosis. Alternative to this, AMPK localization could be assessed by immunofluorescent labeling of macrophages from LDLr-KO and ApoE-KO mice. Assessing if AMPK localization to the plasma membrane (co-localized with LDLr) or any other organelle (e.g. the lysosome) could be assessed in response to atherogenic modified LDL or pharmacological AMPK activators to investigate any differences in AMPK trafficking or localization within macrophages of each genotype (LDLr-KO and ApoE-KO).

ApoE is a secreted protein that travels through circulation, thus genetic ablation of the protein may be having numerous effects within WB physiology. Genetic removal of ApoE has shown to decreased expression of miRNA-146a in monocytes and macrophages but not in other myeloid and lymphoid cells. This is important in the context of atherosclerosis because within monocytes/macrophages miRNA-146a plays a role in dampening inflammation through the negative regulation of NF-κB in cells[219]. Another aspect of ApoE regulatory effects that is important to consider is its effect on hematopoiesis itself. Comparing LDLr-KO and ApoE-KO mice, it was shown that within ApoE-KO mice there is greater hematopoietic stem cell (HSC) proliferation, monocytosis, and leads to enhanced monocyte accumulation in

atherosclerosis compared to the LDLr-KO mouse model[220]. Taken together, in ApoE-KO mice, circulating monocytes may be primed to a more pro-inflammatory phenotype that could lead to increased localization to areas or lesion formation where expression of AMPKα1 may be crucial for monocyte-to-macrophage differentiation. Its possible that once in the developing lesion myeloid AMPKα1 may be exhibiting anti-atherogenic properties as exhibited in LDLr-KO mice, however it is not sufficient to combat increased myeloid cell chemotaxis. Based on what's known within literature, we speculate that ablation of either the LDLr or ApoE effects myeloid cells at different stages of atherogenesis providing a possible explanation between differences in phenotypes observed.

Speculating that myeloid AMPK may be either beneficial or detrimental in atherogenesis at different stages of disease progression between different genetic models of atherosclerosis highlights that timing may be crucial for interpretation of data. Focusing on the duration of each study, its plausible that the phenotypes observed are impacted by the duration of the study. It is possible that myeloid AMPK's role may have an oscillating role in atherogenesis, where during earlier stages it contributes to monocyte-to-macrophage differentiation, but exhibits anti-atherogenic properties at later stages in disease progression. Since *in vivo* interrogations within atherosclerosis are often intensive in terms of labor and time, its unlikely that studies are designed to look at early, intermediate, and advanced atherosclerosis within a single study.

If AMPK signaling is playing an oscillating role in atherogenesis, performing a study with only one time point may not be sufficient to completely understand what is actually taking place during the progression of atherosclerosis. Instead, we suggest that studies into AMPK signaling within atherosclerosis should look at least both an early and late time point to ensure phenotypic differences are present/absent at more than one stage of disease development.

Additional to this, we suggest that interrogating AMPK signaling within atherosclerosis using WB or cell type specific knockout models should not be sufficient to better our understanding of potential causative or preventative pathways regulated by AMPK. In place, we highly suggest future investigations begin to incorporate the use of knock-in mouse models, where AMPK regulation to a specific substrate could be removed through single point mutation (e.g. Ser871Ala on HMGCR). This would allow interrogation into specific AMPK-regulated pathways within atherosclerosis, and hopefully would mitigate any off-target effects or feedback loops caused by complete genetic removal of AMPK signaling.

In summary, our study suggests that myeloid AMPK and an intervening with a 6-week A769662 therapy were insufficient in protecting against atherogenesis. However, with our trending results we are optimistic that perhaps our experimental duration and treatment regime did not capture the maximum effect for myeloid AMPK and its activation within atherosclerosis. It would be important to address in future studies, if a longer therapeutic window (used as a preventative measure) may be effective enough to significantly protect against the progression of atherosclerosis. Regardless, since these studies are often time and labor intensive, we believe the next stage of investigations probing into AMPK in the context of atherosclerosis should move away from global or cell-type specific knockout models and in place incorporate knock-in models to specifically test distinct regulated processes such as autophagy or cholesterol synthesis. By removing AMPK's regulation of a single substrate, it could be possible to tease out the most beneficial pathways regulated by AMPK, possibly highlighting new therapeutic strategies and co-treatments for the most efficient way to combat atherosclerosis.

3.4 Materials and Methods:

Animal Studies: All experiments conducted were in accordance with the Canadian Council of Animal Care and approved by the Animal Care Committee at the University of Ottawa. All mice were housed in ventilated cages at ~23 °C and maintained on a 12/12 h light-dark cycle with *ad libitum* access to a standard rodent chow (44.2% carbohydrates, 6.2% fat, and 18.6% crude protein; diet T.2018, Harlan Teklad). Dr. Benoit Viollet graciously donated mice with both PRKAA1 and PRKAA2 floxed alleles on a C57Bl/6J background. Double floxed AMPKα1α2 mice were crossed with $LysM^{Cre}$ (LysM-Cre; C57Bl/6J background) hemizygous mice to produce MacKO mice along with AMPKα1α2-floxed control littermate mice (herein referred to as WT). At 10 weeks of age mice were injected intravenously (via tail vein injection) with 2.5 $x10^{10}$ genome copies of a mouse PCSK9-AAV (Asp377Tyr). Immediately following viral infection mice were placed on a WD to induce hypercholesterolemia. After 6 weeks, male and female WT and MacKO mice were assigned to groups that received daily intraperitoneal injections of either 30 mg/kg A769662 or a vehicle control (5% DMSO in PBS) for a further 6 weeks. Body weights were monitored weekly for the first 6 weeks, then monitored every second day during the last 6 weeks of intervention to ensure accurate dosage for treatment. Blood samples were collected at baseline and biweekly (following a 4-6 hour fast). After 12 weeks on the WD, mice were anaesthetized with a ketamine and xylazine mixture (150 mg/kg ketamine and 10 mg/kg xylazine), exsanguinated by cardiac puncture, and perfused with PBS. Tissues of interest were removed and either snap frozen in liquid nitrogen or placed in 10% formalin. The heart and aorta were carefully isolated and placed in 10% formalin and stored at 4 °C until processing.

Cardiac Tissue Embedding and Sectioning: Hearts were fixed in 10% formalin for 48 hours at 4°C, with sequential changing the formalin (at minimum 2 changes daily). Hearts were then transferred into sterile 20% sucrose (Bioshop) PBS solution for 72 h at 4°C, with bi-daily changes the sucrose solution. Prior to embedding, hearts were removed and dried gently of excess sucrose solution. A razor blade was used to cut transversely at roughly the central location of the heart. The top half (containing the aortic sinus) was embedded within a standard sized tissue cryomold (VWR) with then optimal cutting temperature medium (Thermo Fisher Scientific) was added to the cryomold to ensure the heart was fully submerged, each cassette was flash frozen with liquid nitrogen and stored at -80°C. The aortic sinus was sectioned using a cryostat (Leica CM 1850 cryostat) at 10 µm serial sections at -20 °C. Each given slide (Thermo Fisher Scientific) contained (at least) 6 serial selections collected at 100 µm intervals, spanning at least 600 µm on a total of 10 slides.

Oil Red O Staining: Slides containing aortic sinus cross sections were taken out of the -80°C freezer and let equilibrate at room temperature for 2 min, following slides were fixed in 10% formalin in a coplin jar for 10 min at room temperature. While fixation occurred, Oil Red O (Sigma-Aldrich) working solution (30 mL of 0.5% Oil Red O in isopropanol + 20 mL ddH_2O) was prepared and let equilibrate for 10 min. Following equilibration, the Oil Red O working solution was filtered initially with a coffee filter followed by filtration through a 0.45 µm syringe filter (VWR). Slides were washed once in 60% isopropanol and then stained in Oil Red O working solution for 5-15 min. Slides were washed twice with 60% isopropanol and then twice with PBS prior to hematoxylin counter staining (Cedarlane). Slides were washed twice with ddH_2O, once dry slides aqueous mounting media was added and a 1 ½ cover slide (Thermo Fisher Scientific) was mounted on the slide. Slides were imaged at 20X magnification

and tiled together with the EVOS FL auto 2. Atherosclerotic lesions denoted by positive Oil Red O staining and were selected and quantified using Image J analysis software. Each data point is representative of the summation of plaque area quantified from 4 sections spanning 400 µm within the aortic sinus from one animal.

Peritoneal macrophage isolation: Mice received an intraperitoneal injection of 1 mL sterile 3% thioglycolate medium (Sigma-Aldrich) four days prior to harvest to induce an inflammatory response for recruitment of immune cells. At harvest, mice were euthanized by cervical dislocation, the abdominal skin was removed to expose the peritoneal cavity. 10 mL of ice-cold PBS was slowly injected within the peritoneal cavity through a 20G needle, without removing the needle from the peritoneum, PBS and any free-floating peritoneal cells were slowly withdrawn back into the syringe. The 20G needle was removed and cells were slowly ejected into a sterile 50 mL conical tube (FroggaBio) and placed on ice until all isolations were completed. The cells were then spun down at 400 x *g* for 5 min at 4 °C, the supernatant was removed and the cell pellet was gently re-suspended in 10-30 mL culture media. Cells were seeded onto 1-3 100 mm cell culture plates and let adhere for 16 h, cells were then washed twice with PBS then gently scraped in complete DMEM and seeded onto 6-well tissue culture plate as needed.

Immunoblotting: Peritoneal cells were washed twice with ice-cold PBS, then cells were scrapped in 60-120 µL cell lysis buffer. For *ex vivo* liver samples ~20-30 mg of tissue was placed in a 2 mL reinforced bead mill tube (VWR) with three 2.8 mm ceramic beads (VWR) with 350-500 µL cell lysis buffer, then placed in a MagNA Lyser (Roche) tissue homogenizer for 40 sec at 6000 RPM. Following lysis protein was spun down 14000 RPM at 4 °C for 5 min,

the protein lysate was placed into a new microfuge tube and the pellet was discarded. Protein preparation and immunoblotting was performed as described in **Chapter 1**.

Immunofluorescent Labeling: Slides containing aortic sinus cross sections were taken out of the -80 °C freezer and let equilibrate at room temperature for 2 min, slides were then fixed in 2% PFA for 20 minutes. Following fixation, a hydrophobic marker (Millipore) was used to create barriers around all sections present on the slides. Slides were washed once in PBS then blocked/permeabilized with PBS containing 5% fatty-acid free BSA, 0.2% Triton X-100 and Tween-20. Samples were washed with PBS then co-stained with anti-mouse antibodies of interest (refer to **Appendix A**) for 1 hour in antibody solution (2% BSA, 0.1% Triton X-100 and Tween-20 in PBS) at room temperature in a dehumidified chamber (shielded from light). Samples were washed twice with PBS then incubated with anti-FITC Alexa-488 conjugated secondary anti-body (refer to **Appendix A**) for 1 hour at room temperature in a dehumidified chamber. Samples were washed then incubated in 300 nM DAPI (Thermo Fisher Scientific) for 5 min at room temperature shielded from light. Samples were washed twice in PBS, ProLong Gold antifade reagent (Invitrogen) was added to slides then mounted with 1 1/2 coverslip (Corning). Fluorescent microscopy images were taken using the EVOS FL Auto 2 Imaging System using a 20X magnification. All fluorescent images were processed and quantified using Image J analysis software.

Plaque CD68 Composition: Firstly, we defined and selected lesions from immunofluorescent images using Image J software. Selected lesion areas were quantified for specific regional analysis. The lesions underwent thresholding to measure positive areas of fluorescence (where

CD68 is expressed) within the plaque being defined as CD68+ area. The percent CD68+ area within the plaque was calculated as follows:

$$\%\ \text{CD68 Positive Plaque Area} = ((\text{CD68 positive Lesion Area}) \div (\text{Total Lesion Area})) * 100$$

Each reported value was the average of three sections within the aortic sinus of one animal, the exact same regions within the aortic sinus were quantified and compared for all animals.

Plaque Arg1 Composition: Firstly, plaque CD68 composition was assessed as above. Selected lesion areas were quantified for specific regional analysis. The CD68+ areas selected were used to provide an overlay for Arg1-specific channel. The area was then taken and results were reported as CD68+Arg1+ area as a fraction of the total plaque area.

Plaque CC3 Composition: Firstly, plaque CD68 composition was assessed as above. Selected lesion areas were quantified for specific regional analysis. The CD68+ areas selected were used to provide an overlay for CC3-specific channel. The area was then taken and results were reported as CD68+CC3+ area as a fraction of the total plaque area.

Lesion Autophagy: Firstly, we defined and selected lesions from immunofluorescent images using Image J software. Within selected regions we quantified single-channel fluorescent intensity values corresponding to p62 expression. The mean, median, and modal fluorescent intensities were analyzed within the plaque for each section, only the mean relative fluorescent intensity were reported. Each reported value was the average of three sections within the aortic sinus of one animal, the exact same regions were quantified and compared for all animals.

Plasma Lipid Determination: Mice were fasted for 4 hours prior to tail bleed (or cardiac puncture at experimental end point). Blood was left at room temperature for 30 min to allow to clot, then spun down at 3000 RPM for 10 min to allow for phase separation. The top opaque yellow phase (plasma) was collected, aliquoted and stored at -20 °C. Plasma was thawed and analyzed accordingly by the commercially available Infinity-cholesterol kit (Thermo Fisher Scientific) and the Triglyceride colorimetric assay kit (Cayman Chemical) as per manufacturer's instructions.

Liver Cholesterol Determination: In brief, ~30 mg of liver was homogenized in 500 µL PBS, liver lysate was snap frozen and thawed on ice twice to ensure full cellular lysis. Liver lysates were spun down at 14000 RPM for 5 min at 4 °C, the supernatant was placed within a new microfuge tube and the pellet was discarded. Following, 200 µL of lysate was used to perform a Bligh and Dyer lipid extraction[221]. Isolated lipids within the chloroform phase were then evaporated under nitrogen and re-suspended in 50 µL of isopropanol. Cholesterol was measured using the commercially available Infinity-cholesterol kit as per manufacturer's instructions and normalized to tissue weight.

Plasma Inflammatory Cytokine Analysis: Plasma cytokines were analyzed and quantified using the MSD MULTI-SPOT Assay system Meso Scale technologies. In brief, 25 µL of terminal plasma was used for determination of Meso Scales Pro-inflammatory Panel 1 (mouse) kit as per manufacturer's instructions.

Statistics: Statistical analysis using a one-way ANOVA was completed for Figure 11 (C), and Figure 2 (B-D). Analysis was performed comparing the mean of each group to the mean of

WT control. Statistical analysis using a two-way ANOVA was completed for Figure 15, Figure 16 (A and B), Figure 17 (B), Figure 18 (B and C), Figure 19, Figure 20 (A and B), and Figure 21 (A-I). Analysis was performed with multiple comparisons comparing the mean value for each group to the mean value to the mean value of alternate groups. Statistical significance was only reported between genotypes of the same treatment, or treatments within genotype in reference to the untreated control. Statistical significance is represented as follows for each Figure (if applicable); *P<0.05, **P<0.005, ***P<0.001. All statistics were done using Prism 8 software.

4.0 CHAPTER 3 – Investigating AMPK's suppression of cholesterol synthesis in the context of atherosclerosis.

4.1 Study Rationale:

Improving whole body and lesion cholesterol homeostasis has been a sought-after therapeutic approach to ameliorate the progression of atherosclerosis. In humans, the most common therapy to combat excessive cholesterol levels is to inhibit endogenous cholesterol synthesis through statin therapy, which uses pharmacological inhibitors of the rate-limiting enzyme in *de novo* cholesterol synthesis, HMGCR. The atheroprotective effects of statin therapy reduce the incidence and severity of atherosclerosis by reducing circulating cholesterol levels, however, statins have also been shown to possess pleiotropic effects showing a protection against atherogenesis independent on modulating circulating lipids[222–224]. HMGCR catalyzes the reduction of HMG-CoA to mevalonate, where mevalonate can be used as a pre-cursor for cholesterol synthesis, steroid hormone synthesis, or isoprenoid synthesis.

Recently, myeloid HMGCR expression was investigated in the context of atherosclerosis by the Cre-mediated deletion of HMGCR driven by the LysM promoter in LDLr-KO mice (HMGCR$^{M\Phi}$/LDLr-DKO). HMGCR$^{M\Phi}$/LDLr-DKO mice, which lack myeloid HMGCR expression, developed significantly less atherosclerosis than LDLr-KO control animals. HMGCR$^{M\Phi}$/LDLr-DKO mice had less inflammatory myeloid-derived monocytes and macrophages, which led to reduced myeloid cell chemotaxis into developing lesions[225]. Furthermore, the reduction of myeloid cell chemotaxis in HMGCR$^{M\Phi}$/LDLr-DKO animals led to significantly less lesion development in comparison to LDLr-KO control animals. Importantly, this highlighted that regulating HMGCR activity within the myeloid compartment may be a relevant method to combat atherosclerosis.

Since its discovery, AMPK has been known as an endogenous regulator of HMGCR, where it provides an inhibitory phosphate to HMGCR at Ser871 (in rodents). The anti-atherogenic effects of statin therapy in addition to the recent findings of myeloid HMGCR expression being causative in atherogenesis allowed us to speculate about the contribution of AMPK regulation of HMGCR in the context of atherosclerosis. We **hypothesized** that AMPK's inhibition of HMGCR is atheroprotective, however we further speculate that AMPK suppression within the hematopoietic compartment alone is sufficient to combat atherogenesis. Utilizing the HMGCR Ser871Ala mouse model (KI) that is insensitive to AMPK's regulation, we sought to test our hypothesis with two cohorts of mice to assess endogenous regulation of HMGCR activity within WB and the hematopoietic compartment in the context of atherosclerosis. All cohorts of mice were made susceptible to atherogenesis with the gain-of-function PCSK9-AAV (Asp377Tyr), which provides continued degradation of the LDL receptor leading to hypercholesterolemia on a WD (see **Chapter 2**).

4.2 RESULTS:

4.2.1 HMGCR KI macrophages have enhanced sterol synthesis insensitive to AMPK-activation while still possessing AMPK regulation of fatty acid synthesis.

We first sought out to confirm that macrophages isolated from KI mice were insensitive to AMPK-regulation, in addition we wanted to assess if there existed any feedback regulation to accommodate enhanced levels of mevalonate production in KI cells. We measured sterol and FA synthesis in cultured macrophages by radiolabeled acetate incorporation into saponifiable (FAs) and non-saponifiable (sterols) fractions following lipid extraction[226]. We observed that BMDMs isolated from HMGCR KI animals had elevated sterol synthesis (non-saponifiable lipids) basally and were insensitive to inhibition mediated by pharmacological AMPK activation with either 991 or A769662 (Figure 22A, refer to **Appendix B**). Despite elevated rates of sterol synthesis, we observed no difference in FA synthesis under basal or AMPK activated condition (Figure 22B) between KI and WT BMDMs, supporting the notion that KI cells experience normal signaling to other AMPK nodes.

4.2.2 Cholesterol uptake and total cholesterol content are unaffected by AMPK's regulation of HMGCR.

We observed previously that macrophages isolated from KI mice had increased rates of incorporation of radiolabeled acetate into sterols (Figure 22A), following this we wanted to address whether increased mevalonate production lead to alterations in cholesterol uptake (possibly due to alterations in protein prenylation) or total cholesterol content. We show that BMDM isolated from KI mice, had similar levels of acute acLDL uptake both basally and in AMPK activated conditions (Figure 23A). Additionally, we observed comparable levels of

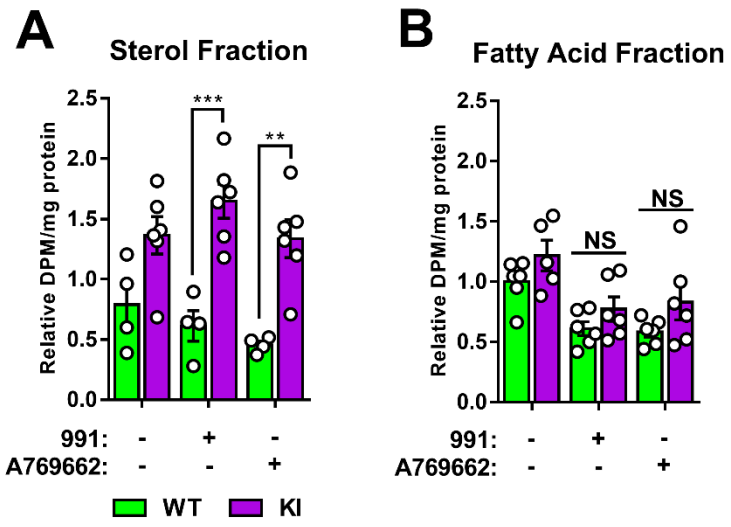

Figure 22. HMGCR KI macrophages have enhanced sterol synthesis that is unresponsive to AMPK activation but retain normal levels of fatty acid synthesis subject to AMPK regulation. (A and B) WT and KI BMDMs were isolated and co-treated for 4 h with 0.5 µCu/mL ^{3}H-acetate ± 991 or A769662. Lipids were separated into two fractions; saponifiable (A; sterol) and non-saponifiable (B; fatty-acids) for separate analysis. (A and B) [991]: 10 µM, [A769662]: 100 µM, [^{3}H-Acetate]: 0.5 µCi/mL, [^{3}H-Cholesterol]: 0.5 µCi/mL. Datum is representative of 4-6 independent experiments from BMDMs isolated from separate WT and HMGCR-KI mice. Datum is reported as the mean value ± SEM, where **P<0.005 and ***P<0.001 was calculated by a two-way ANOVA using Prism8 software.

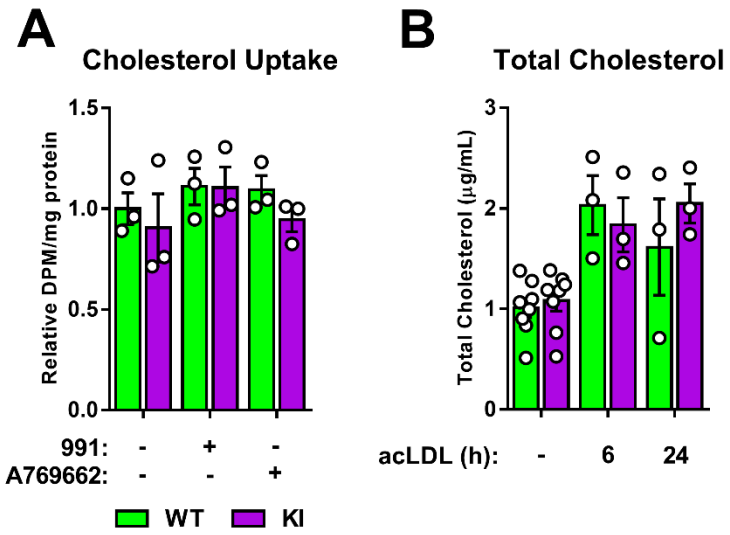

Figure 23. Macrophage AMPK's inhibition of HMGCR does affect basal cholesterol content or acute cholesterol uptake. (A) WT and KI BMDMs were isolated and cells were incubated for 30 min with acLDL(^{3}H-Cholesterol) ± 991 or A769662. Following, cells were lysed and radioactivity was measured within cell lysate and made relative to protein content to assess relative acLDL(^{3}H-Cholesterol) uptake. (B) WT and KI BMDMs were isolated and incubated with acLDL for either 6 or 24 h. Media was removed, cells were washed and processed for cholesterol determination by Amplex Red Cholesterol Assay Kit as manufacturers instructions. (a and b) [991]: 10 µM, [A769662]: 100 µM, [acLDL]: 50 µg/mL, [^{3}H-Cholesterol]: 0.5 µCi/mL. Datum is representative of 3-8 independent experiments from BMDMs isolated from separate WT and HMGCR-KI mice. Datum is reported as the mean value ± SEM, where results were found insignificant calculated by a two-way ANOVA using Prism8 software.

total cholesterol content between WT and KI macrophages under basal and in lipid-laden conditions (acLDL incubation; Figure 23B). Taken together with our previous findings of enhanced acetate incorporation into sterol fractions by KI cells (Figure 22A), these results suggest that enhanced sterol production may lead to alternative metabolic fates than cholesterol within KI macrophages.

4.2.3 AMPK's suppression of cholesterol synthesis does not affect basal or stimulated cholesterol efflux to extracellular cholesterol acceptors.

Macrophages isolated from KI animals had enhanced levels of sterol production (Figure 22A), while maintaining total cholesterol content comparable to WT BMDM. We speculated that enhanced mevalonate production within KI macrophages may being accommodated by enhancing cholesterol efflux to extracellular acceptors HDL and ApoA-I. In BMDM isolated from WT and KI animals, we lipid-loaded with acLDL(^{3}H-Cholesterol) and addressed their potential to export cholesterol specifically to HDL and ApoA-I under basal, AMPK-activated, and LXR-stimulated conditions (Figure 24). We observed that KI macrophages had the same rate of cholesterol efflux to ApoA-I (Figure 24A) and HDL (Figure 24B) under basal and in 'primed' conditions (T0901317 treated) as WT control BMDM. Surprisingly, we did not observe any increases in cholesterol efflux to either acceptor in response to AMPK activation in WT or KI BMDM (Figure 24). Taken together, this datum supports the notion that KI BMDM are not accommodating increased rates of mevalonate production by augmenting cholesterol efflux.

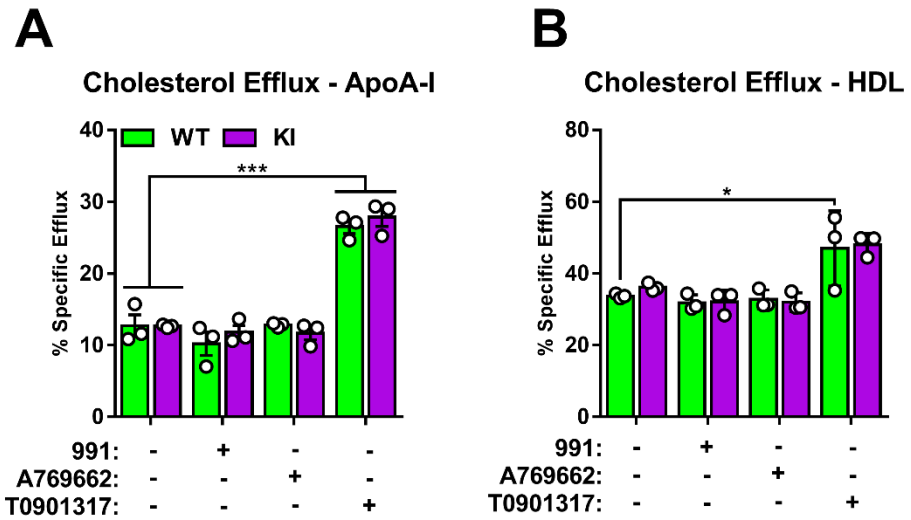

Figure 24. Macrophage AMPK's suppression of HMGCR does not alter basal or stimulated cholesterol efflux to ApoA-I or HDL. (A and B) WT and KI BMDMs were isolated and plated to assess cholesterol efflux to BSA, ApoA-I, and HDL, respectively. BMDMs were lipid loaded with acLDL(^{3}H-Cholesterol) for 24h, radioactive media was then removed and cells were equilibrated for 2 h in equilibration media (DMEM supplemented with 0.2% BSA, 0.1% FBS, and 1% antibiotics). Following media was removed and replenished with fresh equilibration media or equilibration media supplemented with either (A) ApoA-I or (B) HDL. WT and KI BMDMs in respective medias were treated with ± 991, A769662, T0901317 for 24 h. At endpoint all medium was collected and BMDMs were lysed, radioactivity was measured within the media and lysate and cholesterol efflux and percent specific cholesterol were calculated as stated in methods. (A and B) [991]: 10 µM, [A769662]: 100 µM, [T0901317]: 10 µM, [acLDL]: 50 µg/mL, [^{3}H-Cholesterol]: 0.5 µCu/mL, [ApoA-I]: 5 µg/mL, [HDL]: 50 µg/mL. Datum is representative of 3 independent experiments from BMDMs isolated from separate WT and HMGCR-KI mice. Datum is reported as the mean value ± SEM, where *P<0.05 and ***P<0.001 was calculated by a two-way ANOVA using Prism8 software.

4.2.4 HMGCR KI have differential transcript expression for genes within both the mevalonate and isoprenoid pathways.

We sought to further address any potential differences between WT and KI BMDM that may explain our previous findings. To accomplish this, we measured relative transcript expression in pathways related to mevalonate metabolism to probe for any possible differences. In BMDM isolated from KI mice, we observed significant increased transcript expression of HMGCR, farnesyl diphosphate farnesyl transferase 1 (*Fdft1*; $p = 0.07$), and mevalonate kinase (*Mvk*), suggesting AMPK's suppression of HMGCR triggers feedback regulation of transcript expression in proteins involved in mevalonate metabolism (Figure 25). In addition, we observed significantly lower transcript expression of *Dhcr24* ('24-Dehydrocholesterol reductase), an enzyme succeeding HMGCR in the biosynthetic pathway for cholesterol, which may help accommodate sterol levels in response to enhanced HMCGR activity (Figure 25). Additionally, in KI macrophages, we observed a significant increase in *Ggpps* (Geranylgeranyl diphosphate synthase 1) a protein important within the prenylation pathway (Figure 25). Both these genes are important in protein prenylation, where mevalonate is used as a precursor molecule for isoprenoid synthesis necessary for post-translation addition of isoprenoid moieties to proteins. This shed lights on protein prenylation as a possible modulated pathway to accommodate enhanced mevalonate production in KI BMDM.

4.2.5 Assessing AMPK's suppression of whole-body HMGCR in the context of atherosclerosis.

To address the role of AMPK's inhibition of WB HMGCR, we induced hypercholesterolemia by transduced WT and KI mice with the PCSK9-AAV (WT^{WB} and

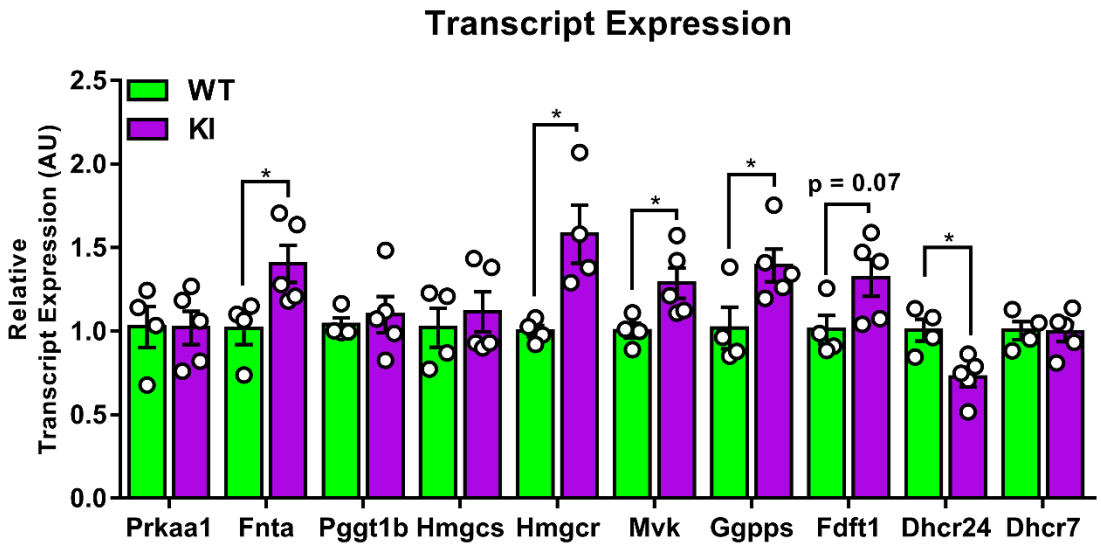

Figure 25. Differential transcript expression of genes within the mevalonate and isoprenoid synthesis pathways within HMGCR BMDMs. Quantitative polymerase chain reaction of WT and KI BMDMs relative transcript expression of genes involved in mevalonate and isoprenoid pathways. Datum is representative of 4-5 independent experiments from BMDMs isolated from separate WT and HMGCR-KI mice. Datum is reported as the mean value ± SEM, where *P<0.05 was calculated between genotypes of a single gene by a student's t test using Prism8 software.

KI^{WB}, respectively), then placed mice on a WD for 16-weeks (Figure 26A). Both WT^{WB} and KI^{WB} animals regardless of sex steadily gained weight for the duration of the 16-week WD feeding period (Figure 26B). On average, male mice gained more weight than their female genotype equivalents, however the Ser871Ala mutation within male and female KI^{WB} animals had no effect on weight gain (Figure 26C).

4.2.6 AMPK's suppression of whole-body HMGCR protects against lesion generation.

We assessed atherogenesis by staining for neutral lipids (with Oil Red O) within the aortic sinus, then measuring lesion size (Figure 27). We observed in male and female mice that lack AMPK's regulation of HMGCR developed significantly larger lesions (Figure 27A). These results support our hypothesis that AMPK's regulation of HMGCR protects against the development of atherosclerosis. Despite KI^{WB} animals only lacking AMPK regulation to one substrate, HMGCR, its enzymatic product mevalonate could be shuttled into synthetic pathways for cholesterol, steroid hormones, or prenylation that could be contributing to the phenotype observed. Additionally, within our global knock-in model we were unsure if the phenotype observed was dependent on signaling within the lesion, or if other tissues contributed or dictated lesion progression.

4.2.7 KI^{WB} animals have elevated total hepatic cholesterol but retain normal levels of circulating total cholesterol.

HMGCR's enzymatic product mevalonate has multiple metabolic fates possible, however with cholesterol being intimately linked to atherosclerosis this became the obvious choice for initial investigations. The liver is responsible for maintaining WB lipid homeostasis and lipoprotein metabolism, we speculated that the phenotype observed may be driven by

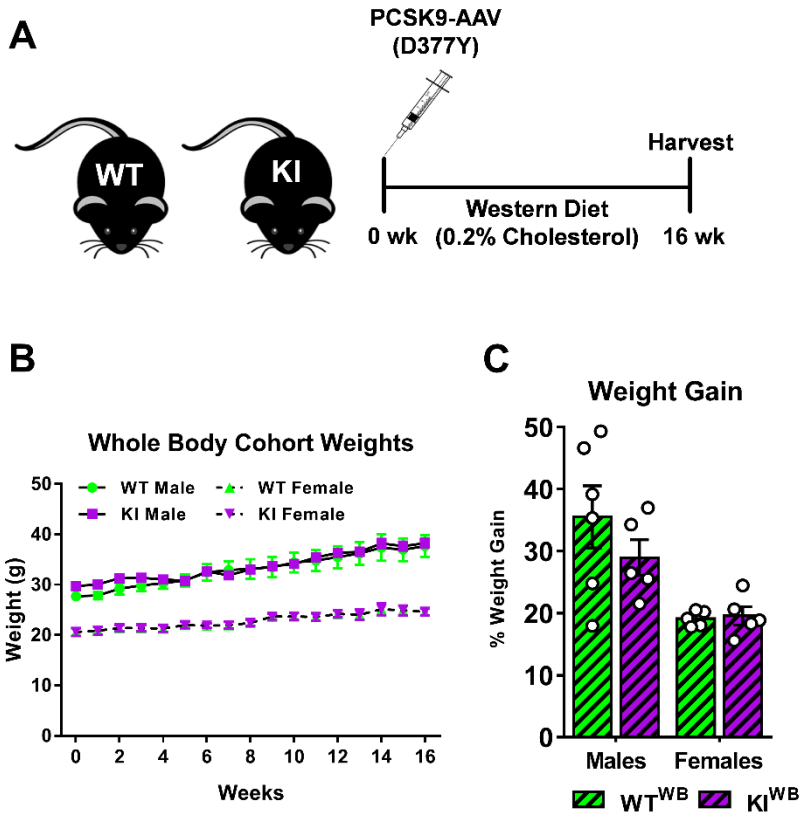

Figure 26. AMPK's negative regulation of whole-body cholesterol synthesis does not impact WD-induced weight gain. (A) Experimental schematic describing PCSK9-AAV transduction of WB WT and KI mice. (B) Weekly monitoring of WD-induced weight gain for WB WT and KI mice (WT^{WB} and KI^{WB}, respectively). (C) Quantification of percent weight gain assessed from basal to end point weight gain. Datum is representative of 5-6 WT^{WB} and KI^{WB} mice. Datum is reported as the mean value ± SEM, where results (C) were found insignificant calculated by a two-way ANOVA using Prism8 software.

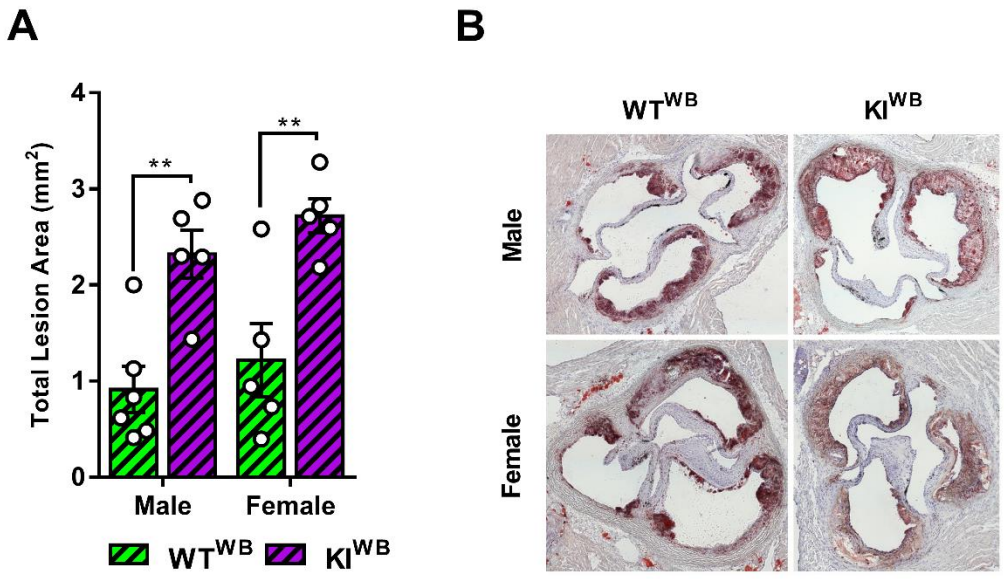

Figure 27. AMPK's negative regulation of whole-body HMGCR protects against the progression of atherosclerosis. (A) Quantification of lesion size in HMGCR KI WB cohort; lesions were stained and quantified from Oil Red O stained slides using Image J software, each data point is representative of the summation of lesion size from 7 serial sections (10 µm thick) spanning the same 700 µm within the aortic sinus of each animal. (B) Representative brightfield image of Oil Red O stained aortic sinus from WT^{WB} and KI^{WB} depicting lesions. Datum is representative of 5-6 WT^{WB} and KI^{WB} mice. Datum is reported as the mean value ± SEM, where **P<0.005 was calculated by a two-way ANOVA using Prism8 software.

altered signaling within the liver in KI^{WB} animals. We observed that male KI^{WB} animals trended to have elevated total hepatic cholesterol content in comparison to WT control animals, while female KI^{WB} animals had significantly higher total hepatic cholesterol (Figure 28A). Following this, we wanted to address if altered hepatic cholesterol content contributed to alterations in total circulating cholesterol, however we observed in both male and female mice had comparable levels of circulating total cholesterol (Figure 28B), which is suggestive that circulating lipid levels causative in the phenotype observed.

4.2.8 Whole-body inflammation does not contribute to accelerated lesion development in KI^{WB} animals.

Alterations in signaling within inflammation can indicate either regression or progression of atherosclerosis. We wanted to probe into levels of inflammatory chemical messengers within animals from the WB cohort to assess if changes in the inflammatory profile may contribute to the phenotypes observed within our study. We looked at various endpoint pro- and anti-inflammatory chemical messengers within circulation (IFN-γ, IL-10, IL-12p70, IL-2, IL-5, IL-6, TNF-α, KC, and IL-1β) however we did not observe any discernible trend between WT and KI animals (Figure 29A-I). Taken together, this datum suggests that inflammation within KI^{WB} animals is not dictating their susceptibility to atherogenesis, however further testing and experimentation is warranted.

4.2.9 Assessing the contribution of AMPK's inhibition of HMGCR within the hematopoietic compartment in the context of atherosclerosis.

It has been shown that the ablation of HMGCR expression in the myeloid compartment is atheroprotective[225], and we observed that AMPK's suppression of WB HMGCR protects

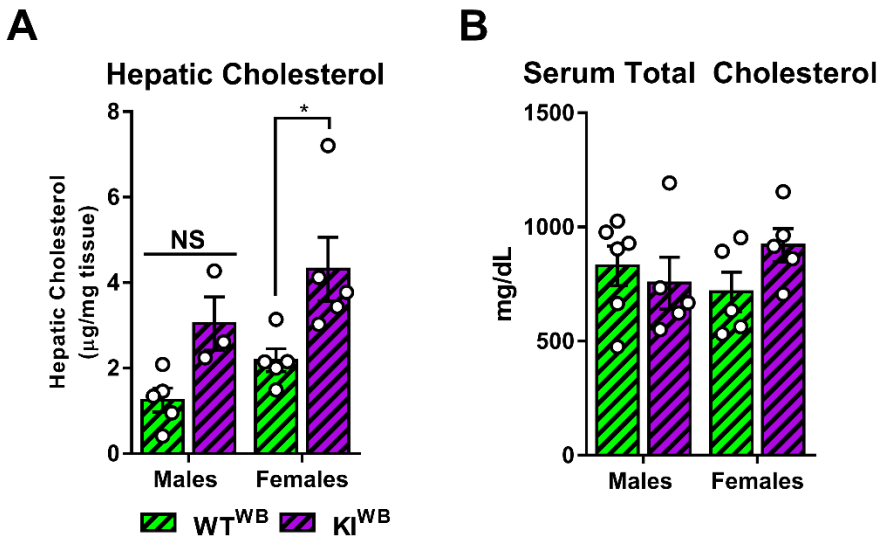

Figure 28. Total hepatic cholesterol content is affected by the Ser871Ala KI mutation within the WB, but it does not alter total levels of circulating cholesterol. (A) Relative hepatic cholesterol from the WT^{WB} and KI^{WB} mice. Lipids were isolated from hepatic tissue via Bligh and Dyer lipid extraction. Following isolation, lipids were evaporated down and re-suspended in isopropanol and total cholesterol was measured using Infinity Cholesterol Kit as per manufacturers instructions. (B) Total cholesterol from plasma collected from endpoint blood. Total cholesterol was measured using the Infinity Cholesterol kit as per manufacturers instructions. Datum is representative of 5-6 WT^{WB} and KI^{WB} mice. Datum is reported as the mean value ± SEM, where *$P<0.05$ was calculated by a two-way ANOVA using Prism8 software.

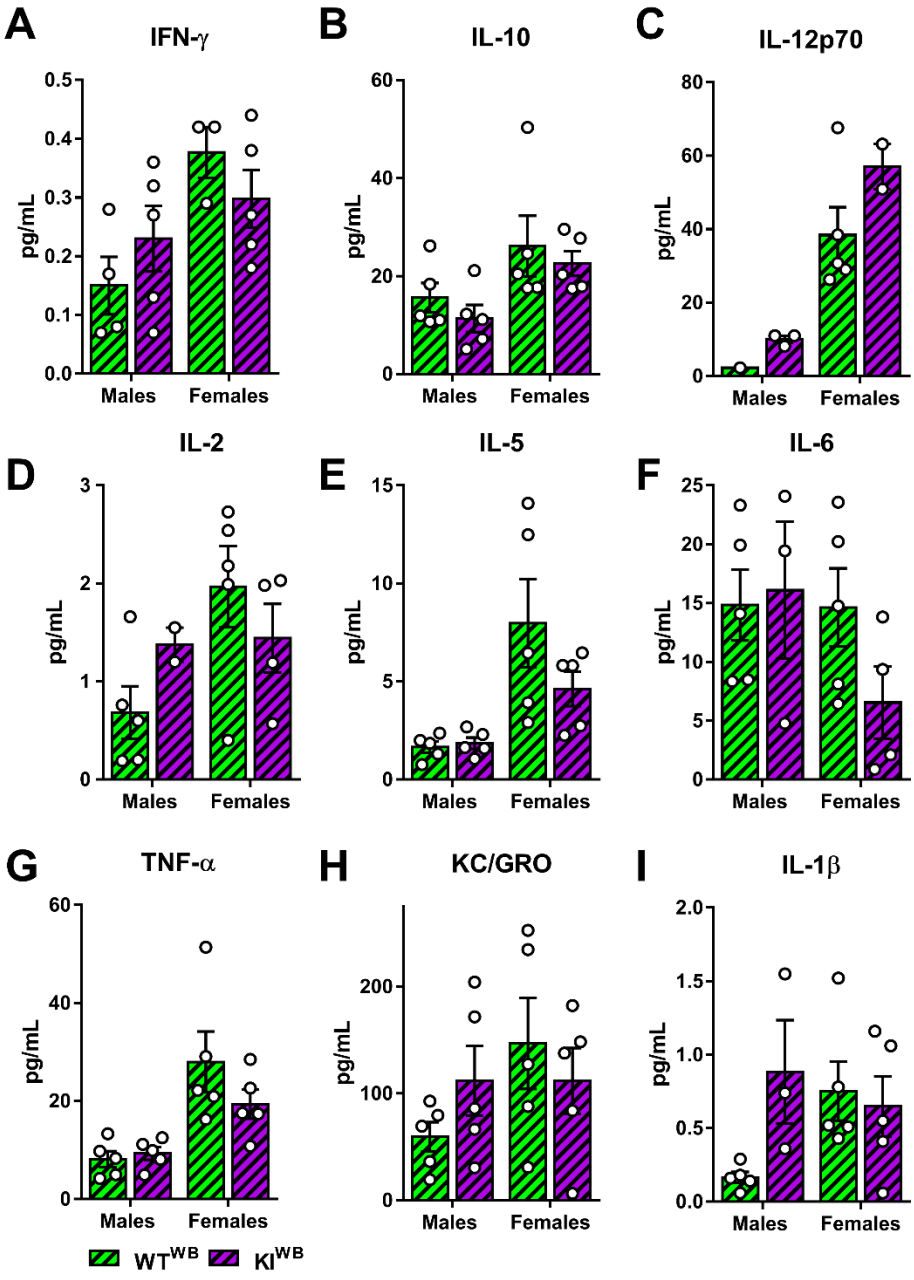

Figure 29. AMPK's negative regulation of whole-body cholesterol synthesis on circulating inflammatory messengers in atherosclerosis. (A-E) Circulating cytokines were analyzed and quantified using the MSD MULTI-SPOT Assay system (Meso Scale Technologies) for Pro-Inflammatory Panel 1 (mouse) as per manufacturer's instructions. Plasma was isolated from blood obtained by cardiac puncture at experimental end point for assessment of inflammation. (a) IFN-γ (B) IL-10 (C) IL-12p70 (D) IL-2 (E) IL-5 (F) IL-6 (G) TNF-α (H) KC/GRO (I) IL-1β. Datum is representative of 2-5 WT^{WB} and KI^{WB} mice. Datum is reported as the mean value ± SEM, where results found insignificant calculated by a two-way ANOVA using Prism8 software.

against lesion generation, an effect independent of circulating lipids. Knowing this, we speculated that AMPK's signaling to HMGCR within the hematopoietic compartment alone may be sufficient to protect against atherogenesis. To test this, WT mice were lethally irradiated mice then were subjected to a bone marrow transplant (BMT) with bone marrow collected from either WT or KI donor mice producing WT^{BMT} and KI^{BMT} animals, respectively (Figure 30A). Age matched WT^{BMT} and KI^{BMT} animals were transduced with the PCSK9-AAV and placed on a WD for 16-week to mimic the WB study. Similar to their WB counterparts, all mice steadily gained weight on a WD, which was not impacted by AMPK signaling within the hematopoietic compartment (Figure 30B-C).

4.2.10 AMPK's suppression of HMGCR within the hematopoietic compartment is atheroprotective.

Following 16-weeks of WD-feeding, we assessed the development of atherosclerosis within the aortic sinus of each animal for all groups. Neutral lipids within the aortic sinus were stained with Oil Red O to help visualize and describe all lesion areas (Figure 31B). We observed that female mice developed on average larger lesions than their male counterparts (Figure 31A) as previously documented[227,228]. Similar to the WB cohort, we observed that male and female KI^{BMT} animals developed significantly more plaque in comparison with WT^{BMT} control animals (Figure 31A). Despite having significantly more plaque, KI^{BMT} animals generated smaller lesions on average in reference to their genotype equivalents in the WB cohort (Figure 27). Comparing KI^{BMT} to KI^{WB} animals highlights that AMPK's suppression of hematopoietic HMGCR is atheroprotective, however it brings to light that AMPK's regulation of HMGCR in other tissues may be contributing to lesion formation.

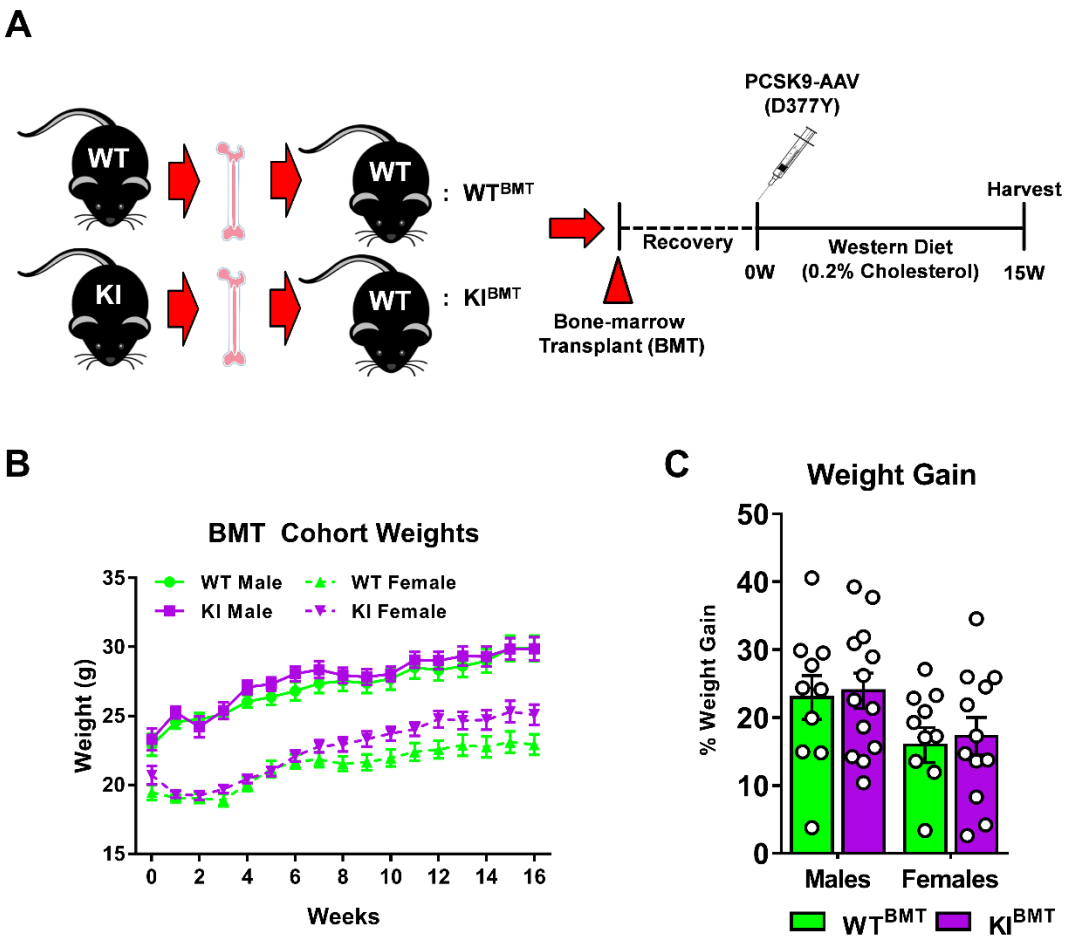

Figure 30. AMPK's negative regulation of hematopoietic cholesterol synthesis does not impact WD-induced weight gain. (A) Experimental schematic describing PCSK9-AAV transduction of WT BMT mice. (B) Weekly monitoring of WD-induced weight gain for BMT WT and KI mice (WT^{BMT} and KI^{BMT}, respectively). (C) Quantification of percent weight gain assessed from basal to end point weight gain. Datum is representative of 10-13 WT^{BMT} and KI^{BMT} mice. Datum is reported as the mean value ± SEM, where results (C) were found insignificant calculated by a two-way ANOVA using Prism8 software.

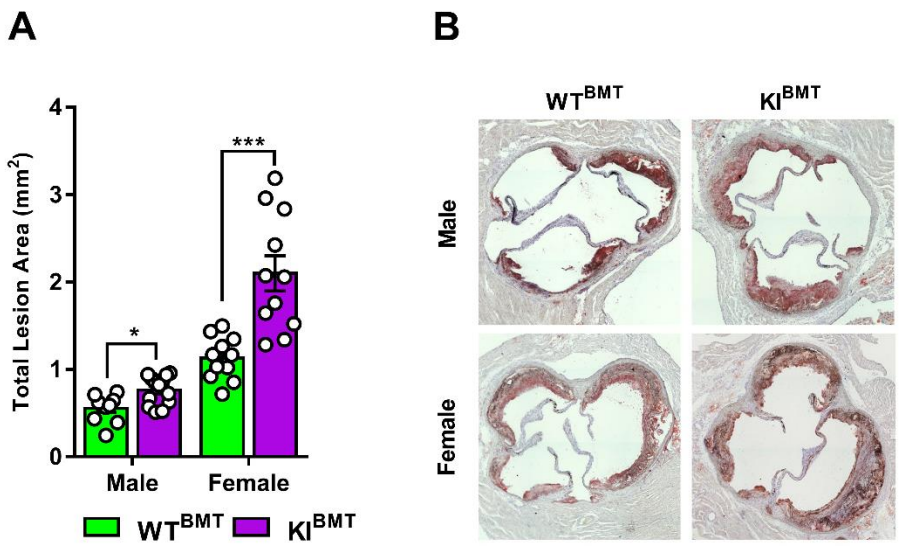

Figure 31. AMPK's negative regulation of hematopoietic cholesterol synthesis protects against the progression of atherosclerosis. (A) Quantification of lesion size in BMT cohort; lesions were stained and quantified from Oil Red O stained slides using Image J software, each data point is representative of the summation of lesion size from 7 serial sections (10 µm thick) spanning the same 700 µm within the aortic sinus of each animal. (A) Quantification of lesion size in HMGCR KI BMT cohort; lesions were stained and quantified from Oil Red O stained slides using Image J software, each data point is representative of the summation of lesion size from 7 serial sections (10 µm thick) spanning the same 700 µm within the aortic sinus of each animal. (B) Representative brightfield image of Oil Red O (ORO) stained aortic sinus from WT^{BMT} and KI^{BMT} depicting lesions. Datum is representative of 10-13 WT^{BMT} and KI^{BMT} mice. Datum is reported as the mean value ± SEM, where *P<0.05 and ***P<0.001 was calculated by a two-way ANOVA using Prism8 software.

4.2.11 AMPK's suppression of HMGCR within the hematopoietic compartment does not impact hepatic cholesterol or total circulating lipids.

Similar to the WB cohort, we thought it was important to address the possibility of altered hepatic cholesterol and circulating lipids within the BMT cohort. Dissimilar to the WB cohort, WT^{BMT} and KI^{BMT} animals had comparable levels of total hepatic cholesterol, which was predicted since KI^{BMT} animals should retain normal AMPK signaling within the liver (Figure 32A). Similar to the results obtained from the WB cohort, levels of total cholesterol and TG were equivalent between WT^{BMT} and KI^{BMT} animals that highlights that the phenotype exhibited by KI^{BMT} animals is not likely due to alterations in circulating total cholesterol in male animals (Figure 32B). We did observe a significant increase in total circulating cholesterol in female KI^{BMT} animals, which had much larger lesions that their respective male counterparts (Figure 32B). This is suggestive that there may exist sex-specific effects within these animals that are additionally contributing to larger lesion formation that is absent from the male cohorts, however future studies are required to further elaborate on sex-specific effects within our study.

4.2.12 Myeloid chemotaxis is not affected by AMPK's suppression of hematopoietic HMGCR.

Genetic removal of HMGCR from myeloid cells was shown to be atheroprotective, an effect that was partially explained by reduced myeloid cell chemotaxis within lesions from animals devoid of myeloid HMGCR[225]. We sought out to determine if myeloid chemotaxis was an underlining mechanism that promoted lesion development within KI^{BMT} animals (Figure 33A). We sought to address potential differences in myeloid content by staining for

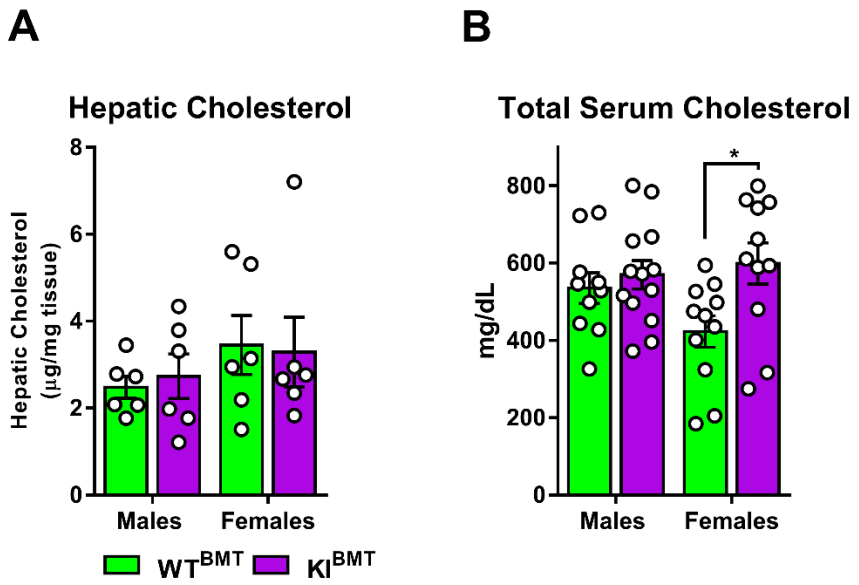

Figure 32. Total hepatic cholesterol content is unaffected by the Ser871Ala KI mutation within the hematopoietic compartment, however may be implicated in circulating total cholesterol levels in in female mice. (A) Relative hepatic cholesterol from the WT^{BMT} and KI^{BMT} mice. Lipids were isolated from hepatic tissue via Bligh and Dyer lipid extraction. Following isolation, lipids were evaporated down and re-suspended in isopropanol and total cholesterol was measured using Infinity Cholesterol Kit as per manufacturers instructions. (B) Total circulating cholesterol from plasma collected from endpoint blood. Total cholesterol was measured using the Infinity Cholesterol kit as per manufacturers instructions. Datum is representative of 10-13 WT^{BMT} and KI^{BMT} mice. Datum is reported as the mean value ± SEM, where *$P<0.05$ was calculated by a two-way ANOVA using Prism8 software.

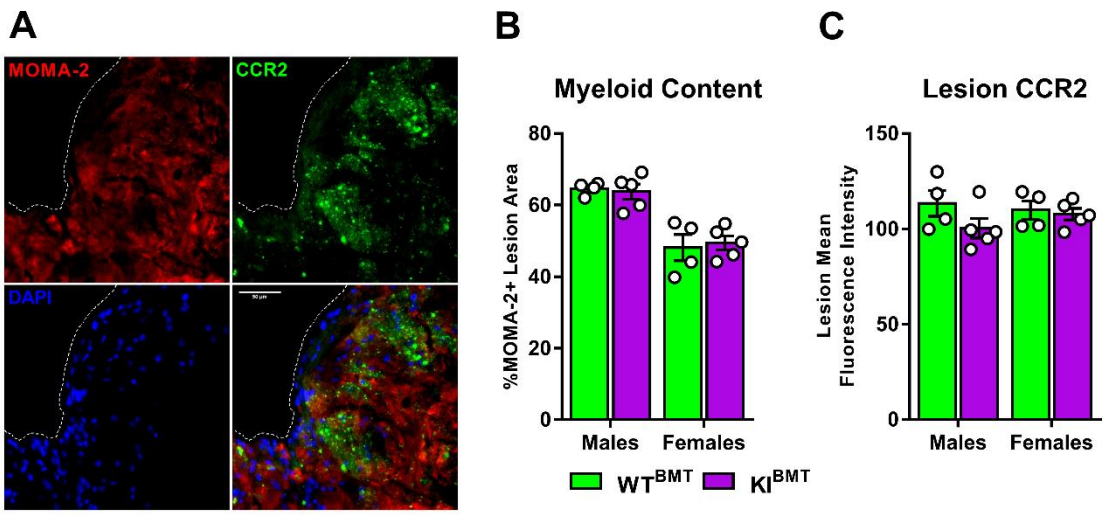

Figure 33. AMPK's regulation of hematopoietic cholesterol synthesis does not alter myeloid recruitment into developing lesions. (a) Representative close up image of immunofluorescent labeled atherosclerotic lesion (MOMA-2; RED, CCR2: GREEN, DAPI; BLUE). The white dotted-line represents the luminal lesion border. (b and c) Quantification of myeloid content (b; MOMA-2) and myeloid attractant protein (c; CCR2) within male WT^{BMT} and KI^{BMT} mice. Scale bar = 50 µm. All images were processed and quantified using Image J software. Data represents the mean value ± SEM (n = 4-5/group). Datum is reported as the mean value for 4-5 male WT^{BMT} and KI^{BMT} mice, where the results were found to be insignificant calculated by a two-way ANOVA using Prism8 software.

MOMA-2 (to label monocytes and macrophages) within the aortic sinus for BMT animals. In tandem, we additionally stained for CCR2 within lesions for the BMT mice, to probe for any alterations in myeloid recruitment into the developing lesion (Figure 33A). To our surprise, we observed no changes in lesion MOMA-2 and CCR2 expression in KI^{BMT} compared to WT^{BMT} mice regardless of sex (Figure 33B-C). This suggests that myeloid chemotaxis isn't driving the phenotypic difference observed, and larger lesion size within KI^{BMT} likely due to an alternative factor.

4.2.13 Circulating inflammatory messengers does not explain KI animals' susceptibility to atherogenesis.

Despite our evidence suggesting that KI^{WB} animals did not have significantly altered systemic inflammation, we wanted to address whether the same findings were apparent within the BMT cohort. We predicted that changes in systemic inflammation, if present, should be greater in animals lacking global regulation of HMGCR by AMPK. We observed no significant differences were observed, suggesting shifts in either pro- or anti-inflammatory signaling molecules within the BMT cohort (Figure 34A-I). This is suggestive that AMPK's inhibition of HMGCR isn't affecting systemic inflammation during the development of atherosclerosis.

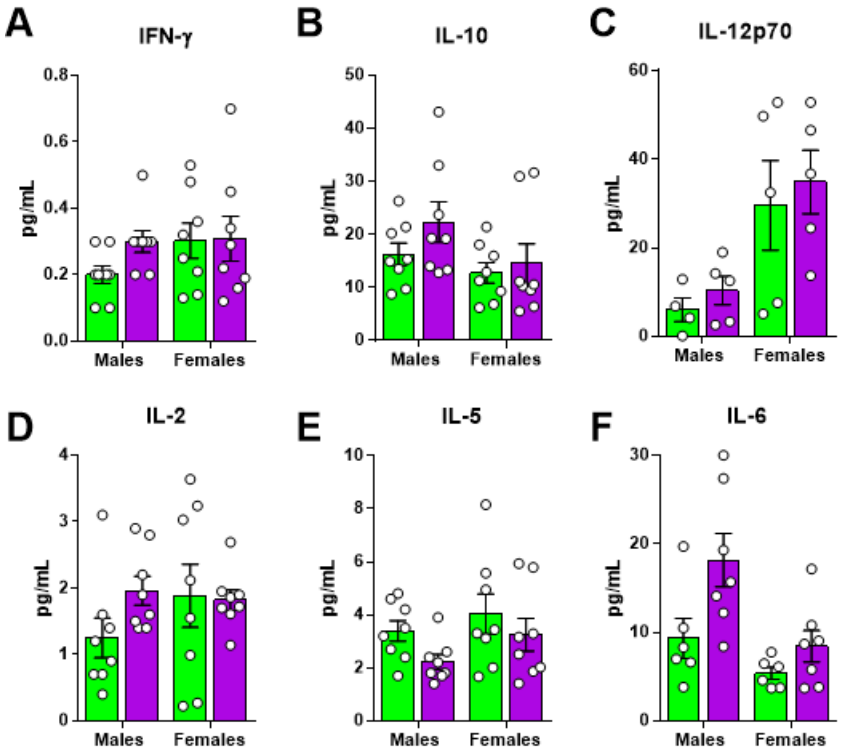
A
IFN-γ
pg/mL
0.8
0.6
0.4
0.2
0.0
Males
Females
B
IL-10
pg/mL
50
40
30
20
10
0
Males
Females
C
IL-12p70
pg/mL
60
40
20
0
Males
Females
D
IL-2
pg/mL
4
3
2
1
0
Males
Females
E
IL-5
pg/mL
10
8
6
4
2
0
Males
Females
F
IL-6
pg/mL
30
20
10
0
Males
Females

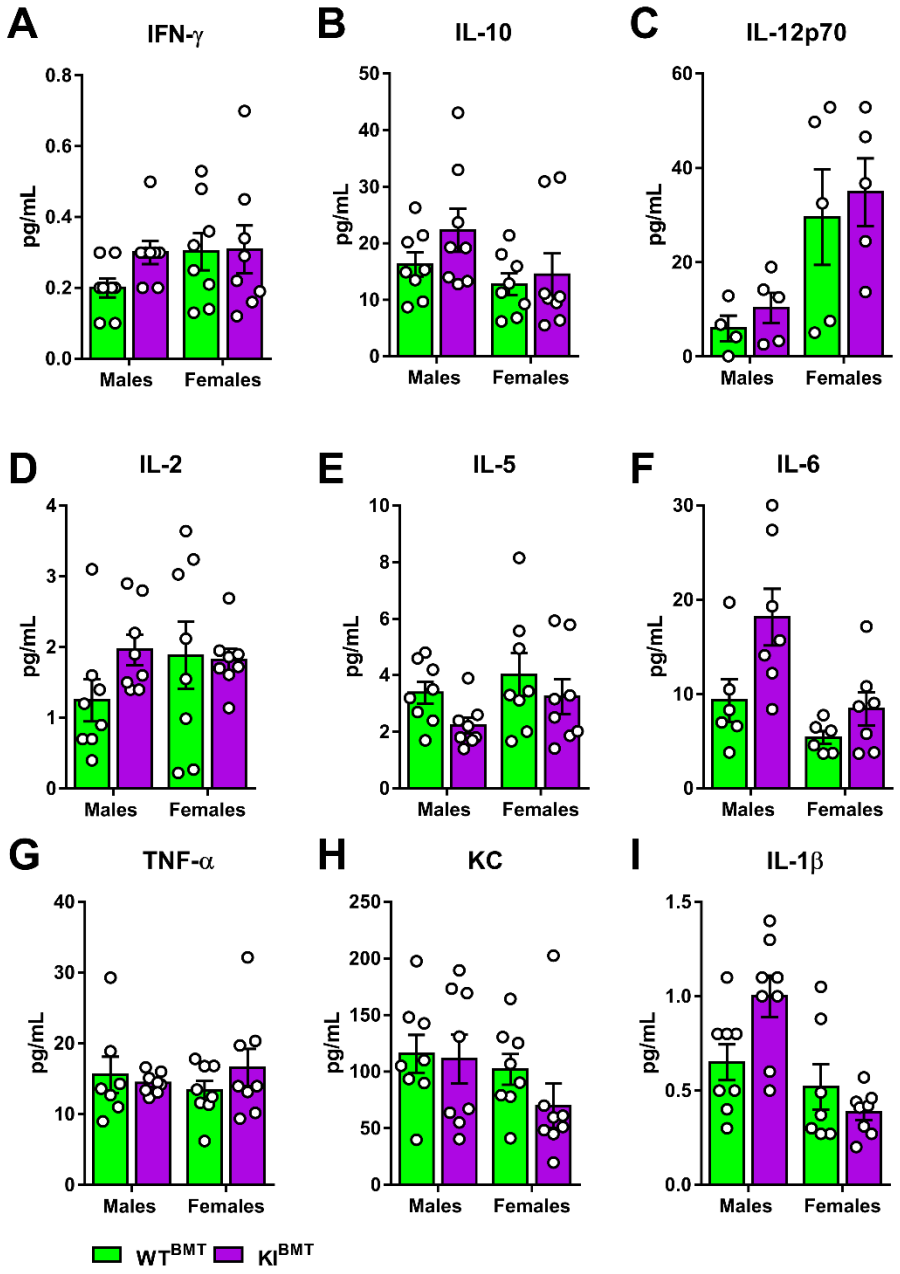

Figure 34. AMPK's negative regulation of hematopoietic cholesterol synthesis on circulating inflammatory messengers in atherosclerosis. (A-E) Circulating cytokines were analyzed and quantified using the MSD MULTI-SPOT Assay system (Meso Scale Technologies) for Pro-Inflammatory Panel 1 (mouse) as per manufacturer's instructions. Plasma was isolated from blood obtained by cardiac puncture at experimental end point for assessment of atherosclerosis. (A) IFN-γ (B) IL-10 (C) IL-12p70 (D) IL-2 (E) IL-5 (F) IL-6 (G) TNF-α (H) KC/GRO (I) IL-1β. Datum is representative of 4-8 WT^{BMT} and KI^{BMT} mice. Datum is reported as the mean value ± SEM, where results found insignificant calculated by a two-way ANOVA using Prism8 software.

4.3 DISCUSSION:

Since the results of the 4S trial (Scandinavian simvastatin survival study) in the 1990s, combating endogenous cholesterol synthesis by HMGCR suppression has been known as an effective strategy to combat the progression of atherosclerosis in humans[229]. Recently, the role of HMGCR within the myeloid compartment has been expanded on by describing a protective effect against lesion development in LDLr-KO mice devoid of myeloid HMGCR expression ($HMGCR^{M\Phi}$/LDLr-DKO). Reduced lesion content within $HMGCR^{M\Phi}$/LDLr-DKO mice was explained in part by reduction in inflammatory myeloid cells within circulation and less myeloid content within lesions[225]. Outside of its role in cholesterol synthesis, mevalonate (HMGCR's enzymatic product) is an essential precursor for steroid hormones, geranyl pyrophosphate, and farnesyl pyrophosphate, where the latter two are essential for protein prenylation. Thus, methods to downregulate or remove HMGCR activity within the myeloid compartment may exhibit diverse anti-atherogenic mechanisms not linked to cholesterol metabolism.

AMPK is an endogenous regulator of HMGCR through reversible phosphorylation. We sought to determine the role of AMPK-mediated inhibition of HMGCR in the development of atherosclerosis. In cultured KI BMDM, we observed increased acetate incorporation into saponifiable lipids (sterols) that was insensitive to AMPK inhibition stimulated by pharmacological AMPK activators 991 and A769662 (Figure 22). Despite increased level of acetate incorporation into sterols, total cholesterol content in basal and lipid-loaded conditions were comparable between WT and KI BMDM (Figure 23). We predicted that in KI BMDM, which possess increased acetate incorporation into saponifiable lipids but equivalent cholesterol content to WT BMDM, possess feedback regulation to cholesterol uptake and/or cholesterol efflux may to accommodate for excess sterol production. However, we observed

no difference in acLDL-cholesterol uptake (Figure 23) or cholesterol efflux to extracellular acceptors ApoA-I or HDL (Figure 24).

In order to interrogate potential differences exhibited by KI BMDM, we assessed relative transcript expression for genes within mevalonate metabolism and protein prenylation (Figure 25). In KI macrophages we observed a significant upregulation of HMGCR and mevalonate kinase (Figure 25), which is indicative that AMPK's suppression of HMGCR causes feedback regulation to suppress transcript expression of *Hmgcr*, *Fnta* and *Mvk*. However, we observed a down regulation of *Dhcr24* (`24-Dehydrocholesterol Reductase) an enzyme succeeding HMGCR, FTNA, and MVK in the biosynthetic pathway for cholesterol, which may be a mechanism to accommodate increased cholesterol synthesis at a later stage in the synthetic pathway. Additionally, we observed that select genes within the protein prenylation pathways (*Ggpps* and *Fdft1*; Figure 25) were upregulated, which may highlight prenylation as the main pathway to utilize increased mevalonate flux.

In support of our hypotheses, we observed that male and female mice with genetic disruption of AMPK signaling to HMGCR within the WB led to significantly larger lesion burden in comparison to respective WT^{WB} control animals (Figure 27). The accelerated atherogenesis observed in male and female KI^{WB} animals could be a lesion specific effect or may be dependent on by multiple tissues. The liver is responsible for maintaining WB cholesterol homeostasis through regulation of lipoprotein metabolism and homeostasis. In mice lacking HMGCR expression within hepatic tissue exclusively (HMGCR-LKO), it was observed that there was a significant decrease in hepatic acetate incorporation into cholesterol and total cholesterol levels. With lower levels of cholesterol within hepatic tissue isolated from HMGCR-KO mice, there was a significant increase in diglycerides and triglycerides[230].

We predicted that altered signaling to hepatic HMGCR within KI^{WB} mice may be contributing to the phenotype through alteration in hepatic cholesterol content and/or levels of circulating lipids. We measured total cholesterol within all animals and observed an increase in hepatic tissue isolated from KI^{WB} mice, but not WT^{WB} mice as predicted (Figure 28). Despite having elevated total hepatic cholesterol, we did not observe a difference between WT^{WB} and KI^{WB} mice in levels of circulating total cholesterol from blood collected at endpoint (Figure 28). This is suggestive that altered AMPK signaling to HMGCR in hepatic tissue is not contributing to altered lipoprotein metabolism, however we cannot rule out that the cholesterol distribution may vary between various lipoprotein fractions. In future studies it would be important to fractionate serum obtained from blood and assess cholesterol distribution within HDL, LDL, and VLDL proportions to fully address possible changes of circulating cholesterol within KI^{WB} animals.

We then sought out to determine if the accelerated atherosclerosis developed by male and female KI^{WB} animals was an immune cell specific effect. To accomplish this, we lethally irradiated WT mice, then transplanted bone marrow from either WT or KI mice to address AMPK's regulation of HMGCR within the hematopoietic compartment alone was atheroprotective. We observed that male and female KI^{BMT} animals developed significantly larger lesions within their aortic sinus compared to WT^{BMT} control animals (Figure 31). However, on average it was observed that the lesion size in KI^{BMT} animals was smaller compared to KI^{WB} animals. This depicts a protective role for AMPK-mediated suppression within the hematopoietic compartment alone, while highlighting a role for other tissues in contributing to the phenotypes observed.

Lipid rafts (LR) are microdomains within the plasma membrane that are composed of an assembly of proteins, cholesterol, and sphingolipids and are implicated in signal

transduction in HSC[231]. It was shown that the common β subunit of the GM-CSF and IL-3 receptors is localized to LRs in HSCs within ApoE-KO mice, and is important for HSC expansion in the bone marrow and spleen[232]. Additionally, enhanced cholesterol content in ABCA1/ABCG1-DKO mice was shown to increase HSPC mobilization and extramedullary hematopoiesis[233]. It is possible that in KI HSC, increased mevalonate production could lead to increases in LR cholesterol content or promote the retribution of cholesterol to LRs leading to elevated levels of hematopoiesis and immune cell infiltration within the developing lesion. Within HMGCR$^{M\Phi}$/LDLr-DKO animals[225], which lack endogenous cholesterol synthesis, the opposite is true, where it was observed that there is less myeloid inflammation and reduced myeloid infiltration into lesions.

To investigate whether myeloid cell inflammation and chemotaxis contributed to the phenotype observed in KI^{BMT} animals, we investigated lesion myeloid content and chemotaxis by quantifying the presence of monocyte/macrophage marker (MOMA-2) in tandem with CCR2 (an important receptor for myeloid chemotaxis) within the lesions (Figure 33). We did not detect any observable difference in lesion myeloid content or CCR2 expression, this supports the notion that myeloid inflammation and chemotaxis are not contributing to the phenotype observed. Furthermore, we addressed systemic inflammation within the WB and BMT cohort and concluded that circulating levels of pro- and anti-inflammatory messengers are not driving the phenotype observed in either cohort.

Statins largely contribute to reductions in atherosclerosis through inhibition of HMGCR resulting in plasma cholesterol lowering effects, however there been observations of a pleiotropic effect for statin therapy to protect against atherosclerosis independent of circulating lipids. HMGCR's enzymatic product mevalonate can be used as a precursor for generation of intermediate species farnesyl diphosphate (FPP) and geranylgeranyl diphosphate

(GGPP) that can be covalently linked to canonical C-terminal CXXX-motif on prenylated proteins (e.g. KRAS, RAS and RHO GTPases)[234]. Protein prenylation is a post-translational modification where lipid moieties are covalently linked to proteins aiding in their localization and association with plasma membranes. Prenylation is a crucial first step for membrane targeting and binding, both the Ras family of GTPases and heterotrimeric G-proteins all depend on prenylation for correct protein trafficking, which affects numerous processes such as growth, cell motility, and apoptosis[235]. We speculate that there is potential for increased flux of the HMGCR product, mevalonate, being shuttled to alternate fates such as use as a precursor for isoprenoid production, which may be a leading contributor to the phenotype observed in KI animals.

Dysregulation of prenylated proteins has been predicted to impact the development of atherosclerosis, where mutations in Ras are present in human atherosclerotic plaque[236]. Protein prenylation can impact numerous important cellular processes that may affect the development of atherosclerosis, studies have looked at specific branches of protein prenylation to aid in the understanding of its possible roles within atherogenesis. Investigating Ras function in atherosclerosis was performed using the inhibitor with farnesyl thiosalicylic acid (FTA) to assess atherosclerosis in ApoE-KO mice. FTA treatment was found to protect against atherogenesis in ApoE-KO mice fed either a WD or chow diet. Additionally, in WD-fed mice, FTA reduced fatty streak production in early atherosclerosis, and reduced lesion formation in late atherosclerosis[237]. Mechanistically, this was explained by reduction of NF-κB and VCAM-1 expression within the lesion microenvironment, dampened inflammation and reduced myeloid cell recruitment[237]. Expanding on the specificity of prenylated pathways during atherosclerosis, it was shown that blocking farnesylation within Manumycin A reduced Ras activation, Ras farnesylation, as well as Raf-1 phosphorylation in isolated aortas from ApoE-

KO mice. Additionally, this led to reduction of superoxide generation within the aorta, attributing to its significant protection from lesion generation in vehicle-treated ApoE-KO animals[238].

The role of GGPP-dependent prenylation within atherosclerosis was investigated by genetically removing Geranylgeranyl transferase type 1 (GGTase-I) from myeloid cells (by a Cre-mediated deletion driven by the LysM promoter) on an LDLr-KO background (GGTase-I$^{M\Phi}$/LDLr-DKO). They characterized the effect of removing GGPP prenylation on macrophage cholesterol efflux to ApoA-I and HDL. Macrophages isolated from GGTase-I$^{M\Phi}$/LDLr-DKO had improved cholesterol efflux to ApoA-I and HDL than LDLr-KO control macrophages[239]. Additionally, in cultured LDLr-KO macrophages, it was shown that pharmacologically inhibiting both GGPP and FPP prenylation (with GGTI and FTI, respectively) increased cholesterol efflux. Furthermore, BMDM isolated form GGTase-I$^{M\Phi}$/LDLr-DKO mice had increased rates of RCT *in vivo*, compared to LDLr-KO control BMDM[239].

When fed a WD for 12- and 24-weeks, it was observed that GGTase-I$^{M\Phi}$/LDLr-DKO mice developed significantly less atherosclerosis than LDLr-KO control animals. Additionally, GGTase-I$^{M\Phi}$/LDLr-DKO animals had reduced myeloid component within their lesions (less MOMA-2 staining), and significantly larger proportion of CD4+ T-cells. Despite possessing improved cholesterol homeostasis, and being protected against atherogenesis, GGTase-I$^{M\Phi}$/LDLr-DKO animals were observed to have more systemic inflammation than LDLr-KO control animals. However, despite improvements of cholesterol homeostasis and protection from atherosclerosis, GGTase-I$^{M\Phi}$/LDLr-DKO mice exhibited more inflammation both systemically and within cultured macrophages[239]. Taken together, this study showed that genetically disrupting GGTase-I-mediated prenylation improves cholesterol efflux and is

atheroprotective, however does negatively impact inflammation, this highlights the complexity of prenylation within the progression of atherosclerosis.

Taken together, these studies show instances where inhibiting prenylation (farnesylation and geranylgeranylation) exhibit protective effect against atherogenesis. In both the KI^{WB} and KI^{BMT} animals with our study, AMPK cannot provide its inhibitory phosphate to HMGCR at Ser871. However, despite increased activity of HMGCR in KI BMDM, total cholesterol does not change thus the enzymatic product mevalonate must be shuttled elsewhere to serve purposes outside of cholesterol biosynthesis. We speculate that mevalonate is being shuttled into the prenylation pathway, which would corresponding to enhanced prenylation of proteins that could be detrimental within atherosclerosis and a plausible explanation of the phenotype we've observed in both KI^{WB} and KI^{BMT} animals.

In future studies, it will be important to address the differences in the prenylome between WT and KI cells to give insight on which pathways may be exhibiting anti- or pro-atherogenic effects. With the adoption of 'click chemistry', where fluorescent tags can be covalently linked to GGPP or FPP, we could assess global changes in prenylation exhibited in KI cells by flow cytometry under basal and AMPK activated conditions. If excess mevalonate produced by HMGCR in KI cells is being shuttled in the prenylation pathway, we predict that we would see a global increase of labeled GGPP and FPP incorporation in KI cells, but not WT. If there is a significant difference in the prenylome between WT and KI cells, it would be important to address the role of increased protein prenylation has during atherosclerosis.

In mice lacking hepatic HMGCR expression, it was shown that supplementation of mevalonate within the drinking water attenuated liver dysfunction and hypercholesterolemia in addition to restoring levels of membrane associated H-RAS and Rac1[230]. Adopting this line of experimentation within our research model would be important to address if

supplementation of mevalonate or isoprenoids in addition to the WD could induce accelerated atherosclerosis in WT mice similarly to the extent we observed in KI^{WB} and KI^{BMT} animals. If excess mevalonate is leading to increased flux into isoprenoid synthesis, we would predict by supplementing isoprenoids within the diet/water of WT, but not KI animals, may produce a comparable phenotype. If this does not alter lesion formation in WT mice, this would suggest a role outside of the protein prenylation to explain the phenotype produced by KI animals.

Systemic AMPK activation therapy has shown to be atheroprotective in ApoE-KO mice, which is explained by reduction of myeloid cell chemotaxis into developing lesions[181,182]. This comparison mirrors the phenotypic comparison of LDLr-KO mice to LDLr-KO mice lacking myeloid HMGCR expression, where removal of myeloid HMGCR reduces chemotaxis of myeloid cells into developing lesions[225]. Incorporation of a treatment regime to activate AMPK systemically in WT and KI atherogenic mice is an important next step following this study. Determining whether extended systemic AMPK activation therapy could rescue the phenotype exhibited by KI animals (WB and BMT), may shed light on the contribution of other processes relevant in atherosclerosis that AMPK is regulating. If AMPK activation therapy does not recue the phenotype it could illuminate AMPK's negative regulation of HMGCR as a leading anti-atherogenic process, which may have been missed within studies focussing on total removal of AMPK-regulated processes in whole-body or myeloid cells specifically.

Alternative to cholesterol synthesis and protein prenylation, increased mevalonate production in KI animals may be accommodating by increased flux to steroid hormone production. In order to interrogate any possible differences in hormone production, measurements between WT and KI mice (under basal and WD conditions) circulating hormones could be assessed with relative ease using commercially available kits or ELISAs

(enzyme-linked immunosorbent assay). This line of investigation may be beneficial to help explain any sex specific differences observed as well, such as significantly increased circulating cholesterol in KI^{BMT} female mice (Figure 32) and altered circulating inflammatory messengers (Figure 34).

Taken together, these results support that AMPK's regulation of WB and hematopoietic HMGCR is protective against atherogenesis. This was without changes or alteration of myeloid chemotaxis within developing lesions. This study shows the importance of utilizing knock-in mouse models to interrogate specific questions on AMPK signaling in the pathogenesis of disease, specifically atherosclerosis and highlights the importance of interrogating specific AMPK-regulated pathways in addition to global and cell-type specific knockout studies.

3.5 MATERIALS AND METHODS:

Animal Studies: All experiments conducted were in accordance with the Canadian Council of Animal Care and approved by the Animal Care Committee at the University of Ottawa. All mice were housed in ventilated cages at ~23 °C and maintained on a 12/12-hour light-dark cycle with *ad libitum* access to a standard rodent chow (44.2% carbohydrates, 6.2% fat, and 18.6% crude protein; diet T.2018, Harlan Teklad). All WT and HMGCR Ser871Ala KI mice described are on a C57Bl/6J background. For BMT experiments bone-marrow from four WT and four KI donor mice was isolated (as described in **Chapter 1**) and pooled (per genotype) for both the male and female cohorts. WT recipient mice were lethally irradiated with two doses of 450 RADs (900 RADs total) 1-2 hours prior to transplantation. Following successful transplantation, mice were monitored for 4 weeks for recovery. After recovery, mice were injected intravenously with 2.5 $x10^{10}$ genome copies of a mouse PCSK9-AAV (D377Y). This plasmid was obtained from Addgene (plasmid # 58376; which was a kindly deposited by Dr. Jacob Bentzon), and packaged in an AAV8 by the Penn Vector Core at the University of Pennsylvania. Immediately following viral infection mice were placed on a WD (40% kcal from fat, 43% kcal from carbohydrate, 17% kcal from protein, with 0.2% cholesterol – Research Diets D12079) to induce hypercholesterolemia. In tandem, WT and HMGCR-KI mice at 12 weeks of age were injected intravenously with 2.5 $x10^{10}$ genome copies of a mouse PCSK9-AAV (Asp377Tyr) and placed on the WD. After 16 weeks of WD feeding, mice from both cohorts were anaesthetized with a ketamine and xylazine mixture (150 mg/kg ketamine and 10 mg/kg xylazine), exsanguinated by cardiac puncture, and perfused with PBS. Tissues of interest were removed and either snap frozen in liquid nitrogen or placed in 10% formalin

(Sigma-Alrich). The heart and aorta were carefully isolated and placed in 10% formalin and stored at 4 °C until processing.

Cardiac Tissue Embedding and Sectioning: Processing and sectioning of the tissue was completed as described in **Chapter 2**. Each slide contains 9 serial selections collected at 100 µm intervals, spanning at least 400-900 µm on a total of 10 slides.

Oil Red O Staining: Staining and imaging was completed as described in **Chapter 2**. Each data point is representative of the summation of plaque area quantified from 7 sections spanning 700 µm within the aortic sinus from one animal.

Cholesterol Efflux: Cholesterol efflux was performed as previously described in **Chapter 2**. A769662 (100 µM), 991 (10 µM; Abintio Bioscience), and T0901317 (10 µM; Torcis) were used as treatments for the duration of the efflux to HDL and ApoA-I.

Measuring lipid synthesis within macrophages: WT and KI BMDMs were harvested and plated within a 6-well tissue culture plate at a density of 1.2 million cells per well (triplicate wells plated for each genotype) in culture media (as previously described in **Chapter 1**). Measurements in lipid synthesis was performed as dictated in Springer's AMPK Methods and Protocols[226], where BMDMs were treated with either A769662 (100 µM), 991 (10 µM), or 0.2% v/v DMSO for 4 hours.

Measuring macrophage cholesterol uptake: WT and KI BMDMs were harvested and plated within a 6-well tissue culture plate at a density of 1.2 million cells per well (triplicate wells

plated for each genotype) in culture media (as previously described in **Chapter 1**). Macrophage cholesterol uptake was analyzed by acute uptake of acLDL (50 µg/mL) in culture. The day prior to experimental start, acLDL was incubated with ^{3}H-cholesterol (0.5 µCi/mL) in culture media overnight at 37ºC. The following day BMDMs were incubated with radiolabeled-acLDL for 30 min. Following, all media was removed and cells were washed twice with ice-cold PBS prior to lysis with 250 µL NaOH (0.1 M). The lysate (125 µL) was transferred into a 7 mL scintillation vial containing 5 mL of liquid scintillation fluid. All samples radioactivity was measured by analyzing on a liquid scintillation counter. Protein determination was performed on 25 µL of protein lysate via the Pierce's BCA assay (as previously described in **Chapter 1**). Cholesterol uptake was expressed by normalizing cellular lysate DPM (disintegrations per minute) to mg/mL of protein.

Macrophage mevalonate pathway transcript expression analysis: WT and KI BMDMs were harvested and plated within a 12-well tissue culture plate at a density of 0.6 million cells per well (triplicate wells plated for each genotype) in culture media (as previously described in **Chapter 1**). All BMDMs were lysed with TriPure as described in **Chapter 1**.

RNA Isolation: RNA isolations were performed as previously described in **Chapter 1**.

RNA quantification: RNA quantification was performed as previously described in **Chapter 1**.

cDNA synthesis: The synthesis of cDNA from RNA was performed as previously described in **Chapter 1**.

Quantitative PCR: Quantitative PCR was preformed as previous described in **Chapter 1** for all genes (refer to **Appendix A**).

Immunofluorescent Labeling: Immunofluorescent labeling was performed as described in **Chapter 2**, however MOMA-2-Alexa-647 (refer to **Appendix A**) and CCR2-FITC (refer to **Appendix A**) were used in place of CD68 and p62, respectively.

Lesion Myeloid Content: Firstly, we defined and selected lesions from immunofluorescent images using Image J software. Selected lesion areas were quantified for specific regional analysis. The lesions underwent thresholding to measure positive areas of fluorescence (where MOMA-2 is expressed) within the plaque being defined as MOMA-2+ area. The percent MOMA-2+ area within the plaque was calculated as follows:

$$\%\ \text{MOMA2 Positive Plaque Area} = (\text{(MOMA2 positive Lesion Area)} \div \text{(Total Lesion Area)}) * 100$$

Each reported value was the average of three sections within the aortic sinus of one animal, the exact same regions within the aortic sinus were quantified and compared for all animals.

Lesion CCR2 Expression: Firstly, we defined and selected lesions from immunofluorescent images using Image J software. Within selected regions we quantified single-channel fluorescent intensity values corresponding to CCR2 expression. We analyzed the mean, median, and modal fluorescent intensities for the combined plaque within a section, only report the mean fluorescent intensity were reported. Each reported value was the average of three sections within the aortic sinus of one animal, the exact same regions were quantified and compared for all animals.

Plasma Lipid Determination: Plasma lipid determination was completed as described in **Chapter 2**.

Liver Cholesterol Determination: Liver cholesterol determination was completed as described in **Chapter 2**.

Plasma Inflammatory Cytokine Analysis: Plasma cytokines were analyzed and quantified using the MSD MULTI-SPOT Assay system Meso Scale technologies. In brief, 25 µL of terminal plasma was used for determination of Meso Scales Pro-inflammatory Panel 1 (mouse) kit as per manufacturer's instructions.

Statistics: Statistical analysis using a two-way ANOVA was completed for Figure 22 (A and B), Figure 23 (A and B), Figure 24 (A and B), Figure 26 (C), Figure 27 (A), Figure 28 (A and B), Figure 29 (A-I), Figure 31 (A), Figure 32 (A and B), Figure 33 (B and C), and Figure 34 (A-I). Analysis was performed with multiple comparisons comparing the mean value for each group to the mean value to the mean value of alternate groups. Statistical analysis using a student's t test was completed for Figure 25 for genotype comparisons for all genes listed. Statistical significance was only reported between genotypes of the same treatment, or treatments within genotype in reference to the untreated control. Statistical significance is represented as follows for each Figure (if applicable); *$P<0.05$, **$P<0.005$, ***$P<0.001$. All statistics were done using Prism 8 software.

INTEGRATED DISCUSSION AND CONCLUSIONS

Atherosclerosis is a multifactorial disease. Accumulated plaque within vasculature restricts blood flow that leads associated co-morbidities such as myocardial infarction and stroke, and CVD, all of which remain a principal source of morbidity and economic burden amongst Canadians for the last century[1]. There are numerous genetic factors ranging in both complexity and severity that predispose an individual to the development of atherosclerosis. Heritable diseases such as familial hypercholesterolemia and type 2 diabetes impact WB lipid homeostasis that can lead to lipid retention within vessel walls[240,241]. Alternatively, more common complications that lead to hypertension or altered circulating lipoprotein profiles can also lead to susceptibility within seemingly healthy individuals. In tandem with the numerous environmental factors such as diet, smoking, and exercise, the susceptibility and prominence of atherosclerosis amongst Canadians warrants additional research into therapies that both prevent and ameliorate atherosclerosis.

Notwithstanding the plasticity of cell types involved in atherogenesis, myeloid derived monocytes/macrophages are a major component in lesion development with additional roles in continuation of inflammatory nature of the lesion microenvironment[22,242,243]. Myeloid-derived macrophages are responsible for the unregulated uptake of modified LDL variants, where cholesterol is extracted, esterified, then stored in cytoplasmic LD. Accumulation of these lipid droplets leads to lipid latency within these macrophages that directly contribute to increased lesion size and the continuation of pro-inflammatory signaling that further recruits of immune cells into the developing lesion[23]. Understanding these crucial pathways during disease progression has led to genetic and pharmacological approaches to combat disease

generation by enhancing macrophage cholesterol metabolism and dampening inflammation to prevent the progression of atherosclerosis.

The master regulator of cellular energetics, AMPK, is implicated in many anti-atherogenic processes such as (but not limited to) suppression of endogenous cholesterol synthesis, RCT, autophagy, and resolution of inflammation[86,173,215]. We describe in **Chapter 1**, a pathway that links macrophage uptake of atherogenic oxLDL to modulation of AMPK activity, which was previously observed but never characterized[200]. The unregulated uptake and storage of modified LDL variants within myeloid leads to lesion generation within vasculature, thus there is an initial disconnect when understanding how or why this process leads to activation of AMPK. However, we speculate that this may have evolved as a compensatory pathway, such that excessive modified LDL uptake triggers AMPK signaling to pathways that aid in accommodating excess sterol burden in macrophages.

We describe that two physiologically relevant modified LDL variants, agLDL and oxLDL, stimulate AMPK-specific signaling to ACC (Figure 1). When BMDM were co-incubated with the CaMKKβ inhibitor, STO-609, both agLDL and oxLDL-induced AMPK activation was blunted, however it remained elevated in reference to untreated cells (Figure 2). A similar result was observed when either ionic calcium release from the ER or NPC1 was chemically inhibited. This is suggestive that the CaMKKβ/Ca^{2+} is involved in agLDL/oxLDL mediated AMPK activation, however is not solely responsible for these signaling events. We observed a trending increase in AMP: ATP ratios in response to acute uptake of agLDL and oxLDL by BMDM, which allows for speculation of LKB1's potential role within these pathways, however further experimentation is required to confirm these results (Figure 3). It was documented in two separate experiments that within macrophages isolated from the

peritoneum of thioglycolate-elicited mice, that oxLDL both perturbed lysosome function and enhanced nuclear enrichment of TFEB[183]. Knowing that BMDM AMPK stimulates autophagy (Figure 6) and enhances the expression of key genes within autophagy and lysosomal biogenesis (Figure 8), we speculated that modified LDL may be enhancing BMDM AMPK signaling to promote lysosomal biogenesis to accommodate excessive lipid burden. Despite our original predictions, we did not observe a similar response to agLDL or oxLDL within our macrophage model (BMDM) as previously reported for macrophages isolated from the peritoneum from thioglycolate-elicited mice (Figure 9).

Within atherosclerosis, there is a disconnect for the role of myeloid AMPKα1 signaling, where it has been show important for recruitment and differentiation of monocytes to macrophages attributing to more atherosclerosis in ApoE-KO mice[200], but reduces myeloid recruitment and lesion size in LDLr-KO mice[179]. We know that BMDM cultured with modified LDL variants have enhanced AMPK signaling (Figure 1), however this could fit in with either a protective or causative mechanism proposed by both confounding studies. To address this *in vivo*, we performed a study to preferentially activate lesion AMPK by packaging A769662 (a specific activator of AMPK) within NP decorated with Collagen IV binding peptide, which has been shown to improve delivery and accumulation within atherosclerotic lesions[197].

In our preliminary study, we show that A769662-NP therapy was insufficient in altering lesion generation within WD-fed LDLr-KO mice (Figure 11). Systemic activation of AMPK with various AMPK activators (including A769662) has shown to protect against atherogenesis within ApoE-KO mice, however this is accomplished by lengthy treatment times of daily injections for 10-12 weeks. We could not rule out that the timing, dosage, or duration of A769662-NP therapy was inadequate to alter lesion generation in LDLr-KO mice, thus we

designed a second study to interrogate myeloid AMPK and its subsequent activation within atherogenesis. To accomplish this, we utilized animals that lack myeloid AMPKα1α2 expression and their floxed littermate controls (WT equivalent) and made them susceptible to WD-induced atherogenesis through PCSK9-AAV transduction (Figure 15). At the experimental halfway point (week 6), we intervened with daily systemic injections of A769662 to determine whether the potential protective effects from A769662 administration are dependent on myeloid AMPK expression, or if other tissues are attributing to the protective effect previously observed[198,212].

We observed within our model, neither A769662 therapy or myeloid AMPK impacted lesion generation assessed by H&E staining (Figure 16). However, when staining for total neutral lipids (with Oil Red O), we observed that albeit not significant, myeloid AMPK and A769662 have a trending effect to restrict lipid content within the aortic sinus (Figure 16). The potential for myeloid AMPK and its subsequent activation to reduce lesion lipid levels fits in with our speculations that modified LDL enhances AMPK signaling to promote responses to accommodate lipid burden. We observed in **Chapter 1** that in BMDMs, both agLDL and oxLDL did not promote transcript expression of TFEB and TFEB-regulated genes important for lysosomal biogenesis and autophagy (Figure 9). Similarly, we show that within the lesion microenvironment, neither myeloid deletion of AMPK or A769662-therapy altered the expression of p62, a key marker of autophagy (Figure18).

Myeloid chemotaxis is causative in the progression of atherosclerosis, where myeloid The role of myeloid AMPKα1 within chemotaxis during the progression of atherosclerosis remains elusive, since its been observed to both protect and contribute depending on the animal model used[179,180]. We investigated the total amount of CD68 expression within the lesion as a

marker for macrophage-like cells. We observed no discernible differences between genotype or treatment groups (Figure 17). Taken together, we speculated that myeloid AMPK is protecting against atherogenesis through regulation of lesion lipid content, and not by modulating myeloid chemotaxis or autophagy. Although AMPK is implicated in numerous aspects of lipid metabolism, we hypothesized that AMPK may be regulating lipid content within the atherosclerotic microenvironment through inhibition of HMGCR, the rate limiting enzyme in cholesterol synthesis.

To address the role of AMPK's suppression of HMGCR during atherosclerosis, we utilized the Ser871Ala HMGCR mouse model that retains normal AMPK signaling to all of its substrates except HMGCR. With reports showing a protective role for WB AMPK activation by pharmacological activators in ApoE-KO mice, we wanted to address our hypothesis that AMPK's suppression of HMGCR within the WB is atheroprotective. We accomplished this by transducing WT and KI mice with the PCSK9-AAV, mice were then placed on a WD for 16-weeks. In support of our hypothesis, we observed that in mice lacking AMPK's regulation of HMGCR developed significantly more atherosclerosis (Figure 27). Although hepatic total cholesterol levels were altered between WT and KI mice, we observed no difference in total levels of circulating cholesterol that allowed us to speculate this phenotype is not being driven by the liver processes (Figure 28).

Knowing that myeloid deletion of HMGCR protects against lesion generation in LDLr-KO mice[225], and that WB AMPK-mediated suppression of HMGCR is atheroprotective, we hypothesized that AMPK's inhibition of HMGCR within the hematopoietic compartment alone is atheroprotective. To assess this, we performed a BMT into WT recipient mice, and reconstituted their hematopoietic compartment by transplantation of bone-marrow from either

WT or KI donor animals. Following, transduced these mice with the PCSK9-AAV and placed them on a WD for 16-weeks. Following, we assessed lesion generation within the aortic sinus of all mice. In support of our hypothesis, we observed that removing AMPK's signaling to HMGCR within the hematopoietic compartment significantly accelerated lesion development (Figure 31).

Reduction of myeloid HMGCR expression was shown to protect against atherogenesis through modulation of myeloid cell inflammation and chemotaxis, however within our model we observed no evidence for variations in monocyte/macrophage content or markers for myeloid recruitment (Figure 33). Despite not knowing the exact mechanism by which hematopoietic HMGCR suppression by AMPK protects against lesion generation, in tandem with our findings from **Chapter 1** and **Chapter 2** we speculate that within the lesion microenvironment AMPK is regulating lipid levels to combat lesion progression.

In conclusion, we show the potential for hematopoietic AMPK signaling to beneficially alter lipid homeostasis to protect against the development of atherosclerosis. This protective effect likely involved managing lesion lipid content through modulation of HMGCR activity, however additional studies are warranted for confirmation. We highlight the need for more studies looking at AMPK's regulation to a single substrate (such as HMGCR) in the context of atherosclerosis to better understand and delineate potential causative and protective mechanisms.

REFERENCES:

1. Canada, P. H. A. of. Heart disease in Canada: Highlights from the Canadian Chronic Disease Surveillance System, 2017. *aem* https://www.canada.ca/en/public-health/services/publications/diseases-conditions/heart-disease-canada-fact-sheet.html (2017).
2. Konstantinov, I. E., Mejevoi, N., Anichkov, N. M. & Anichkov, N. N. Nikolai N. Anichkov and His Theory of Atherosclerosis. *Tex. Heart Inst. J.* **33**, 7 (2006).
3. Gofman, J. W. *et al.* The Role of Lipids and Lipoproteins in Atherosclerosis. *Science* **111**, 166–186 (1950).
4. Brown, M. S., Dana, S. E. & Goldstein, J. L. Regulation of 3-hydroxy-3-methylglutaryl coenzyme A reductase activity in human fibroblasts by lipoproteins. *Proc. Natl. Acad. Sci. U. S. A.* **70**, 2162–2166 (1973).
5. Goldstein, J. L. & Brown, M. S. Familial hypercholesterolemia: identification of a defect in the regulation of 3-hydroxy-3-methylglutaryl coenzyme A reductase activity associated with overproduction of cholesterol. *Proc. Natl. Acad. Sci. U. S. A.* **70**, 2804–2808 (1973).
6. Brown, M. S., Dana, S. E. & Goldstein, J. L. Regulation of 3-hydroxy-3-methylglutaryl coenzyme A reductase activity in cultured human fibroblasts. Comparison of cells from a normal subject and from a patient with homozygous familial hypercholesterolemia. *J. Biol. Chem.* **249**, 789–796 (1974).
7. Brown, M. S. & Goldstein, J. L. A receptor-mediated pathway for cholesterol homeostasis. *Science* **232**, 34–47 (1986).
8. Ishibashi, S. *et al.* Hypercholesterolemia in low density lipoprotein receptor knockout mice and its reversal by adenovirus-mediated gene delivery. *J. Clin. Invest.* **92**, 883–893 (1993).
9. Lagace, T. A. PCSK9 and LDLR degradation: regulatory mechanisms in circulation and in cells. *Curr. Opin. Lipidol.* **25**, 387–393 (2014).
10. Elguindy, A. & Yacoub, M. H. The discovery of PCSK9 inhibitors: A tale of creativity and multifaceted translational research. *Glob. Cardiol. Sci. Pract.* **2013**, 343–347 (2013).

11. Farnier, M. PCSK9: From discovery to therapeutic applications. *Arch. Cardiovasc. Dis.* **107**, 58–66 (2014).
12. Kumar, S., Kang, D.-W., Rezvan, A. & Jo, H. Accelerated atherosclerosis development in C57Bl6 mice by overexpressing AAV-mediated PCSK9 and partial carotid ligation. *Lab. Investig. J. Tech. Methods Pathol.* **97**, 935–945 (2017).
13. Goettsch, C. *et al.* A single injection of gain-of-function mutant PCSK9 adeno-associated virus vector induces cardiovascular calcification in mice with no genetic modification. *Atherosclerosis* **251**, 109–118 (2016).
14. Khoo, J. C., Miller, E., McLoughlin, P. & Steinberg, D. Enhanced macrophage uptake of low density lipoprotein after self-aggregation. *Arterioscler. Dallas Tex* **8**, 348–358 (1988).
15. Rosenfeld, M. E., Palinski, W., Ylä-Herttuala, S., Butler, S. & Witztum, J. L. Distribution of oxidation specific lipid-protein adducts and apolipoprotein B in atherosclerotic lesions of varying severity from WHHL rabbits. *Arterioscler. Dallas Tex* **10**, 336–349 (1990).
16. Palinski, W. *et al.* Low density lipoprotein undergoes oxidative modification in vivo. *Proc. Natl. Acad. Sci. U. S. A.* **86**, 1372–1376 (1989).
17. Salonen, J. T. *et al.* Autoantibody against oxidised LDL and progression of carotid atherosclerosis. *Lancet Lond. Engl.* **339**, 883–887 (1992).
18. Talbot, R. M., del Rio, J. D. & Weinberg, P. D. Effect of fluid mechanical stresses and plasma constituents on aggregation of LDL. *J. Lipid Res.* **44**, 837–845 (2003).
19. Virella, G. *et al.* Definition of the immunogenic forms of modified human LDL recognized by human autoantibodies and by rabbit hyperimmune antibodies. *J. Lipid Res.* **45**, 1859–1867 (2004).
20. Zhang, L. *et al.* Morphology and structure of lipoproteins revealed by an optimized negative-staining protocol of electron microscopy. *J. Lipid Res.* **52**, 175–184 (2011).
21. Lu, M. & Gursky, O. Aggregation and fusion of low-density lipoproteins in vivo and in vitro. *Biomol. Concepts* **4**, 501–518 (2013).

22. Schumski, A., Winter, C., Döring, Y. & Soehnlein, O. The Ins and Outs of Myeloid Cells in Atherosclerosis. *J. Innate Immun.* **10**, 479–486 (2018).
23. Moore, K. J., Sheedy, F. J. & Fisher, E. A. Macrophages in atherosclerosis: a dynamic balance. *Nat. Rev. Immunol.* **13**, 709–721 (2013).
24. Flynn, M. C., Pernes, G., Lee, M. K. S., Nagareddy, P. R. & Murphy, A. J. Monocytes, Macrophages, and Metabolic Disease in Atherosclerosis. *Front. Pharmacol.* **10**, (2019).
25. Nicholson Andrew C., Frieda S., Pearce A. & Silverstein Roy L. Oxidized LDL Binds to CD36 on Human Monocyte-Derived Macrophages and Transfected Cell Lines. *Arterioscler. Thromb. Vasc. Biol.* **15**, 269–275 (1995).
26. Podrez, E. A. *et al.* Macrophage scavenger receptor CD36 is the major receptor for LDL modified by monocyte-generated reactive nitrogen species. https://www.jci.org/articles/view/8574/pdf (2000) doi:10.1172/JCI8574.
27. Park, Y. M. CD36, a scavenger receptor implicated in atherosclerosis. *Exp. Mol. Med.* **46**, e99 (2014).
28. Llorente-Cortés, V. & Badimon, L. LDL receptor-related protein and the vascular wall: implications for atherothrombosis. *Arterioscler. Thromb. Vasc. Biol.* **25**, 497–504 (2005).
29. Kruth, H. S. Sequestration of aggregated low-density lipoproteins by macrophages. *Curr. Opin. Lipidol.* **13**, 483–488 (2002).
30. Moore, K. J. & Freeman, M. W. Scavenger Receptors in Atherosclerosis: Beyond Lipid Uptake. *Arterioscler. Thromb. Vasc. Biol.* **26**, 1702–1711 (2006).
31. Libby, P. *et al.* Atherosclerosis. *Nat. Rev. Dis. Primer* **5**, 1–18 (2019).
32. Ouimet, M. *et al.* Autophagy Regulates Cholesterol Efflux from Macrophage Foam Cells via Lysosomal Acid Lipase. *Cell Metab.* **13**, 655–667 (2011).
33. Ohashi, R., Mu, H., Wang, X., Yao, Q. & Chen, C. Reverse cholesterol transport and cholesterol efflux in atherosclerosis. *QJM Mon. J. Assoc. Physicians* **98**, 845–856 (2005).

34. Rohatgi, A. Reverse Cholesterol Transport and Atherosclerosis: Heterogeneous Observations by Vascular Bed and Plaque Architecture. *Arterioscler. Thromb. Vasc. Biol.* **39**, 2–4 (2019).
35. Wang, M.-D., Franklin, V. & Marcel, Y. L. In Vivo Reverse Cholesterol Transport From Macrophages Lacking ABCA1 Expression Is Impaired. *Arterioscler. Thromb. Vasc. Biol.* **27**, 1837–1842 (2007).
36. Ouimet, M., Barrett, T. J. & Fisher, E. A. HDL and Reverse Cholesterol Transport. 14.
37. Glomset, J. A. The plasma lecithin:cholesterol acyltransferase reaction. *J. Lipid Res.* **9**, 155–167 (1968).
38. Milasan, A., Ledoux, J. & Martel, C. Lymphatic network in atherosclerosis: the underestimated path. *Future Sci. OA* **1**, (2015).
39. Vuorio, T. *et al.* LYMPHATIC VESSEL INSUFFICIENCY IN HYPERCHOLESTEROLEMIC MICE ALTERS LIPOPROTEIN LEVELS AND PROMOTES ATHEROGENESIS. *Arterioscler. Thromb. Vasc. Biol.* **34**, 1162–1170 (2014).
40. Miller, N. E. *et al.* Lipoprotein remodeling generates lipid-poor apolipoprotein A-I particles in human interstitial fluid. *Am. J. Physiol. - Endocrinol. Metab.* **304**, E321–E328 (2013).
41. Dikkers, A. & Tietge, U. J. Biliary cholesterol secretion: More than a simple ABC. *World J. Gastroenterol. WJG* **16**, 5936–5945 (2010).
42. Paalvast, Y., de Boer, J. F. & Groen, A. K. Developments in intestinal cholesterol transport and triglyceride absorption. *Curr. Opin. Lipidol.* **28**, 248–254 (2017).
43. Feig, J. E. Regression of Atherosclerosis: Insights from Animal and Clinical Studies. *Ann. Glob. Health* **80**, 13–23 (2014).
44. Chockalingam, P., Vinayagam, N. S., Chockalingam, V. & Chockalingam, A. Remarkable regression of coronary atherosclerosis: An interplay of pharmacotherapeutic and lifestyle factors. *Indian Heart J.* **68**, 188–189 (2016).
45. Atri, C., Guerfali, F. Z. & Laouini, D. Role of Human Macrophage Polarization in Inflammation during Infectious Diseases. *Int. J. Mol. Sci.* **19**, (2018).

46. A, S.-M. *et al.* Macrophage Plasticity, Polarization, and Function in Health and Disease. *Journal of cellular physiology* vol. 233 https://pubmed.ncbi.nlm.nih.gov/29319160/ (2018).
47. Wolfs, I. M. J., Donners, M. M. P. C. & de Winther, M. P. J. Differentiation factors and cytokines in the atherosclerotic plaque micro-environment as a trigger for macrophage polarisation. *Thromb. Haemost.* **106**, 763–771 (2011).
48. Zhao, L. *et al.* Low-dose oral sirolimus reduces atherogenesis, vascular inflammation and modulates plaque composition in mice lacking the LDL receptor. *Br. J. Pharmacol.* **156**, 774–785 (2009).
49. Stunault, M. I., Bories, G., Guinamard, R. R. & Ivanov, S. Metabolism Plays a Key Role during Macrophage Activation. *Mediators of Inflammation* vol. 2018 e2426138 https://www.hindawi.com/journals/mi/2018/2426138/ (2018).
50. Viola, A., Munari, F., Sánchez-Rodríguez, R., Scolaro, T. & Castegna, A. The Metabolic Signature of Macrophage Responses. *Front. Immunol.* **10**, (2019).
51. Jeon, S.-M. Regulation and function of AMPK in physiology and diseases. *Exp. Mol. Med.* **48**, e245 (2016).
52. Kola, B., Grossman, A. B. & Korbonits, M. The role of AMP-activated protein kinase in obesity. *Front. Horm. Res.* **36**, 198–211 (2008).
53. Coughlan, K. A., Valentine, R. J., Ruderman, N. B. & Saha, A. K. AMPK activation: a therapeutic target for type 2 diabetes? *Diabetes Metab. Syndr. Obes. Targets Ther.* **7**, 241–253 (2014).
54. Viollet, B. *et al.* Targeting the AMPK pathway for the treatment of Type 2 diabetes. *Front. Biosci. Landmark Ed.* **14**, 3380–3400 (2009).
55. Steinberg, G. R. & Kemp, B. E. AMPK in Health and Disease. *Physiol. Rev.* **89**, 1025–1078 (2009).
56. Lin, S.-C. & Hardie, D. G. AMPK: Sensing Glucose as well as Cellular Energy Status. *Cell Metab.* **27**, 299–313 (2018).

57. Crute, B. E., Seefeld, K., Gamble, J., Kemp, B. E. & Witters, L. A. Functional domains of the alpha1 catalytic subunit of the AMP-activated protein kinase. *J. Biol. Chem.* **273**, 35347–35354 (1998).

58. Pang, T. *et al.* Conserved α-Helix Acts as Autoinhibitory Sequence in AMP-activated Protein Kinase α Subunits. *J. Biol. Chem.* **282**, 495–506 (2007).

59. Grahame Hardie, D. Regulation of AMP-activated protein kinase by natural and synthetic activators. *Acta Pharm. Sin. B* **6**, 1–19 (2016).

60. Li, J., Li, S., Wang, F. & Xin, F. Structural and biochemical insights into the allosteric activation mechanism of AMP-activated protein kinase. *Chem. Biol. Drug Des.* **89**, 663–669 (2017).

61. de Souza Almeida Matos, A. L. *et al.* Allosteric regulation of AMP-activated protein kinase by adenylate nucleotides and small-molecule drugs. *Biochem. Soc. Trans.* **47**, 733–741 (2019).

62. Iseli, T. J. *et al.* AMP-activated Protein Kinase β Subunit Tethers α and γ Subunits via Its C-terminal Sequence (186–270). *J. Biol. Chem.* **280**, 13395–13400 (2005).

63. Dzamko, N. *et al.* AMPK β1 Deletion Reduces Appetite, Preventing Obesity and Hepatic Insulin Resistance. *J. Biol. Chem.* **285**, 115–122 (2010).

64. Warden, S. M. *et al.* Post-translational modifications of the beta-1 subunit of AMP-activated protein kinase affect enzyme activity and cellular localization. *Biochem. J.* **354**, 275–283 (2001).

65. McBride, A., Ghilagaber, S., Nikolaev, A. & Hardie, D. G. The Glycogen-Binding Domain on the AMPK β Subunit Allows the Kinase to Act as a Glycogen Sensor. *Cell Metab.* **9**, 23–34 (2009).

66. Hunter, R. W., Treebak, J. T., Wojtaszewski, J. F. P. & Sakamoto, K. Molecular mechanism by which AMP-activated protein kinase activation promotes glycogen accumulation in muscle. *Diabetes* **60**, 766–774 (2011).

67. Jin, X., Townley, R. & Shapiro, L. Structural insight into AMPK regulation: ADP comes into play. *Struct. Lond. Engl. 1993* **15**, 1285–1295 (2007).

68. Townley, R. & Shapiro, L. Crystal structures of the adenylate sensor from fission yeast AMP-activated protein kinase. *Science* **315**, 1726–1729 (2007).

69. Xiao, B. *et al.* Structural basis for AMP binding to mammalian AMP-activated protein kinase. *Nature* **449**, 496–500 (2007).

70. Yan, Y., Zhou, X. E., Xu, H. E. & Melcher, K. Structure and Physiological Regulation of AMPK. *Int. J. Mol. Sci.* **19**, (2018).

71. Gu, X. *et al.* Deconvoluting AMP-activated protein kinase (AMPK) adenine nucleotide binding and sensing. *J. Biol. Chem.* **292**, 12653–12666 (2017).

72. Fullerton, M. D. *et al.* Single phosphorylation sites in Acc1 and Acc2 regulate lipid homeostasis and the insulin–sensitizing effects of metformin. *Nat. Med.* **19**, 1649–1654 (2013).

73. Pollard, A. E. *et al.* AMPK activation protects against diet induced obesity through Ucp1-independent thermogenesis in subcutaneous white adipose tissue. *Nat. Metab.* **1**, 340–349 (2019).

74. Garcia, D. *et al.* Genetic Liver-Specific AMPK Activation Protects against Diet-Induced Obesity and NAFLD. *Cell Rep.* **26**, 192-208.e6 (2019).

75. Carlson, M., Osmond, B. C. & Botstein, D. Mutants of yeast defective in sucrose utilization. *Genetics* **98**, 25–40 (1981).

76. Woods, A. *et al.* LKB1 Is the Upstream Kinase in the AMP-Activated Protein Kinase Cascade. *Curr. Biol.* **13**, 2004–2008 (2003).

77. Hawley, S. A. *et al.* 5′-AMP Activates the AMP-activated Protein Kinase Cascade, and Ca^{2+} /Calmodulin Activates the Calmodulin-dependent Protein Kinase I Cascade, via Three Independent Mechanisms. *J. Biol. Chem.* **270**, 27186–27191 (1995).

78. Hawley, S. A. *et al.* Complexes between the LKB1 tumor suppressor, STRADα/β and MO25α/β are upstream kinases in the AMP-activated protein kinase cascade. *J. Biol.* **2**, 28 (2003).

79. Hurley, R. L. *et al.* The Ca^{2+} /Calmodulin-dependent Protein Kinase Kinases Are AMP-activated Protein Kinase Kinases. *J. Biol. Chem.* **280**, 29060–29066 (2005).

80. Shaw, R. J. *et al.* The tumor suppressor LKB1 kinase directly activates AMP-activated kinase and regulates apoptosis in response to energy stress. *Proc. Natl. Acad. Sci.* **101**, 3329–3335 (2004).

81. Zhang, Y.-L. *et al.* AMP as a low-energy charge signal autonomously initiates assembly of AXIN-AMPK-LKB1 complex for AMPK activation. *Cell Metab.* **18**, 546–555 (2013).

82. Zhang, C.-S. *et al.* The Lysosomal v-ATPase-Ragulator Complex Is a Common Activator for AMPK and mTORC1, Acting as a Switch between Catabolism and Anabolism. *Cell Metab.* **20**, 526–540 (2014).

83. Kim, J., Yang, G., Kim, Y., Kim, J. & Ha, J. AMPK activators: mechanisms of action and physiological activities. *Exp. Mol. Med.* **48**, e224 (2016).

84. Göransson, O. *et al.* Mechanism of action of A-769662, a valuable tool for activation of AMP-activated protein kinase. *J. Biol. Chem.* **282**, 32549–32560 (2007).

85. Sag, D., Carling, D., Stout, R. D. & Suttles, J. AMP-activated protein kinase promotes macrophage polarization to an anti-inflammatory functional phenotype. *J. Immunol. Baltim. Md 1950* **181**, 8633–8641 (2008).

86. Galic, S. *et al.* Hematopoietic AMPK β1 reduces mouse adipose tissue macrophage inflammation and insulin resistance in obesity. *J. Clin. Invest.* **121**, 4903–4915 (2011).

87. Zhu, Y. P., Brown, J. R., Sag, D., Zhang, L. & Suttles, J. AMP-activated protein kinase regulates IL-10-mediated antiinflammatory signaling pathways in macrophages. *J. Immunol. Baltim. Md 1950* **194**, 584–594 (2015).

88. Murakami, M. *et al.* mTOR Is Essential for Growth and Proliferation in Early Mouse Embryos and Embryonic Stem Cells. *Mol. Cell. Biol.* **24**, 6710–6718 (2004).

89. Gangloff, Y.-G. *et al.* Disruption of the Mouse mTOR Gene Leads to Early Postimplantation Lethality and Prohibits Embryonic Stem Cell Development. *Mol. Cell. Biol.* **24**, 9508–9516 (2004).

90. Laplante, M. & Sabatini, D. M. mTOR Signaling. *Cold Spring Harb. Perspect. Biol.* **4**, (2012).

91. Luo, Y., Xu, W., Li, G. & Cui, W. Weighing In on mTOR Complex 2 Signaling: The Expanding Role in Cell Metabolism. *Oxid. Med. Cell. Longev.* **2018**, (2018).

92. Yip, C. K., Murata, K., Walz, T., Sabatini, D. M. & Kang, S. A. Structure of the human mTOR Complex I and its implications for rapamycin inhibition. *Mol. Cell* **38**, 768–774 (2010).

93. Mao, Z. & Zhang, W. Role of mTOR in Glucose and Lipid Metabolism. *Int. J. Mol. Sci.* **19**, (2018).

94. Grahammer, F. *et al.* mTORC2 critically regulates renal potassium handling. *J. Clin. Invest.* **126**, 1773–1782 (2016).

95. Schaub, T. *et al.* mTORC1 and mTORC2 Differentially Regulate Cell Fate Programs to Coordinate Osteoblastic Differentiation in Mesenchymal Stromal Cells. *Sci. Rep.* **9**, 20071 (2019).

96. Lamming, D. W. & Sabatini, D. M. A central role for mTOR in lipid homeostasis. *Cell Metab.* **18**, (2013).

97. Alers, S., Löffler, A. S., Wesselborg, S. & Stork, B. Role of AMPK-mTOR-Ulk1/2 in the regulation of autophagy: cross talk, shortcuts, and feedbacks. *Mol. Cell. Biol.* **32**, 2–11 (2012).

98. Weichhart, T., Hengstschläger, M. & Linke, M. Regulation of innate immune cell function by mTOR. *Nat. Rev. Immunol.* **15**, 599–614 (2015).

99. Song, X. *et al.* mTOR attenuates the inflammatory response in cardiomyocytes and prevents cardiac dysfunction in pathological hypertrophy. *Am. J. Physiol. - Cell Physiol.* **299**, C1256–C1266 (2010).

100. Holroyd, A. K. & Michie, A. M. The role of mTOR-mediated signaling in the regulation of cellular migration. *Immunol. Lett.* **196**, 74–79 (2018).

101. Castro, C. *et al.* Rapamycin attenuates atherosclerosis induced by dietary cholesterol in apolipoprotein-deficient mice through a p27 Kip1 -independent pathway. *Atherosclerosis* **172**, 31–38 (2004).

102. Pakala, R., Stabile, E., Jang, G. J., Clavijo, L. & Waksman, R. Rapamycin attenuates atherosclerotic plaque progression in apolipoprotein E knockout mice: inhibitory effect on monocyte chemotaxis. *J. Cardiovasc. Pharmacol.* **46**, 481–486 (2005).

103. Gadioli, A. L. N. *et al.* Oral rapamycin attenuates atherosclerosis without affecting the arterial responsiveness of resistance vessels in apolipoprotein E-deficient mice. *Braz. J. Med. Biol. Res.* **42**, 1191–1195 (2009).

104. Mueller, M. A., Beutner, F., Teupser, D., Ceglarek, U. & Thiery, J. Prevention of atherosclerosis by the mTOR inhibitor everolimus in LDLR−/− mice despite severe hypercholesterolemia. *Atherosclerosis* **198**, 39–48 (2008).

105. Beutner, F. *et al.* Effect of everolimus on pre-existing atherosclerosis in LDL-receptor deficient mice. *Atherosclerosis* **222**, 337–343 (2012).

106. Baetta, R. *et al.* Everolimus inhibits monocyte/macrophage migration in vitro and their accumulation in carotid lesions of cholesterol-fed rabbits. *J. Pharmacol. Exp. Ther.* **328**, 419–425 (2009).

107. Chen, W. Q. *et al.* Oral rapamycin attenuates inflammation and enhances stability of atherosclerotic plaques in rabbits independent of serum lipid levels. *Br. J. Pharmacol.* **156**, 941–951 (2009).

108. Zhai, C. *et al.* Selective inhibition of PI3K/Akt/mTOR signaling pathway regulates autophagy of macrophage and vulnerability of atherosclerotic plaque. *PloS One* **9**, e90563 (2014).

109. Wang, X. *et al.* Knockdown of mTOR by lentivirus-mediated RNA interference suppresses atherosclerosis and stabilizes plaques via a decrease of macrophages by autophagy in apolipoprotein E-deficient mice. *Int. J. Mol. Med.* **32**, 1215–1221 (2013).

110. Kwiatkowski, D. J. & Manning, B. D. Tuberous sclerosis: a GAP at the crossroads of multiple signaling pathways. *Hum. Mol. Genet.* **14**, R251–R258 (2005).

111. Gwinn, D. M. *et al.* AMPK phosphorylation of raptor mediates a metabolic checkpoint. *Mol. Cell* **30**, 214–226 (2008).

112. Hurley, J. H. & Young, L. N. Mechanisms of Autophagy Initiation. *Annu. Rev. Biochem.* **86**, 225–244 (2017).

113. Glick, D., Barth, S. & Macleod, K. F. Autophagy: cellular and molecular mechanisms. *J. Pathol.* **221**, 3–12 (2010).

114. Ravikumar, B. *et al.* Regulation of Mammalian Autophagy in Physiology and Pathophysiology. *Physiol. Rev.* **90**, 1383–1435 (2010).

115. Jiang, P. & Mizushima, N. Autophagy and human diseases. *Cell Res.* **24**, 69–79 (2014).

116. Levine, B. & Kroemer, G. Autophagy in the Pathogenesis of Disease. *Cell* **132**, 27–42 (2008).

117. Razani, B. *et al.* Autophagy Links Inflammasomes to Atherosclerotic Progression. *Cell Metab.* **15**, 534–544 (2012).

118. Kim, J., Kundu, M., Viollet, B. & Guan, K.-L. AMPK and mTOR regulate autophagy through direct phosphorylation of Ulk1. *Nat. Cell Biol.* **13**, 132–141 (2011).

119. Russell, R. C., Yuan, H.-X. & Guan, K.-L. Autophagy regulation by nutrient signaling. *Cell Res.* **24**, 42–57 (2014).

120. Zhang, D. *et al.* AMPK regulates autophagy by phosphorylating BECN1 at threonine 388. *Autophagy* **12**, 1447–1459 (2016).

121. Jang, M. *et al.* AMPK contributes to autophagosome maturation and lysosomal fusion. *Sci. Rep.* **8**, 1–10 (2018).

122. Pan, T., Kondo, S., Le, W. & Jankovic, J. The role of autophagy-lysosome pathway in neurodegeneration associated with Parkinson's disease. *Brain* **131**, 1969–1978 (2008).

123. Panigrahi, I. *et al.* Niemann-Pick Disease: An Underdiagnosed Lysosomal Storage Disorder. *Case Reports in Genetics* vol. 2019 e3108093 https://www.hindawi.com/journals/crig/2019/3108093/ (2019).

124. Oyarzún, J. E. *et al.* Lysosome motility and distribution: Relevance in health and disease. *Biochim. Biophys. Acta Mol. Basis Dis.* **1865**, 1076–1087 (2019).

125. Sardiello, M. *et al.* A Gene Network Regulating Lysosomal Biogenesis and Function. *Science* **325**, 473–477 (2009).

126. Settembre, C. *et al.* TFEB links autophagy to lysosomal biogenesis. *Science* **332**, 1429–1433 (2011).

127. Palmieri, M. *et al.* Characterization of the CLEAR network reveals an integrated control of cellular clearance pathways. *Hum. Mol. Genet.* **20**, 3852–3866 (2011).

128. Yao, Y., Jones, E. & Inoki, K. Lysosomal Regulation of mTORC1 by Amino Acids in Mammalian Cells. *Biomolecules* **7**, (2017).

129. Rabanal-Ruiz, Y. & Korolchuk, V. I. mTORC1 and Nutrient Homeostasis: The Central Role of the Lysosome. *Int. J. Mol. Sci.* **19**, (2018).

130. Vega-Rubin-de-Celis, S., Peña-Llopis, S., Konda, M. & Brugarolas, J. Multistep regulation of TFEB by MTORC1. *Autophagy* **13**, 464–472 (2017).

131. Settembre, C. *et al.* A lysosome-to-nucleus signalling mechanism senses and regulates the lysosome via mTOR and TFEB. *EMBO J.* **31**, 1095–1108 (2012).

132. Nezich, C. L., Wang, C., Fogel, A. I. & Youle, R. J. MiT/TFE transcription factors are activated during mitophagy downstream of Parkin and Atg5. *J. Cell Biol.* **210**, 435–450 (2015).

133. Martina, J. A., Chen, Y., Gucek, M. & Puertollano, R. MTORC1 functions as a transcriptional regulator of autophagy by preventing nuclear transport of TFEB. *Autophagy* **8**, 903–914 (2012).

134. Roczniak-Ferguson, A. *et al.* The Transcription Factor TFEB Links mTORC1 Signaling to Transcriptional Control of Lysosome Homeostasis. *Sci. Signal.* **5**, ra42 (2012).

135. Xu, Y. *et al.* YWHA/14-3-3 proteins recognize phosphorylated TFEB by a noncanonical mode for controlling TFEB cytoplasmic localization. *Autophagy* **15**, 1017–1030 (2019).

136. Shin, H.-J. R. *et al.* AMPK–SKP2–CARM1 signalling cascade in transcriptional regulation of autophagy. *Nature* **534**, 553–557 (2016).

137. Young, N. P. *et al.* AMPK governs lineage specification through Tfeb-dependent regulation of lysosomes. *Genes Dev.* **30**, 535–552 (2016).

138. Li, X. *et al.* Nucleus-Translocated ACSS2 Promotes Gene Transcription for Lysosomal Biogenesis and Autophagy. *Mol. Cell* **66**, 684-697.e9 (2017).

139. Li, C. *et al.* Nuclear AMPK regulated CARM1 stabilization impacts autophagy in aged heart. *Biochem. Biophys. Res. Commun.* **486**, 398–405 (2017).

140. El-Houjeiri, L. *et al.* The Transcription Factors TFEB and TFE3 Link the FLCN-AMPK Signaling Axis to Innate Immune Response and Pathogen Resistance. *Cell Rep.* **26**, 3613-3628.e6 (2019).

141. Collodet, C. *et al.* AMPK promotes induction of the tumor suppressor FLCN through activation of TFEB independently of mTOR. *FASEB J.* **33**, 12374–12391 (2019).

142. Eberlé, D., Hegarty, B., Bossard, P., Ferré, P. & Foufelle, F. SREBP transcription factors: master regulators of lipid homeostasis. *Biochimie* **86**, 839–848 (2004).

143. Shimano, H. & Sato, R. SREBP-regulated lipid metabolism: convergent physiology — divergent pathophysiology. *Nat. Rev. Endocrinol.* **13**, 710–730 (2017).

144. Moslehi, A. & Hamidi-zad, Z. Role of SREBPs in Liver Diseases: A Mini-review. *J. Clin. Transl. Hepatol.* **6**, 332–338 (2018).

145. Li, Y. *et al.* AMPK phosphorylates and inhibits SREBP activity to attenuate hepatic steatosis and atherosclerosis in diet-induced insulin-resistant mice. *Cell Metab.* **13**, 376–388 (2011).

146. Han, Y. *et al.* Post-translational regulation of lipogenesis via AMPK-dependent phosphorylation of insulin-induced gene. *Nat. Commun.* **10**, (2019).

147. Kawaguchi, T., Takenoshita, M., Kabashima, T. & Uyeda, K. Glucose and cAMP regulate the L-type pyruvate kinase gene by phosphorylation/dephosphorylation of the carbohydrate response element binding protein. *Proc. Natl. Acad. Sci.* **98**, 13710–13715 (2001).

148. Ortega-Prieto, P. & Postic, C. Carbohydrate Sensing Through the Transcription Factor ChREBP. *Front. Genet.* **10**, 472 (2019).

149. Sato, S. *et al.* Metabolite Regulation of Nuclear Localization of Carbohydrate-response Element-binding Protein (ChREBP) ROLE OF AMP AS AN ALLOSTERIC INHIBITOR. *J. Biol. Chem.* **291**, 10515–10527 (2016).

150. Kawaguchi, T., Osatomi, K., Yamashita, H., Kabashima, T. & Uyeda, K. Mechanism for Fatty Acid "Sparing" Effect on Glucose-induced Transcription REGULATION OF CARBOHYDRATE-RESPONSIVE ELEMENT-BINDING PROTEIN BY AMP-ACTIVATED PROTEIN KINASE. *J. Biol. Chem.* **277**, 3829–3835 (2002).

151. Oort, M. M. van *et al.* Effects of AMPK activators on the sub-cellular distribution of fatty acid transporters CD36 and FABPpm. *Arch. Physiol. Biochem.* **115**, 137–146 (2009).

152. Jeppesen, J. *et al.* Contraction-induced skeletal muscle FAT/CD36 trafficking and FA uptake is AMPK independent. *J. Lipid Res.* **52**, 699–711 (2011).

153. Samovski, D., Su, X., Xu, Y., Abumrad, N. A. & Stahl, P. D. Insulin and AMPK regulate FA translocase/CD36 plasma membrane recruitment in cardiomyocytes via Rab GAP AS160 and Rab8a Rab GTPase. *J. Lipid Res.* **53**, 709–717 (2012).

154. Schreurs, M., Kuipers, F. & van der Leij, F. R. Regulatory enzymes of mitochondrial beta-oxidation as targets for treatment of the metabolic syndrome. *Obes. Rev. Off. J. Int. Assoc. Study Obes.* **11**, 380–388 (2010).

155. Qu, Q., Zeng, F., Liu, X., Wang, Q. J. & Deng, F. Fatty acid oxidation and carnitine palmitoyltransferase I: emerging therapeutic targets in cancer. *Cell Death Dis.* **7**, e2226 (2016).

156. Hopkins, T. A., Dyck, J. R. B. & Lopaschuk, G. D. AMP-activated protein kinase regulation of fatty acid oxidation in the ischaemic heart. *Biochem. Soc. Trans.* **31**, 207–212 (2003).

157. O'Neill, H. M., Holloway, G. P. & Steinberg, G. R. AMPK regulation of fatty acid metabolism and mitochondrial biogenesis: implications for obesity. *Mol. Cell. Endocrinol.* **366**, 135–151 (2013).

158. Herzig, S. & Shaw, R. J. AMPK: guardian of metabolism and mitochondrial homeostasis. *Nat. Rev. Mol. Cell Biol.* **19**, 121–135 (2018).

159. Eichner, L. J. & Giguère, V. Estrogen related receptors (ERRs): a new dawn in transcriptional control of mitochondrial gene networks. *Mitochondrion* **11**, 544–552 (2011).

160. Jäger, S., Handschin, C., St.-Pierre, J. & Spiegelman, B. M. AMP-activated protein kinase (AMPK) action in skeletal muscle via direct phosphorylation of PGC-1α. *Proc. Natl. Acad. Sci. U. S. A.* **104**, 12017–12022 (2007).

161. Zong, H. *et al.* AMP kinase is required for mitochondrial biogenesis in skeletal muscle in response to chronic energy deprivation. *Proc. Natl. Acad. Sci. U. S. A.* **99**, 15983–15987 (2002).

162. Garcia-Roves, P. M., Osler, M. E., Holmström, M. H. & Zierath, J. R. Gain-of-function R225Q mutation in AMP-activated protein kinase gamma3 subunit increases mitochondrial biogenesis in glycolytic skeletal muscle. *J. Biol. Chem.* **283**, 35724–35734 (2008).

163. O'Neill, H. M. *et al.* AMP-activated protein kinase (AMPK) beta1beta2 muscle null mice reveal an essential role for AMPK in maintaining mitochondrial content and glucose uptake during exercise. *Proc. Natl. Acad. Sci. U. S. A.* **108**, 16092–16097 (2011).

164. Tanner, C. B. *et al.* Mitochondrial and performance adaptations to exercise training in mice lacking skeletal muscle LKB1. *Am. J. Physiol. Endocrinol. Metab.* **305**, E1018-1029 (2013).

165. Lantier, L. *et al.* AMPK controls exercise endurance, mitochondrial oxidative capacity, and skeletal muscle integrity. *FASEB J. Off. Publ. Fed. Am. Soc. Exp. Biol.* **28**, 3211–3224 (2014).

166. Mottillo, E. P. *et al.* Lack of Adipocyte AMPK Exacerbates Insulin Resistance and Hepatic Steatosis through Brown and Beige Adipose Tissue Function. *Cell Metab.* **24**, 118–129 (2016).

167. Hasenour, C. M. *et al.* 5-Aminoimidazole-4-carboxamide-1-β-d-ribofuranoside (AICAR) Effect on Glucose Production, but Not Energy Metabolism, Is Independent of Hepatic AMPK in Vivo. *J. Biol. Chem.* **289**, 5950–5959 (2014).

168. Afonso, M. S. *et al.* Molecular Pathways Underlying Cholesterol Homeostasis. *Nutrients* **10**, (2018).

169. Ohashi, K. *et al.* Early embryonic lethality caused by targeted disruption of the 3-hydroxy-3-methylglutaryl-CoA reductase gene. *J. Biol. Chem.* **278**, 42936–42941 (2003).

170. Carling, D., Clarke, P. R., Zammit, V. A. & Hardie, D. G. Purification and characterization of the AMP-activated protein kinase. *Eur. J. Biochem.* **186**, 129–136 (1989).

171. Loh, K. *et al.* Inhibition of Adenosine Monophosphate–Activated Protein Kinase–3-Hydroxy-3-Methylglutaryl Coenzyme A Reductase Signaling Leads to Hypercholesterolemia and Promotes Hepatic Steatosis and Insulin Resistance. *Hepatol. Commun.* **3**, 84–98 (2018).

172. Li, D. *et al.* Adenosine Monophosphate-activated Protein Kinase Induces Cholesterol Efflux from Macrophage-derived Foam Cells and Alleviates Atherosclerosis in Apolipoprotein E-deficient Mice. *J. Biol. Chem.* **285**, 33499–33509 (2010).

173. Fullerton, M. D. *et al.* Salicylate improves macrophage cholesterol homeostasis via activation of Ampk. *J. Lipid Res.* **56**, 1025–1033 (2015).

174. Dong, Y. *et al.* Reduction of AMP-activated Protein Kinase Alpha 2 Increases Endoplasmic Reticulum Stress and Atherosclerosis In Vivo. *Circulation* **121**, 792–803 (2010).

175. Wang, Q. *et al.* Activation of AMP-activated protein kinase is required for berberine-induced reduction of atherosclerosis in mice: the role of uncoupling protein 2. *PloS One* **6**, e25436 (2011).

176. Ding, Y. *et al.* AMP-Activated Protein Kinase Alpha 2 Deletion Induces VSMC Phenotypic Switching and Reduces Features of Atherosclerotic Plaque Stability. *Circ. Res.* **119**, 718–730 (2016).

177. Cai, Z. *et al.* Ablation of Adenosine Monophosphate-Activated Protein Kinase α1 in Vascular Smooth Muscle Cells Promotes Diet-Induced Atherosclerotic Calcification In Vivo. *Circ. Res.* **119**, 422–433 (2016).

178. Fisslthaler, B. *et al.* Myeloid-Specific Deletion of the AMPKα2 Subunit Alters Monocyte Protein Expression and Atherogenesis. *Int. J. Mol. Sci.* **20**, (2019).

179. Cao, Q. *et al.* Myeloid Deletion of α1AMPK Exacerbates Atherosclerosis in LDL Receptor Knockout (LDLRKO) Mice. *Diabetes* **65**, 1565–1576 (2016).

180. Zhang, M. *et al.* AMP-activated Protein Kinase α1 Promotes Atherogenesis by Increasing Monocyte-to-macrophage Differentiation. *J. Biol. Chem.* jbc.M117.779447 (2017) doi:10.1074/jbc.M117.779447.

181. Ma, A., Wang, J., Yang, L., An, Y. & Zhu, H. AMPK activation enhances the anti-atherogenic effects of high density lipoproteins in apoE−/− mice. *J. Lipid Res.* **58**, 1536–1547 (2017).

182. Wang, J., Ma, A., Zhao, M. & Zhu, H. AMPK activation reduces the number of atheromata macrophages in ApoE deficient mice. *Atherosclerosis* **258**, 97–107 (2017).

183. Emanuel, R. *et al.* Induction of Lysosomal Biogenesis in Atherosclerotic Macrophages Can Rescue Lipid-Induced Lysosomal Dysfunction and Downstream Sequelae. *Arterioscler. Thromb. Vasc. Biol.* **34**, 1942–1952 (2014).

184. Samovski, D. *et al.* Regulation of AMPK Activation by CD36 Links Fatty Acid Uptake to β-Oxidation. *Diabetes* **64**, 353–359 (2015).

185. Bahar, E., Kim, H. & Yoon, H. ER Stress-Mediated Signaling: Action Potential and Ca2+ as Key Players. *Int. J. Mol. Sci.* **17**, (2016).

186. Yao, S. *et al.* Endoplasmic Reticulum Stress Promotes Macrophage-derived Foam Cell Formation by Up-regulating Cluster of Differentiation 36 (CD36) Expression. *J. Biol. Chem.* **289**, 4032–4042 (2014).

187. Sanson Marie *et al.* Oxidized Low-Density Lipoproteins Trigger Endoplasmic Reticulum Stress in Vascular Cells. *Circ. Res.* **104**, 328–336 (2009).

188. Ivanova, E. A. & Orekhov, A. N. The Role of Endoplasmic Reticulum Stress and Unfolded Protein Response in Atherosclerosis. *Int. J. Mol. Sci.* **17**, (2016).

189. Chistiakov, D. A., Sobenin, I. A., Orekhov, A. N. & Bobryshev, Y. V. Role of Endoplasmic Reticulum Stress in Atherosclerosis and Diabetic Macrovascular Complications. *BioMed*

Research International https://www.hindawi.com/journals/bmri/2014/610140/ (2014) doi:https://doi.org/10.1155/2014/610140.

190. Li, Y. *et al.* CD36 plays a negative role in the regulation of lipophagy in hepatocytes through an AMPK-dependent pathway. *J. Lipid Res.* **60**, 844–855 (2019).

191. Rafieian-Kopaei, M., Setorki, M., Doudi, M., Baradaran, A. & Nasri, H. Atherosclerosis: Process, Indicators, Risk Factors and New Hopes. *Int. J. Prev. Med.* **5**, 927–946 (2014).

192. Linton, M. F. *et al.* The Role of Lipids and Lipoproteins in Atherosclerosis. in *Endotext* (eds. Feingold, K. R. et al.) (MDText.com, Inc., 2000).

193. Gu, X. *et al.* Conformational heterogeneity of the allosteric drug and metabolite (ADaM) site in AMP-activated protein kinase (AMPK). *J. Biol. Chem.* **293**, 16994–17007 (2018).

194. Pinkosky, S. L. *et al.* Long-chain fatty acyl-CoA esters regulate metabolism via allosteric control of AMPK β1 isoforms. *Nat. Metab.* (2020) doi:10.1038/s42255-020-0245-2.

195. García-Tardón, N. & Guigas, B. Determination of Adenine Nucleotide Concentrations in Cells and Tissues by High-Performance Liquid Chromatography. *Methods Mol. Biol. Clifton NJ* **1732**, 229–237 (2018).

196. Ouimet, M. *et al.* Mycobacterium tuberculosis induces the miR-33 locus to reprogram autophagy and host lipid metabolism. *Nat. Immunol.* **17**, 677–686 (2016).

197. Fredman, G. *et al.* Targeted nanoparticles containing the proresolving peptide Ac2-26 protect against advanced atherosclerosis in hypercholesterolemic mice. *Sci. Transl. Med.* **7**, 275ra20 (2015).

198. Ma, A., Wang, J., Yang, L., An, Y. & Zhu, H. AMPK activation enhances the anti-atherogenic effects of high density lipoproteins in apoE−/− mice. *J. Lipid Res.* **58**, 1536–1547 (2017).

199. Cool, B. *et al.* Identification and characterization of a small molecule AMPK activator that treats key components of type 2 diabetes and the metabolic syndrome. *Cell Metab.* **3**, 403–416 (2006).

200. Zhang, M. *et al.* AMP-activated Protein Kinase α1 Promotes Atherogenesis by Increasing Monocyte-to-macrophage Differentiation. *J. Biol. Chem.* jbc.M117.779447 (2017) doi:10.1074/jbc.M117.779447.

201. Cao, Q. *et al.* Myeloid deletion of α1AMPK exacerbates atherosclerosis in low density lipoprotein receptor knockout (LDLRKO) mice. *Diabetes* (2016) doi:10.2337/db15-0917.

202. Feil, S. *et al.* Transdifferentiation of Vascular Smooth Muscle Cells to Macrophage-Like Cells During Atherogenesis. *Circ. Res.* **115**, 662–667 (2014).

203. Albarrán-Juárez, J., Kaur, H., Grimm, M., Offermanns, S. & Wettschureck, N. Lineage tracing of cells involved in atherosclerosis. *Atherosclerosis* **251**, 445–453 (2016).

204. Sergin, I. *et al.* p62-enriched inclusion bodies in macrophages protect against atherosclerosis. *Sci. Signal.* **9**, ra2 (2016).

205. Gregory, C. D. & Devitt, A. The macrophage and the apoptotic cell: an innate immune interaction viewed simplistically? *Immunology* **113**, 1–14 (2004).

206. Yoon, K. W. Dead cell phagocytosis and innate immune checkpoint. *BMB Rep.* **50**, 496–503 (2017).

207. Gordon, S. & Plüddemann, A. Macrophage Clearance of Apoptotic Cells: A Critical Assessment. *Front. Immunol.* **9**, 127 (2018).

208. Jt, H., Dy, K., Oj, P. & Ms, K. Resveratrol protects ROS-induced cell death by activating AMPK in H9c2 cardiac muscle cells. *Genes Nutr.* **2**, 323–326 (2008).

209. Wang, Y.-S. *et al.* AMP-activated protein kinase protects against necroptosis via regulation of Keap1-PGAM5 complex. *Int. J. Cardiol.* **259**, 153–162 (2018).

210. Li, J. *et al.* AMP-activated protein kinase agonist N 6 -(3-hydroxyphenyl)adenosine protects against fulminant hepatitis by suppressing inflammation and apoptosis. *Cell Death Dis.* **9**, 1–13 (2018).

211. Barialai, L. *et al.* AMPK activation protects astrocytes from hypoxia-induced cell death. *Int. J. Mol. Med.* **45**, 1385–1396 (2020).

212. Wang, J., Ma, A., Zhao, M. & Zhu, H. AMPK activation reduces the number of atheromata macrophages in ApoE deficient mice. *Atherosclerosis* **258**, 97–107 (2017).

213. Conde, E. *et al.* Specific pattern of LKB1 and phospho-acetyl-CoA carboxylase protein immunostaining in human normal tissues and lung carcinomas. *Hum. Pathol.* **38**, 1351–1360 (2007).

214. Quan, H. *et al.* AICAR Enhances the Phagocytic Ability of Macrophages towards Apoptotic Cells through P38 Mitogen Activated Protein Kinase Activation Independent of AMP-Activated Protein Kinase. *PLoS ONE* **10**, (2015).

215. Kim, J., Kundu, M., Viollet, B. & Guan, K.-L. AMPK and mTOR regulate autophagy through direct phosphorylation of Ulk1. *Nat. Cell Biol.* **13**, 132–141 (2011).

216. Alers, S., Löffler, A. S., Wesselborg, S. & Stork, B. Role of AMPK-mTOR-Ulk1/2 in the regulation of autophagy: cross talk, shortcuts, and feedbacks. *Mol. Cell. Biol.* **32**, 2–11 (2012).

217. Ouimet, M. *et al.* Autophagy regulates cholesterol efflux from macrophage foam cells via lysosomal acid lipase. *Cell Metab.* **13**, 655–667 (2011).

218. Zhong, S. *et al.* Acetaldehyde dehydrogenase 2 interactions with LDLR and AMPK regulate foam cell formation. *J. Clin. Invest.* **129**, 252–267.

219. Li, K., Ching, D., Luk, F. S. & Raffai, R. L. Apolipoprotein E Enhances microRNA-146a in Monocytes and Macrophages to Suppress Nuclear Factor-κB–Driven Inflammation and Atherosclerosis. *Circ. Res.* **117**, e1 (2015).

220. Murphy, A. J. *et al.* ApoE regulates hematopoietic stem cell proliferation, monocytosis, and monocyte accumulation in atherosclerotic lesions in mice. *J. Clin. Invest.* **121**, 4138–4149 (2011).

221. Bligh, E. G. & Dyer, W. J. A RAPID METHOD OF TOTAL LIPID EXTRACTION AND PURIFICATION. 7.

222. Scandinavian Simvastatin Survival Study Group. Randomised trial of cholesterol lowering in 4444 patients with coronary heart disease: the Scandinavian Simvastatin Survival Study (4S). *The Lancet* **344**, 1383–1389 (1994).

223. Bittencourt, M. S. & Cerci, R. J. Statin effects on atherosclerotic plaques: regression or healing? *BMC Med.* **13**, (2015).

224. Kavalipati, N., Shah, J., Ramakrishan, A. & Vasnawala, H. Pleiotropic effects of statins. *Indian J. Endocrinol. Metab.* **19**, 554–562 (2015).

225. Sakai, K. *et al.* Myeloid HMG-CoA (3-Hydroxy-3-Methylglutaryl-Coenzyme A) Reductase Determines Atherosclerosis by Modulating Migration of Macrophages. *Arterioscler. Thromb. Vasc. Biol.* **38**, 2590–2600 (2018).

226. Foretz, M. & Viollet, B. Measurement of AMPK-Induced Inhibition of Lipid Synthesis Flux in Cultured Cells. *Methods Mol. Biol. Clifton NJ* **1732**, 363–371 (2018).

227. Fairweather, D. Sex Differences in Inflammation During Atherosclerosis. *Clin. Med. Insights Cardiol.* **8**, 49–59 (2015).

228. Man Joshua J., Beckman Joshua A. & Jaffe Iris Z. Sex as a Biological Variable in Atherosclerosis. *Circ. Res.* **126**, 1297–1319 (2020).

229. Randomised trial of cholesterol lowering in 4444 patients with coronary heart disease: the Scandinavian Simvastatin Survival Study (4S). *Lancet Lond. Engl.* **344**, 1383–1389 (1994).

230. Nagashima, S. *et al.* Liver-specific deletion of 3-hydroxy-3-methylglutaryl coenzyme A reductase causes hepatic steatosis and death. *Arterioscler. Thromb. Vasc. Biol.* **32**, 1824–1831 (2012).

231. Alomari, M. *et al.* Role of Lipid Rafts in Hematopoietic Stem Cells Homing, Mobilization, Hibernation, and Differentiation. *Cells* **8**, (2019).

232. Wang, M. *et al.* IL-3/GM-CSF receptor promotes stem cell expansion, monocytosis, and atheroma macrophage burden in mice with hematopoietic Apoe deficiency. *Arterioscler. Thromb. Vasc. Biol.* **34**, 976–984 (2014).

233. Westerterp, M. *et al.* Regulation of hematopoietic stem and progenitor cell mobilization by cholesterol efflux pathways. *Cell Stem Cell* **11**, 195–206 (2012).

234. M, W. & Pj, C. Protein Prenylation: Unique Fats Make Their Mark on Biology. *Nature reviews. Molecular cell biology* vol. 17 https://pubmed.ncbi.nlm.nih.gov/26790532/ (2016).

235. Palsuledesai, C. C. & Distefano, M. D. Protein Prenylation: Enzymes, Therapeutics, and Biotechnology Applications. *ACS Chem. Biol.* **10**, 51–62 (2015).

236. Kiaris, H., Hatzistamou, J. & Spandidos, D. A. Instability at the H-ras minisatellite in human atherosclerotic plaques. *Atherosclerosis* **125**, 47–51 (1996).

237. George, J. *et al.* Functional inhibition of Ras by S-trans,trans-farnesyl thiosalicylic acid attenuates atherosclerosis in apolipoprotein E knockout mice. *Circulation* **105**, 2416–2422 (2002).

238. Sugita, M., Sugita, H. & Kaneki, M. Farnesyltransferase Inhibitor, Manumycin A, Prevents Atherosclerosis Development and Reduces Oxidative Stress in Apolipoprotein E-Deficient Mice. *Arterioscler. Thromb. Vasc. Biol.* **27**, 1390–1395 (2007).

239. Khan, O. M. *et al.* Targeting GGTase-I Activates RHOA, Increases Macrophage Reverse Cholesterol Transport, and Reduces Atherosclerosis in Mice. *Circulation* **127**, 782–790 (2013).

240. Lusis, A. J., Mar, R. & Pajukanta, P. Genetics of atherosclerosis. *Annu. Rev. Genomics Hum. Genet.* **5**, 189–218 (2004).

241. Kovacic, S. & Bakran, M. Genetic Susceptibility to Atherosclerosis. *Stroke Research and Treatment* vol. 2012 e362941 https://www.hindawi.com/journals/srt/2012/362941/ (2012).

242. Koltsova, E. K., Hedrick, C. C. & Ley, K. Myeloid cells in atherosclerosis: a delicate balance of anti-inflammatory and proinflammatory mechanisms. *Curr. Opin. Lipidol.* **24**, 371–380 (2013).

243. Swirski, F. K., Nahrendorf, M. & Libby, P. Mechanisms of Myeloid Cell Modulation of Atherosclerosis. *Microbiol. Spectr.* **4**, (2016).

APPENDIX A:

Table 2. All antibodies and important associated information for all experimental approaches. Rb: Rabbit, Rt: Rat, Mu: Mouse, Gt: Goat.

Antibody name	Host species	Application	Conjugation	Reactivity	Type	Supplier	Cat. #
Phospho-Acetyl-CoA Carboxylase (Ser79)	Rabbit	WB	None	Hu, Ms	Primary	Cell Signaling Technology	3676
Acetyl-CoA Carboxylase	Rabbit	WB	None	Hu, Ms, Rt, Hm	Primary	Cell Signaling Technology	11818
AMPKα	Rabbit	WB	None	Hu, Ms, Rt, Mk, B	Primary	Cell Signaling Technology	2535
Arginase 1 (Arg1)	Sheep	IF	Fluorescein	Hu, Ms, Rt	Primary	R&D Systems	IC5868F
Beclin-1	Rabbit	WB	None	Hu, Ms, Rt, Mk	Primary	Cell Signaling Technology	3495
Beta-Actin	Rabbit	WB	HRP	Hu, Ms, Rt, Mk, B, Pg	Primary	Cell Signaling Technology	5125
Cleaved Caspase-3 (CC3)	Rabbit	IF	AlexaFluor 594	Hu, Ms	Primary	Cell Signaling Technology	8172S
CCR2	Rabbit	IF	DyLight™ 488	Ms, Hu	Primary	Thermo Fisher Scientific	PIPA523046
CD36	Rabbit	WB	None	Hu	Primary	Cell Signaling Technology	14347
CD68	Rat	IF	AlexaFluor 647	Ms	Primary	BioLegend	137004
IREα	Rabbit	WB	None	Hu, Ms, Rt	Primary	Cell Signaling Technology	3294
LC3 A/B	Rabbit	WB	None	Hu, Ms, Rt	Primary	Cell Signaling Technology	4108
Monocytes and Macrophages (MOMA-2)	Rat	IF	None	Ms	Primary	Thermo Fisher Scientific	PIMA180630
p62 (SQSTMI)	Rabbit	IF	Fluorescein	Hu, Ms, Rt	Primary	Novus Biologicals	NBP1-42822F
Phospho-AMPKα (Thr172)	Rabbit	WB	None	Hu, Ms, Rt, Hm, Mk, Dm, Sc	Primary	Cell Signaling Technology	2535
Phospho-Raptor (Ser792)	Rabbit	WB	None	Hu, Ms, Rt	Primary	Cell Signaling Technology	2083
Phospho-ULK1 (Ser555)	Rabbit	WB	None	Hu, Ms	Primary	Cell Signaling Technology	5869
Phospho-ULK1 (Ser757)	Rabbit	WB	None	Hu, Ms, Mk	Primary	Cell Signaling Technology	6888
Raptor	Rabbit	WB	None	Hu, Ms, Rt, Mk	Primary	Cell Signaling Technology	2280
p62 (SQSTM1)	Rabbit	WB	None	Hu, Ms, Rt, Mk	Primary	Cell Signaling Technology	5114
TFEB	Mouse	IF	None	Hu	Primary	My BioSource	MBS120432
ULK1	Rabbit	WB	None	Hu, Ms, Rt, Mk	Primary	Cell Signaling Technology	8054
Anti-rabbit IgG, HRP-linked	Goat	WB	HRP	Rb	Secondary	Cell Signaling Technology	7074
Anti-Fluorescein/Oregon Green	Rabbit	IF	Alexa Fluor 488	Chemical	Secondary	Thermo Fisher Scientific	A-11090
Anti-Mouse IgG (H+L)	Goat	IF	Alexa Fluor 488	Ms	Secondary	Thermo Fisher Scientific	A11001
Anti-Mouse IgG (H+L)	Goat	IF	Alexa Fluor 488	Ms	Secondary	Thermo Fisher Scientific	A11001
Anti-Rat IgG (H+L)	Goat	IF	Alexa Fluor Plus 647	Rt	Secondary	Thermo Fisher Scientific	A21247

Table 3. All Taqman primer probes used for quantitative PCR analysis.

Gene Name	Assay I.D.	Supplier	Cat. #
PRAAK1	Mm01296700_m1	Thermo Fisher Scientific	4331182
Actb	Mm00607939_s1	Thermo Fisher Scientific	4331182
BECN1	Mm00554370_m1	Thermo Fisher Scientific	4331182
DHCR24	Mm00519071_m1	Thermo Fisher Scientific	4331182
DHCR7	Mm00514571_m1	Thermo Fisher Scientific	4331182
FDFT1 (SQS)	Mm01598574_g1	Thermo Fisher Scientific	4331182
GGPS1	Mm00656129_mH	Thermo Fisher Scientific	4331182
HMGCR	Mm01282499_m1	Thermo Fisher Scientific	4331182
HMGCS1	Mm01304569_m1	Thermo Fisher Scientific	4331182
LAL (CPQ)	Mm01164968_m1	Thermo Fisher Scientific	4351372
LC3 (Map1lc3a)	Mm00458724_m1	Thermo Fisher Scientific	4331182
MVK	Mm00445773_m1	Thermo Fisher Scientific	4331182
Pggt1b	Mm00553955_m1	Thermo Fisher Scientific	4331182
TBP	Mm00446973_m1	Thermo Fisher Scientific	4331182
TFEB	Mm00448968_m1	Thermo Fisher Scientific	4331182

APPENDIX B:

Table 4. List of all Figures and location within Thesis.

Figure #	Page #	Figure Title
1	39	Modified LDL variants, agLDL and oxLDL, augment AMPK-specific signaling in BMDM.
2	41	The CaMKKβ/Ca^{2+} pathway is partially involved in regulating AMPK activity in response to agLDL and oxLDL in BMDM.
3	42	Acute incubation with agLDL or oxLDL shifts cellular energy levels in BMDM.
4	44	AMPK links CD36-mediated uptake of oxLDL to early signaling events in autophagy initiation.
5	45	AMPKβ1-KO BMDM show signs of perturbed parameters associated with lysosomal dysfunction.
6	47	Activation of BMDM AMPK regulates signaling events within the autophagy pathway.
7	49	Acute pharmacological activation of BMDM AMPK induces the nuclear localization of TFEB.
8	50	AMPK regulates the transcript and protein expression of TFEB and TFEB-regulated genes important for lysosomal homeostasis and autophagy.
9	52	Modified LDL variants, agLDL and oxLDL, do not modulate TFEB or downstream effector genes through AMPK in BMDMs.
10	73	A769662 embedded within poly-lactic acid nanoparticles induces a robust and sustained increase of AMPK signaling to ACC in BMDM and hepatic tissue.
11	75	A769662-NP therapy is insufficient for reducing WD-induced lesion development in male LDLr-KO mice.
12	77	A769662-NPs do not alter lesion macrophage-like cell frequency, anti-inflammatory marker expression, or apoptotic cell death in male mice.
13	78	Inability to assess AMPK activity in atherosclerotic lesions via immunofluorescent techniques.
14	80	AMPK signaling is retained in liver, but not in primary peritoneal macrophages isolated from thioglycolate-elicited MacKO mice.
15	82	A769662-therapy protects against WD-induced weight gain in male mice.
16	84	Myeloid AMPK and A769662-intervention therapy are insufficient in protecting against the progression of atherosclerosis in male mice.
17	85	Myeloid AMPK and A769662-therapy don't influence macrophage-like cell frequency within developing lesions in male mice.
18	87	Myeloid AMPK and A769662-therapy do not promote lesion autophagy in male mice.
19	89	Myeloid AMPK and A769662-therapy do not protect against the resolution of lesion necrosis in male mice.

20	90	Myeloid AMPK and A769662 therapy do not mitigate anti-atherogenic effects through modulation of total circulating lipids in male or female mice.
21	92	The role of myeloid AMPK and A769662-therapy on circulating inflammatory messengers.
22	112	HMGCR KI macrophages have enhanced sterol synthesis that is unresponsive to AMPK activation but retain normal levels of fatty acid synthesis subject to AMPK regulation.
23	113	Macrophage AMPK's inhibition of HMGCR does affect basal cholesterol content or acute cholesterol uptake.
24	115	Macrophage AMPK's suppression of HMGCR does not alter basal or stimulated cholesterol efflux to ApoA-I or HDL.
25	117	Differential transcript expression of genes within the mevalonate and isoprenoid synthesis pathways within HMGCR BMDMs.
26	119	AMPK's negative regulation of whole-body cholesterol synthesis does not impact WD-induced weight gain.
27	120	AMPK's negative regulation of whole-body HMGCR protects against the progression of atherosclerosis.
28	122	Total hepatic cholesterol content is affected by the Ser871Ala KI mutation within the WB, but it does not alter total levels of circulating cholesterol.
29	123	AMPK's negative regulation of whole-body cholesterol synthesis on circulating inflammatory messengers in atherosclerosis.
30	126	AMPK's negative regulation of hematopoietic cholesterol synthesis does not impact WD-induced weight gain.
31	127	AMPK's negative regulation of hematopoietic cholesterol synthesis protects against the progression of atherosclerosis.
32	129	Total hepatic cholesterol content is unaffected by the Ser871Ala KI mutation within the hematopoietic compartment, however may be implicated in circulating total cholesterol levels in in female mice.
33	130	AMPK's regulation of hematopoietic cholesterol synthesis does not alter myeloid recruitment into developing lesions.
34	132	AMPK's negative regulation of hematopoietic cholesterol synthesis on circulating inflammatory messengers in atherosclerosis.

Table 5. List of compounds for activating macrophage AMPK.

Compound name	Mechanism of action
A769662 (thienopyridone)	Allosteric activation and inhibition of dephosphorylation
AICAR (5-Aminoimidazole-4-carboxamide ribonucleotide)	AMP mimetic
Salicylate	Allosteric activation
Berberine	Increase AMP: ATP ratio
Curcumin	Increase AMP: ATP ratio
Resveratrol	Increase AMP: ATP ratio

Metformin	Increase AMP: ATP ratio
Phenformin	Increase AMP: ATP ratio
Troglitazone	Increase AMP: ATP ratio

Nicholas LeBlond Curriculum Vitae

PERSONAL STATEMENT

I am a self-motivated enthusiastic researcher with 7 years of cumulative research experience that has largely focussed on understanding the molecular mechanism that underpin cardiovascular and metabolic pathologies. I am a critical thinker with an aptitude for developing and improving methodologies and procedures for higher-level data analysis and reporting. My long-term aspiration has always been to be able to work towards the betterment of global health and quality of life through my scientific endeavour.

RESEARCH EXPERIENCE

Doctoral Researcher (09/2014 - 09/2020)

The University of Ottawa, Ottawa, ON.

Mentor: Dr. Morgan Fullerton

Research Projects:

- Myeloid deletion of both AMPK catalytic subunits and therapeutic activation does not alter atherosclerosis in male or female mice.

  (Completed: Tentatively accepted)
- Foam cell formation activates AMPK but uncouples its regulation of autophagy and lysosomal homeostasis.

  (Completed: Submitted)
- Investigating AMPK-mediated suppression of endogenous cholesterol synthesis within hematopoietic-derived immune cells in the context of atherosclerosis.

  (Completed: Co-author review process)

Undergraduate Researcher (05/2013 - 05/2014)

Trent University, Peterborough, ON

Mentor: Dr. Janet Yee and Dr. Steven Rafferty

Research Projects:

- Designing an optimizing a pull-down assay to isolate and identify candidate redox partners for all isoforms of *Giardia lamblia's* Cytochrome b5.
- Characterizing *Giardia lamblia's* putative TATA-binding protein.

SCIENTIFIC SKILLS

- Animal handling and tissue isolations
- Murine *in vivo* models of metabolic disease
- Mammalian cell culture
- Histology
- Analyte isolation and purification (DNA, RNA, protein, and lipids)
- Biochemical and molecular biology techniques (gel electrophoresis, western blotting, PCR, qPCR, immunofluorescent microscopy, and flow cytometry)

ACADEMIC WORK EXPERIENCE

Academic Assistant Molecular Biology, Trent University, Peterborough, ON. (09/2013 - 12/2013)

Academic Assistant Human Anatomy, Trent University, Peterborough, ON. (09/2013 - 12/2013)

Academic Assistant Human Physiology, Trent University, Peterborough, ON. (01/2014 - 05/2014)

- Supported student learning objectives through personalized and small group assistance.
- Mentored students through office hours and one-on-one communication.
- Checked assignments, proctored tests, and provided grades according to university standards.

TEACHING AND MENTORING EXPERIENCE

The University of Ottawa, Ottawa, ON (09/2014 – Present)

- MSc Candidates: 4
- Undergraduates: 9
- Student Volunteers: 4

SCHOLARSHIPS AND AWARDS (TOTAL: $107 074 CAD)

Graduate Student Mentorship Award (2018):	$500 CAD
Excellence Scholarship (2017 - 2018):	$7 074 CAD
Ontario Graduate Scholarship (2017 - 2018):	$15 000 CAD
Admissions Scholarship-Doctorate (2015 - 2020):	$72 000 CAD
Admissions Scholarship-Master's (2014 - 2015):	$12 500 CAD

EDUCATION

Doctorate (Biochemistry), The University of Ottawa, Ottawa, ON.

(09/2014 - 09/2020)

Bachelors of Science (Biology), Trent University, Peterborough, ON.

(09/2009 - 05/2014)

VOLUNTEER EXPERIENCE

Stroll for Liver: Virtual Challenge, The Canadian Liver Foundation. Ottawa, ON. (2020)

Scientific guide/host, Encounters Canada, The University of Ottawa. Ottawa, ON. (2019)

Science and innovation guest lecturer, M M. Robinson High School. Burlington, ON. (2018)

Scientific guide/host, Encounters Canada, The University of Ottawa. Ottawa, ON. (2018)

Event Coordinator, National Canadian Lipoprotein Conference. Ottawa, ON. (2017)

Volunteer cook, Graduate council student lunches, The University of Ottawa. Ottawa, ON. (2014 – 2020)

Co-President of the Biology Undergraduate Society. Trent University, Peterborough, ON. (2013 – 2014)

Biological Sciences Senior Tutor, Trent University. Peterborough, ON. (2013 – 2014)

PUBLICATIONS

Life-time Summary:

- Submitted Journal Articles: 1
- Accepted Journal Articles: 1
- Refereed Journal Articles: 9
- Conference Publications: 20

SUBMITTED JOURNAL ARTICLES:

11. **Nicholas LeBlond**, Julia Nunes, Tyler Smith, Sabrina Robichaud, Marceline Côté, Suresh Gadde, Bruce Kemp, Mireille Ouimet and Morgan Fullerton. Foam cell formation activates AMPK but uncouples its regulation of autophagy and lysosomal homeostasis.
Submitted, under peer-review.
Pre-print deposited on BioRxiv. (doi: https://doi.org/10.1101/2020.08.13.244640)

ACCEPTED JOURNAL ARTICLES:

10. **Nicholas LeBlond**, Peyman Ghorbani, Conor O'Dwyer, Nia Abursley, Julia Nunes, Tyler Smith, Natasha Trzaskalski, Erin Mulvihill, Benoit Viollet, Marc Foretz and Morgan Fullerton. (2020). Myeloid deletion and therapeutic activation of AMP-activated protein kinase (AMPK) do not alter atherosclerosis in male or female mice.
Tentatively accepted at Journal of Lipid Research.
Pre-print deposited on BioRxiv. (doi: https://doi.org/10.1101/2020.07.15.204487)

REFEREED JOURNAL ARTICLES:

9. Conor O'Dwyer*, Rebecca Yaworski*, **Nicholas LeBlond**, Peyman Ghorbani, Julia Nunes, Kaitlyn Margison, Tyler Smith, Kaelan Gobeil Odai, Shauna Han, Morgan Fullerton. (2020). Fatty acid-induced lipotoxicity inhibits choline metabolism independent of ER stress in mouse primary hepatocytes. Hepatology Communications, 4(6).

8. Tyler Smith*, Zaina Kahiel*, **Nicholas LeBlond**, Peyman Ghorbani, Eliya Farah, Marceline Cote, Suresh Gadde, Morgan Fullerton. (2019). Characterization of LXR-activating nanoparticle formulations in primary mouse macrophages. Molecules, 24(20).

7. Corina Stewart, Stephanie Dorion, Marie Ottenbrite, **Nicholas LeBlond**, Tyler Smith, Shirley Qiu, Morgan Fullerton, Darwyn Kobasa, Marceline Côté. (2019). A Diacylglycerol Kinase Inhibitor, R-59-022, Blocks Filovirus Internalization in Host Cells. Viruses, 11(3).

6. Truc Losier, Mercy Akuma, Olivia McKee-Muir, **Nicholas LeBlond**, Yujin Suk, Reham Alsaadi, Zhihao Guo, Ryan Reshke, Subash Sad, François-Xavier Campbell-Valois, Derrick Gibbings, Morgan Fullerton, Ryan Russell. (2019). AMPK Promotes Xenophagy through Priming of Autophagic Kinases upon Detection of Bacterial Outer Membrane Vesicles. Cell reports, 26(8).

5. Kim Loh, Shanna Tam, Lisa Murray-Segal, Kevin Huynh, Peter Meikle, John Scott, Bryce van Denderen, Zhiping Chen, Rohan Steel, **Nicholas LeBlond**, Leah Burkovsky, Conor O'Dwyer, Julia Nunes, Gregory Steinberg, Morgan Fullerton,

Sandra Galic, Bruce Kemp. (2018). Inhibition of Adenosine Monophosphate-Activated Protein Kinase-3-Hydroxy-3-Methylglutaryl Coenzyme A Reductase Signaling Leads to Hypercholesterolemia and Promotes Hepatic Steatosis and Insulin Resistance. Hepatology communications, 3(1).

4. Shayne Snider*, Kaitlyn Margison*, Peyman Ghorbani, **Nicholas LeBlond**, Conor O'Dwyer, Julia Nunes, Thao Nguyen, Hongbin Xu, Steffany Bennett, Morgan Fullerton. (2018). Choline transport links macrophage phospholipid metabolism and inflammation. Journal of Biological Chemistry. 293(29).

3. **Nicholas LeBlond**, Morgan Fullerton. (2018). Methods to Evaluate AMPK Regulation of Macrophage Cholesterol Homeostasis. Methods in molecular biology (Clifton, N.J.), 1732, 477-493.\

2. Meenakshi Sundaram, Kaitlin Curtis, Mohsen Amir Alipour, **Nicholas LeBlond**, Kaitlyn Margison, Rebecca Yaworski, Robin Parks, Adam McIntyre, Robert Hegele, Morgan Fullerton, Zemin Yao. (2017). The apolipoprotein C-III (Gln38Lys) variant associated with human hypertriglyceridemia is a gain-of-function mutation. Journal of lipid research, 58(11).

1. Morgan Fullerton, Rebecca Ford, Chelsea McGregor, **Nicholas LeBlond**, Shane Snider, Stephanie Stypa, Emily Day, Sarka Lhoták, Jonathan Schertzer, Richard Austin, Bruce Kemp, Gregory Steinberg. (2015). Salicylate improves macrophage cholesterol homeostasis via activation of AMPK. Journal of lipid research, 56(5).

PRESENTATIONS AND PUBLISHED ABSTRACTS:

20. Morgan Fullerton. Lecture. (2019). “Immunometabolism links AMPK and atherosclerosis”. National Molecular and Cellular Biology of Lipids Annual Retreat, Edmonton, Canada.

19. **Nicholas LeBlond**. Abstract and Poster Presentation. (2019). “Myeloid AMPK in atherosclerosis: Mechanisms and therapeutic potential”. The University of Ottawa Seminar Day. Ottawa, Canada.

18. Morgan Fullerton. Lecture. (2019). "Immunometabolism links AMPK and atherosclerosis". Provincial, Guelph, Canada.

17. **Nicholas LeBlond**. Abstract and Poster Presentation. (2018). "Myeloid AMPK in Atherosclerosis: associated mechanisms and therapeutic potential". The University of Ottawa Poster Day, Ottawa, Canada.

16. Morgan Fullerton. Lecture. (2018). "Therapeutic targeting of macrophage AMPK in atherosclerosis". National AMPK- From mechanisms to new therapies, Niagara-on-the-Lake, Canada.

15. **Nicholas LeBlond**. Abstract and Poster Presentation. (2017). "Macrophage AMPK links cholesterol and lysosomal homeostasis". The University of Ottawa Seminar Day, Ottawa, Canada.

14. **Nicholas LeBlond**. Lecture. (2017). "Macrophage AMPK links cholesterol and lysosomal homeostasis". National Canadian Lipoprotein Conference, Ottawa, Canada.

13. Morgan Fullerton. Lecture. (2017). "Macrophage AMPK links cholesterol and lysosomal homeostasis". National 3rd European Workshop on AMPK, Île de Porquerolles, France.

12. **Nicholas LeBlond**. (2017). "Macrophage AMPK links cholesterol and lysosomal homeostasis". Canadian Society for Molecular Biosciences, Ottawa, Canada.

11. Morgan Fullerton. Lecture. (2017). "Macrophage AMPK regulation of lipid and lysosomal homeostasis". National Bridging Discovery Research with Therapies, Banff, Canada.

10. Morgan Fullerton. Lecture. (2017). "Regulation of Macrophage Lipid Homeostasis and Immunometabolism". National Trinity Biomedical Sciences Institute, Dublin, Ireland.

9. **Nicholas LeBlond**. Abstract and Poster Presentation. (2017). "Macrophage AMPK links cholesterol and lysosome homeostasis". Ottawa Heart Conference: Inflammation in Cardiometabolic Disease, Ottawa, Canada.

8. **Nicholas LeBlond**. Lecture. (2016). "Macrophage AMPK during atherosclerosis: mechanisms and therapeutic potential". The University of Ottawa Seminar Day. Ottawa, Canada.

7. Morgan Fullerton. Lecture. (2016). "Immunometabolism of macrophage AMP-activated protein kinase". Longhua International Forum on Digestive Diseases, Shanghai, China.

6. **Nicholas LeBlond**. Abstract and Poster Presentation. (2015). "The Role of AMPK and Autophagy in Cholesterol Efflux in Macrophage Foam Cells". University of Ottawa Poster Day, Ottawa, Canada.

5. **Nicholas LeBlond**. Abstract and Poster Presentation. (2015). "Macrophage AMPK regulates lysosome homeostasis". Canadian Lipoprotein conference, Toronto, Canada.

4. Morgan Fullerton. Lecture. (2015). "AMPK-activated protein kinase: Linking inflammation and metabolism". ISN Forefronts Symposium. Immunomodulation of cardio-renal function, Shenzhen, China.

3. Morgan Fullerton. Informal Talk. (2015). "Salicylate restores macrophage cholesterol homeostasis via activation of AMP-activated protein kinase". National Atherosclerosis, Thrombosis and Vascular Biology, San Francisco, United States.

2. **Nicholas LeBlond**. Abstract and Poster Presentation. (2015). "Macrophage AMPK is activated by atherogenic lipoproteins". Canadian Lipoprotein conference, Toronto, Canada.

1. **Nicholas LeBlond**. Lecture. (2014). "A Pulldown Assay to Detect Binding Partners of *Giardia lamblia's* Cytochromes b5". Southern Ontario Undergraduate Student Chemistry Conference, Windsor, Canada.